SYSTEM LEVEL ASSESSMENT OF MOTOR CONTROL THROUGH PATTERNED MICROSTIMULATION IN THE SUPERIOR COLLICULUS

by

Husam A. Katnani

B.S. in Bioengineering, Pennsylvania State University, 2007

Submitted to the Graduate Faculty of

the Swanson School of Engineering in partial fulfillment

of the requirements for the degree of

Doctor of Philosophy

University of Pittsburgh

2012

UNIVERSITY OF PITTSBURGH

SWANSON SCHOOL OF ENGINEERING

This dissertation was presented

by

Husam A. Katnani

It was defended on

May 10, 2012

and approved by

C.R. Olson, Ph.D., Professor, Center of the Neural Basis of Cognition

D.J. Weber, Ph.D., Professor, Bioengineering Department

A.P. Batista, Ph.D., Professor, Bioengineering Department

Dissertation Director: N.J. Gandhi, Ph.D., Professor, Otolaryngology

SYSTEM LEVEL ASSESSMENT OF MOTOR CONTROL THROUGH PATTERNED MICROSTIMULATION IN THE SUPERIOR COLLICULUS

Husam A. Katnani, PhD

University of Pittsburgh, 2012

We are immersed in an environment full of sensory information, and without much thought or effort we can produce orienting responses to appropriately react to different stimuli. This seemingly simple and reflexive behavior is accomplished by a very complicated set of neural operations, in which motor systems in the brain must control behavior based on populations of sensory information. The oculomotor or saccadic system is particularly well studied in this regard. Within a visual environment consisting of many potential stimuli, we control our gaze with rapid eye movements, or saccades, in order to foveate visual targets of interest. A key sub-cortical structure involved in this process is the superior colliculus (SC). The SC is a structure in the midbrain which receives visual input and in turn projects to lower-level areas in the brainstem that produce saccades. Interestingly, microstimulation of the SC produces eye movements that match the metrics and kinematics of naturally-evoked saccades. As a result, we explore the role of the SC in saccadic motor control by manually introducing distributions of activity through neural stimulation.

Systematic manipulation of microstimulation patterns were used to characterize how ensemble activity in the SC is decoded to generate eye movements. Specifically, we focused on three different facets of saccadic motor control. In the first study, we examine the effective influence of microstimulation parameters on behavior to reveal characteristics of the neural mechanisms underlying saccade generation. In the second study, we experimentally verify the predictions of computational algorithms that are used to describe neural mechanisms for saccade generation. And in the third study, we assess where neural mechanisms for decoding occur within the oculomotor network in order to establish the order of operations necessary for saccade generation. The experiments assess different aspects of saccadic motor control, which collectively, reveal properties and mechanisms that contribute to the comprehensive understanding of signal processing in the oculomotor system.

TABLE OF CONTENTS

LIST OF TABLES

LIST OF FIGURES

PREFACE

The chapters of this dissertation, as well as, a large portion of the general introduction have been published or are currently under review for publication.

General Introduction: Gandhi NJ and Katnani HA. "Motor Functions of the Superior Colliculus." Annual Review of Neuroscience, 34:205-31, 2011.

Chapter 2: Katnani HA and Gandhi NJ. "The relative impact of microstimulation parameters on movement generation." Journal of Neurophysiology, 2012 [Epub ahead of print].

Chapter 3: Katnani HA and Gandhi NJ. "A test of spatial temporal decoding mechanisms in the superior colliculus." Journal of Neurophysiology, 107(9):2442-52, 2012.

Chapter 4: Katnani HA, Van Opstal AJ and Gandhi NJ. "Analysis of stimulation-evoked saccades perturbed by blinks." PLoS ONE, 2012 [Under Review].

Chapter 5: Katnani HA and Gandhi NJ. "Order of operations for decoding superior colliculus activity for saccade generation." Journal of Neurophysiology, 106(3):1250-9, 2011.

Acknowledgements

First and foremost, I must thank Dr. Neeraj Gandhi (aka Raj). Although his pedigree speaks for itself, my highest praise goes out to him as a mentor, a scientist, and a friend. As his first doctorate student, I can only hope that many more may come to benefit from his mentorship. Dr. Gandhi has found the perfect balance between walking you through a challenge and pushing you to overcome it on your own. His guidance has led me to six publications, one book chapter, and three training grants, all within five years. Dr. Gandhi's passion, enthusiasm, and leadership

have made him and will continue to make him a great advisor for years to come. He is truly a bioengineering gemstone buried in the otolaryngology department.

Recognition must be given to the members that comprise the Gandhi group. Thanks to Joe Mcferron (aka Mr. Labview); the man is an engineer for engineers, which in itself, says enough. Thanks to Uday Jagadisan, a young enthusiastic scientist, who is responsible for many great scientific discussions, whether wanted or not. The future Dr. Jagadisan will definitely have an impact on the neuroscience community. Special thanks go to Bernard Bechara. During my first year of graduate school, Mr. Bechara was finishing his master's degree under Dr. Gandhi. His presence was truly invaluable; if it weren't for him I would not have completed my doctorate degree in five years. He showed me the ins and outs which allowed me to quickly become successful on my own. I must also mention Mr. Bechara's recent voyage into fatherhood with his baby girl, Maya Noor Bechara, who can now say her name was published before she turned one. Last but not least in the Gandhi group is Gloria Foster, the lab manager and vet technician. Gloria's contribution to my life and work is indescribable. Thank you for dog-sitting so many times; you'll never know how much that helped me. Thank you for teaching me how to train and deal with primates. Thank you for always keeping me up-to-date on shots and protocols, and thank you for showing me that sometimes you have to step up and act as a human shield, even if you don't want to. I truly can't thank Gloria enough for all her support.

I must thank my doctorate committee, all of whom are outstanding scientists. Their help, advice, and guidance have fortified my dissertation work, which has led to the successful completion of my doctorate degree. I can only hope to be as successful as each member in my committee. Special thanks to Dr. Batista, who I was fortunate enough to assistant teach with twice. I've learned a great deal about teaching and life from him.

The network of people and opportunities available between the University of Pittsburgh and Carnegie Mellon are outstanding. The bioengineering department and center for the neural basis of cognition (CNBC) have been instrumental in my success. The programs, meetings, and retreats that have been orchestrated by each program have been unbelievably conducive to bringing together all disciplines of science and engineering. Their architecture for teaching and development should be a model system for programs around the nation. A very special thanks to Lynette Spataro, the academic administrator for the bioengineering graduate program and Lisa Bopp, administrative assistant in the CNBC. I have relied on them a countless number of times

for help, and they have always been there to support me. Another very special thanks to Dr. Harvey Borovetz, chair of the Bioengineering department. During recruitment, his continuous confidence and support drove me to choose the University of Pittsburgh, and I am ever grateful that I did. As he promised, the graduate program here has allowed me to flourish as an engineer, scientist, and man.

Dr. John Van Opstal is a magnificent man and scientist that I am so happy to have met and worked with. I have been fortunate enough to collaborate with Dr. Van Opstal twice, once during his sabbatical with the Gandhi group and then again as a result of a training grant that funded my work in his lab. During my trip to his lab in the Netherlands, Dr. Van Opstal was a most gracious host who took me in as family. He is a brilliant, jovial, and passionate individual who has essentially been a second mentor to me. I have published two research articles with Dr. Van Opstal and hope to continue collaborating in the future.

I could not have completed my doctorate degree without my family. Their support and love was a fixture throughout the entire process. My mother, Maha Katnani, sister, Samar Katnani, and father, Dr. Ahmad Katnani are center pieces in my life. Their support, selflessness, and tough love have pushed me to far surpass any of my expectations. My father, especially, has been a tremendous resource in helping me accomplish my degree. My discussions with him ranged from control theory, to signal processing, to neuronal function, to analytical techniques and beyond, and each discussion ended with him teaching me something. His intellect continues to astonish me, and makes me think that I may have earned my degree in the wrong field, as his doctorate in physics seems to provide him with knowledge on all math and science. I am not sure if version 2.0 can live up to version 1.0, but I'll try.

My final acknowledgment goes to the most important person in my life, my best friend and soon to be wife, Michelle Markowitz. She willingly followed me to Pittsburgh to endure the grueling life of being partnered with a graduate student, and despite that, she has shown me nothing but love and support. There is no other person I would rather share the ups and downs of my graduate career with. No matter how depressed or frustrated I got, she always made me smile and realize that tomorrow is another day. I dedicate my dissertation to Michelle; her support was the most critical factor in my success.

1.0 GENERAL INTRODUCTION

Imagine that a basketball player cuts to the hoop, and in doing so realizes that the ball has been lofted up, close to the rim, for him to slam home. To successfully record the alley-oop the player relies on a gamut of sensory information to appropriately guide his actions in performing the task. Visual and auditory cues provide information on the velocity and timing of the ball, proprioceptive signals determine how body position must change relative to the ball and rim, and somatosensory signals confirm catching, grasping, and dunking the ball. This seemingly simple and reflexive behavior for the player is accomplished by a very complicated set of neural operations in the brain. Information about the basketball, the rim, the players, and much more are represented in different regions throughout the brain as distributed neural activity. The activity evolves across both space and time and is integrated and transformed by sensorimotor structures to generate the appropriate motor behavior to allow the basketball player to react and perform. One such structure that is a major node for sensorimotor transformations is the superior colliculus (SC) (Hall and Moschovakis 2004; Sparks and Mays 1990; Stein and Meredith 1993). The SC is sensitive to several sensory modalities (e.g., vision, audition, somatosensation) with a major emphasis residing in visual function. The work encompassed in this dissertation focuses on how an ensemble of collicular motor activity, corresponding to visual stimuli, can be decoded for the behavioral control of fast eye movements or saccades. Saccades allow foveate species to direct gaze to stimuli of interest, which is not only a major component in allowing basketball players to perform, but also in allowing everyday assessment of our visual environment.

1.1 OCULOMOTOR SYSTEM

The oculomotor system comprises a large neural network in the brain. The neural representations of visual stimuli propagate through and are processed by a number of cortical (i.e., visual cortex, frontal eye fields, parietal cortex, etc.) and sub-cortical (basal ganglia, lateral geniculate nucleus, superior colliculus, etc.) structures in order to generate an eye movement. The intent of this thesis is to focus on the motoric functions of the SC by utilizing an electrical stimulus, which primarily activates descending collicular outputs employed on brainstem structures that innervate the eye muscles. In doing so, we eliminate a great deal of complexity in the motor system in an attempt to gain a clear understanding of motor control concepts involved in saccade generation. This perspective does not diminish the role of other processes mediated by the many structures involved in the saccadic system, but their inclusion is beyond the scope of this work.

1.1.1 Superior Colliculus

The superior colliculus is a subcortical structure that resides on the roof of the brainstem and contains seven alternating fibrous and cellular laminae. The structure can essential be thought of as a pipeline, from top layer to bottom layer, with the classification of neurons in each layer defining the progression of sensorimotor transformation. Neurons in the top or superficial layers (stratum zonale, stratum griseum superficiale, and stratum opticum) exclusively respond to sensory visual stimuli appearing at specific locations in the contralateral visual hemi-field. As you move to the bottom, into the intermediate (stratum griseum intermedium, and stratum album intermedium) and deeper (stratum griseum profundum, and stratum album profundum) layers, the cells begin to change primarily to motor function; sensory responses are transformed into motor commands, whereby the output of the SC discharges a vigorous burst that drives lower-level brainstem structures to produce a saccade. The burst exists for only a range of saccade vectors that define each cell's movement field (Straschill and Hoffmann 1970; Wurtz and Goldberg 1972). The response is maximal for a specific amplitude and direction, also known as the center or "hot spot" of the movement field, and graded for increasing and decreasing vectors

(Fig. 1B). Neurons in the SC are organized according to their movement field centers (Fig. 1A) (Sparks et al. 1976). Cells located rostrally within the SC discharge for small-amplitude saccades, whereas units found at more caudal locations discharge for large-size movements. Neurons within the medial and lateral regions are most active during saccades with upward and downward components, respectively. Furthermore, due to the direct input of visual field information from the retina to the SC, the topography of saccade amplitude is logarithmically skewed (Fig. 1A). A disproportionately large amount of SC tissue is allocated for small saccades, corresponding to the high density of projection from the para-foveal space of the retina, whereas a relatively compressed region is attributed for larger amplitude, corresponding to the spare projections from the peripheral space of the retina. In contrast, the saccade direction map along the mediolateral extent of the SC is fairly linear (Ottes et al. 1986).

Motor neurons in the deep layers of the SC bursts for a range of saccades, therefore it follows that a population of cells, generally envisioned as a Gaussian mound, burst to produce a single saccade (Fig. 1C). Several features of the mound are noteworthy. First, the size of the active population and the total number of spikes produced in the motor burst are invariant across all saccades (Anderson et al. 1998; Van Opstal and Goossens 2008). Second, the mound is centered at the site corresponding to the executed saccade vector. Third, the shaping of the spatial distribution of activity is attributed to intrinsic lateral interactions in the collicular layers that exhibit local excitation and distant inhibition (Isa and Hall 2009; Lee et al. 1997; Munoz and Istvan 1998; Pettit et al. 1999). And finally, the population response emits a high-frequency burst just prior to a saccade, in which the firing rate of the burst reflects the velocity of the movement (Goossens and Van Opstal 2000b, 2006; Sparks and Mays 1990; Stanford et al. 1996).

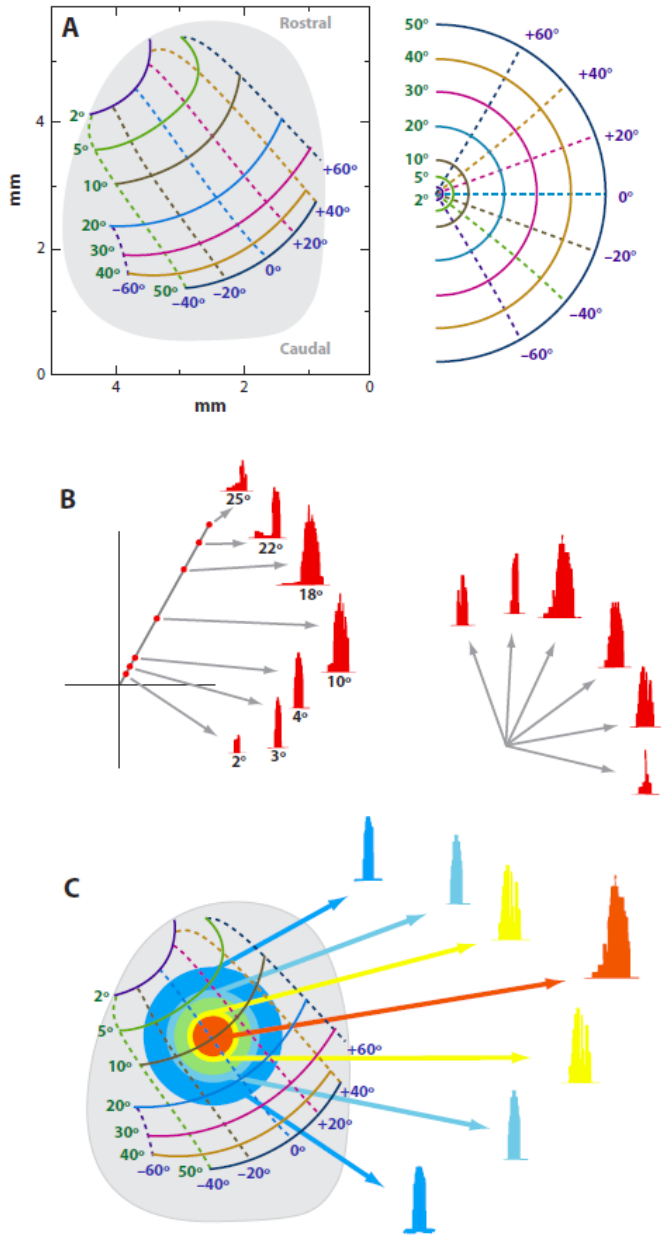

Figure 1. Fundamental properties of the superior colliculus for the generation of saccades **(A)** A schematic of the topographic organization of contralateral saccade vectors (left) is encoded in retinotopic coordinates. Isoradial and isodirectional bands are shown as solid and dashed lines, respectively. The radial and directions bands are identified in green and blue numbers, respectively. Each band is represented in a different color. The mapping of these bands in the contralateral hemifield is shown in the right panel. A disproportionately large amount of SC space is used to produce small amplitude saccades relative to the caudal SC areas that produce larger vectors. **(B)** Neurons in the deep SC layers discharge for a range of saccade amplitudes and directions. Its location on the SC map dictates the optimal vector for which the cell emits its maximal burst. Burst profiles are shown for different amplitude saccades in the optimal direction (left) and for several optimal amplitude saccades in various directions (right). **(C)** Population response for the generation of a saccade can be envisioned as a mound of activity across a large portion of the deep SC layers. The amplitude and direction of the executed saccade typically matches with the vector encoded at the locus of maximal activity. Neurons that are active but are located away from the center exhibit a suboptimal burst. **(B, C):** Adapted from Sparks & Gandhi (2003).

1.1.2 Brainstem Burst Generator and Omnipause Neurons

Descending outputs from the deep layers of the SC project onto the horizontal and vertical saccadic burst generators (BG) found in the paramedian pontine reticular formation (PPRF) and mesencephalic reticular formation of the brainstem, respectively. As a result of the logarithmic topography of the SC, the projections to the PPRF region of the brainstem are believed to be weighted exponentially in order to produce a wide range of saccade amplitudes from a relatively constant output, and to maintain the visual coordinates of stimuli originally relayed from the visual field (inverse of logarithmic topography). Consistent with this notion, the number of terminal boutons deployed from the colliculus to PPRF increases monotonically across the rostral-caudal extent of the SC (Moschovakis et al. 1998). The BG receives its drive from the colliculus and in-turn provides the high frequency discharge responsible for driving the motoneurons that innervate the corresponding eye muscles for horizontal and vertical movement (Moschovakis et al. 1991a; Moschovakis et al. 1991b; Sasaki and Shimazu 1981; Strassman et al. 1986). Furthermore, the peak discharge and duration of the BG burst has been shown to be tightly linked to the peak velocity and duration of saccades (Hepp and Henn 1983; Keller 1974; Luschei and Fuchs 1972; Strassman et al. 1986; Van Gisbergen et al. 1981). In addition, the burst generator is believed to reside in a local feedback loop that operates to ensure the metrics and kinematics of saccades (Goossens and Van Opstal 2000a; Jürgens et al. 1981).

The generation of saccades relies on another group of brainstem neurons called omnipause neurons (OPNs). These neurons are located along the midline in the PPRF and are defined as the inhibitory gate of the saccadic system, supported by a microstimulation study that demonstrated the complete cessation of eye movements during stimulation of the OPN region (Keller 1974). The OPNs discharge at a tonic rate during fixation, inhibiting both the horizontal and vertical BG (Büttner and Büttner-Ennever 1988; Furuya and Markham 1982; Langer and Kaneko 1990; Nakao et al. 1980; Strassman et al. 1987). During the execution of a saccade, in any direction, the OPNs become quiescent for the duration of the movement, only resuming discharge at saccade offset (Keller 1974; Luschei and Fuchs 1972). Furthermore, intracellular and local field recordings have shown that the OPNs are hyperpolarized during saccades, and the temporal profile of the membrane potential is the reciprocal of the saccade velocity waveform (Van Horn et al. 2010; Yoshida et al. 1999). These findings suggest that the OPNs prevent the

premature execution of eye movements until a candidate such as the SC or BG, which have projections to the OPNs, reaches threshold to fire a high-frequency burst that inhibits OPNs and produces a saccade.

1.2 MECHANISMS FOR DECODING COLLICULAR ENSEMBLE ACTIVITY

An important problem in understanding motor control is how populations of distributed neural activity can be deciphered to control behavior. In the saccadic system the question relates to how invariant spatial distributions of collicular activity, which define the desired eye movement, can be transformed into the temporal code needed to drive motoneurons (Sparks and Hartwich-Young 1989). Two controversial models have dominated the oculomotor field in hypothesizing the proper mechanism for deciphering SC activity: vector averaging and vector summation. Early saccade models utilized static-ensemble-coding schemes, in which SC motor activity specifies only the metric coordinates of the saccade displacement. Dynamical properties such as trajectory and kinematics were assumed to be reflected by the operation of a feedback mechanism downstream of the SC, such as in the pons (Jürgens et al. 1981; Robinson 1975) or cerebellum (Lefèvre et al. 1998; Quaia et al. 1999). The vector-averaging model (Fig. 2A) hypothesized that an active population in the SC is computed by taking the weighted average of the vector contribution of each neuron (Lee et al. 1988; Walton et al. 2005). In this format, the level of activity has no direct relation to either saccade trajectory or its kinematics. Early success of the model came from its ability to account accurately for the findings generated from several experiments. Some examples include the following: (a) Simultaneous microstimulation at two points within the SC evokes a single saccade whose amplitude and direction are predicted by the weighted average of the two saccades generated when each site is stimulated independently (Katnani and Gandhi 2011; Robinson 1972). (b) Local inactivation within the SC generates saccades with dysmetria patterns that conform to an averaging hypothesis (Lee et al. 1988). (c) The timing and initial direction of curved saccades, generated by using a double-step paradigm, are accurately predicted by the computation of an averaging scheme (Port and Wurtz 2003).

Experimental findings that dispute the vector-averaging model also exist. For example, stimulation-evoked saccades can have a sigmoidal dependency with current intensity (Van Opstal et al. 1990). Stimulation frequency may also have a similar effect (Groh 2011; Katnani et al. 2012; Stanford et al. 1996). This relationship reveals a flaw in the averaging computation, because a strict interpretation of this mechanism indicates that a single spike in the colliculus can generate a maximal amplitude vector. The model, however, can be appended with the addition of a parameter to demonstrate amplitude dependency, but by doing so the computation essential becomes a summation scheme (Van Opstal and Goossens 2008). Another limitation of the averaging mechanism persists in how the computation can be implemented physiologically. Although network architectures that can accomplish normalization have been proposed (Carandini and Heeger 1994; Groh 2001), there is still no substantial anatomical evidence in the oculomotor system to support this structure.

Vector summation is recognized as a more physiological mechanism for decoding a motor command (Georgopoulos et al. 1986). For deciphering SC output for the generation of saccades, it hypothesizes that each active SC neuron contributes a vector that is weighted by the mean firing rate of the cell (Fig. 2B). The resulting sum of these weighted vectors produces the desired saccade (Van Gisbergen et al. 1987). As with the averaging scheme, this simple summation model also does not incorporate any means to explain saccade kinematics. The strength of the model is exhibited by its simplicity, intuitive nature, and ability to produce normometric saccades. Its shortcomings, however, become prevalent when tested with more complex motivations (i.e., simultaneous stimulation of two SC sites and inactivation), but they too can be accounted for by extending the model with intracollicular connectivity features such as local excitation and distal inhibition (Behan and Kime 1996; Isa and Hall 2009; Lee et al. 1997; McIlwain 1982; Meredith and Ramoa 1998; Munoz and Istvan 1998; Pettit et al. 1999; Takahashi et al. 2010). Initial implementation of lateral interaction was shown through an inhibitory tuning parameter (Van Opstal and Van Gisbergen 1989). The addition of inhibition provided a cutoff during the summation of two vectors to simulate weighted averaging saccades seen with simultaneous stimulation. Moreover, a later model that incorporated both visual and motor layers of the SC (Arai et al. 1994) demonstrated that vector summation can generate normometric, averaging, and express saccades. Yet another version (Badler and Keller 2002) additionally emphasized that lateral interactions shift the locus of ensemble activity when a

subset of model neurons is "inactivated," and the resulting endpoints of simulated saccades match both experimental data and predictions based on an averaging mechanism.

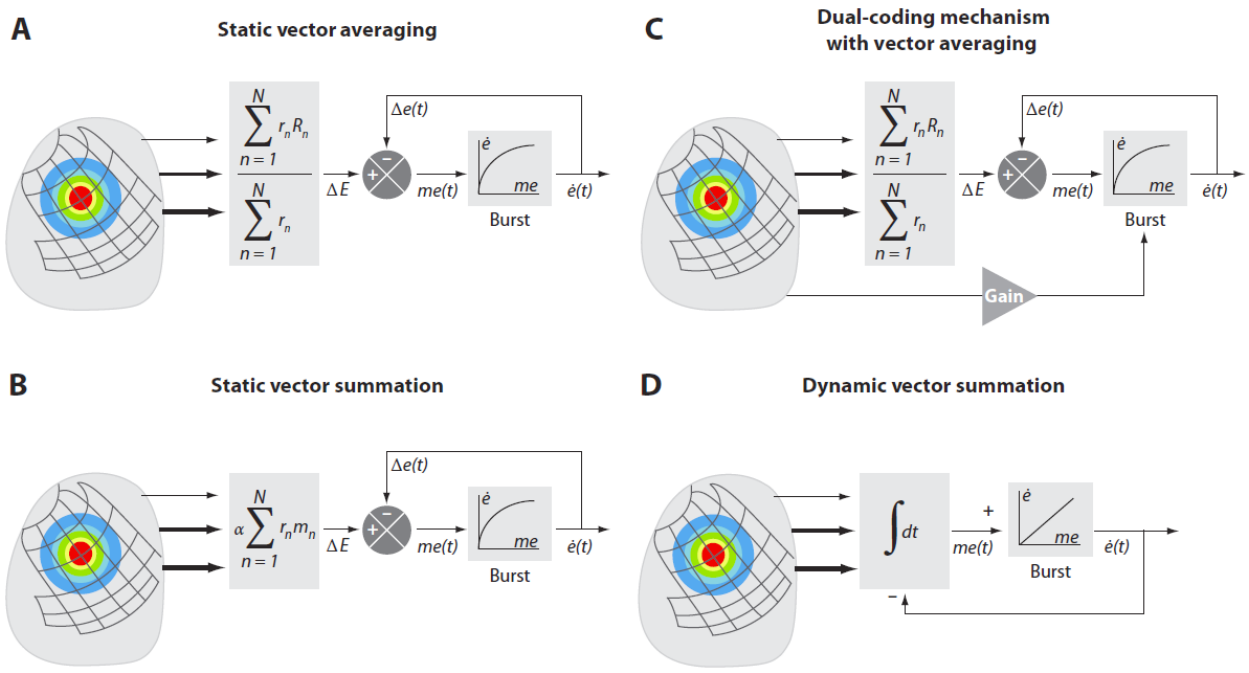

Figure 2. Framework of contemporary models for decoding SC activity for saccade generation **(A)** Static averaging decoding model that defines desired saccade metrics by using a vector averaging computation (r_n is the mean firing rate of cell *n* and $\vec{R}_n$ is the optimal vector encoded by that cell). **(B)** Static summation decoding model uses vector summation to define saccade metrics ($\vec{m}_n$ is the vector contribution of cell *n* and α is a fixed scaling constant). For both static averaging and summation models, the trajectory and kinematics are controlled downstream by *nonlinear* local feedback. **(C)** Dual-coding hypothesis model shares some of the framework of the static vector averaging model. In addition, the firing rate of the SC across time can modulate the gain of the burst generator. In this manner, SC output now contributes to both metrics and kinematics. **(D)** Dynamic summation model integrates across time the spikes from an active population. The accumulating activity specifies the intended movement trajectory. Each spike from an SC cell adds a fixed, site specific "mini" vector contribution to the movement command. In contrast to the other frameworks, the movement is controlled downstream by *linear* feedback. The projections from the SC are weighted (thickness of lines and size of arrows) according to its origin site along the rostral-caudal dimension. Model parameters: ΔE , desired eye displacement; $\Delta e(t)$, current eye displacement; $me(t)$, dynamic motor error; $\dot{e}(t)$, current eye velocity; $\int dt$, temporal integration; "*burst*", brainstem burst generator. Adapted from Goossens & Van Opstal (2006)

The discussion of both models to this point has focused on computation of only the desired saccade movement (metric). However, accumulating evidence suggests that the level of activity within the SC does influence the saccade kinematics. For example, low firing rates in the SC are associated with slow saccades (Berthoz et al. 1986; Van Opstal and Van Gisbergen 1990), and saccade velocity has been shown to scales with the intensity and frequency of

microstimulation in the SC (Stanford et al. 1996; Van Opstal et al. 1990). These findings indicate that the changes in collicular activity across time now become significant to saccade programming. A vector-averaging theory of dynamic ensemble coding has been addressed mainly conceptually (Fig. 2C). In essence, the firing rate of SC activity modulates the gain of the brainstem burst generator (Nichols and Sparks 1996; Sparks and Mays 1990). Hence, an attenuated burst, such as after partial inactivation of the SC or during memory guided saccades, evokes a slower amplitude matched saccade. With this implementation, not only the metrics, but also the kinematics of a movement could be explained by an averaging scheme. A detailed and quantified vector summation computation has also been developed under the theoretical framework of dynamic ensemble coding (Fig. 2D) (Goossens and Van Opstal 2006; Van Opstal and Goossens 2008). The model proposes that a saccade is computed by the vector summation of all individual cell contributions across time. Thus, SC neurons now relate the cumulative number of spikes in the active population to the ongoing eye displacement. With such a scheme, the SC output now specifies the desired saccade trajectory, including its kinematics. Simulations of the model revealed several saccade-related properties that other models cannot incorporate without additional assumptions. First, the decoding computation accounts for stretching of horizontal and vertical saccade components necessary for oblique saccades. Second, SC activity encodes the nonlinear main sequence, in contrast to the long-believed idea that the kinematic nonlinearity originates from a local feedback circuit in the brainstem. Thus, the SC acts as a nonlinear vectorial pulse generator where the spatial temporal activity patterns in the motor SC encode desired saccade kinematics, without having to use nonlinear mechanisms such as normalization of activity. Although the model's mechanism reveals advantageous properties, a shortcoming arises in that the computation will always yield a vector sum when tested with the contribution of two sites. To account for averaging saccades, the model must incorporate an additional saturation criterion that could potentially be introduced through modeled lateral interactions.

1.2.1 Knowledge Gap

The evolution of describing ensemble decoding in the SC has produced two conceptually distinct frameworks that continue to be contrasting equivalents in the field. Predictions of

different neural mechanisms for motor control have provoked many experiments attempting to validate hypotheses and reveal emerging properties, yet a coherent direction has still not been achieved. Furthermore, there is a general ambiguity in the field towards the order of operations involved in the saccadic system, causing qualitative and noncommittal statements on the implementation strategy for motor control. One of the biggest reasons for the obscurity of several concepts involved in saccade generation is that invariant motor commands in the SC generate straight saccades with little variability and near normal kinematics. The lack of variability between saccade-related bursts and resulting behavioral output hinders the ability to characterize relationships, and therefore masks the understanding of underlying mechanisms for saccade generation. The objectives of the studies presented in this thesis are to help elucidate potential properties and mechanisms involved in collicular motor control by utilizing novel methodologies based on microstimulation. By systematically manipulating the range of stimulation parameters, to force variability in the resulting saccade output, we establish an input-output correlation to which the characterization of that relationship contributes insightful information towards the controversial and obscure topics of saccadic motor control.

1.3 RESEARCH OBJECTIVES

Microstimulation in the deep layers of the SC produces saccade vectors that conform to the topographical organization (McHaffie and Stein 1982; Robinson 1972; Straschill and Rieger 1973). It is generally assumed that neural stimulation in the SC also activates a Gaussian distribution, as a result of the metrics and kinematics of stimulation-evoked saccades being nearly equivalent to visually-guided movements (Van Opstal et al. 1990). Although it is not well-known how stimulation can induce patterns of activity that generate saccades similar to those naturally-evoked, evidence suggests that a very small number of neural elements are directly activated by the electric field generated at the microelectrode tip (Histed et al. 2009) and that the population response is recruited through synaptic activation (McHaffie and Stein 1982). As a result, the metrics and kinematics of stimulation-evoked saccades reflect sensitivity to microstimulation parameters (Stanford et al. 1996; Van Opstal et al. 1990), presumably due to

the effectiveness of synaptic transmission generated by different levels of microstimulation strength. We utilize microstimulation in the SC to evoke saccades, and then study the dependencies of saccade characteristics on stimulation parameters to understand how distributed motor activity is processed to generate eye movement behavior.

Collectively, the experiments in this thesis provide a comprehensive overview of how distributed neural activity in the saccadic system can be deciphered to appropriately generate eye movements that allow us to assess our visual environment. In our first study, we take a systematic approach to understanding the sensitivity of the SC to two of the most relevant microstimulation parameters, current intensity and frequency. The two parameters are thought to influence activation patterns in spatial and temporal domains, respectively. Therefore, by varying both current intensity and frequency within a large range, in order to capture the effects of a substantial portion of parameter space, we obtain a correlation between microstimulation input and behavioral output. The input-output relationship allows us to ascertain the sensitivity of motor control to different spatial and temporal features of activity, and therefore, provides insight into the mechanisms underlying saccade generation. The work also provides a first level resource for choosing desired parameter ranges to effectively manipulate behavior, which is utilized to properly design experiments that can further test mechanisms for motor control. Accordingly, in study two we experimentally verify the predictions of computational models, used to describe neural mechanisms for saccade generation, by employing a dual microstimulation methodology that exploits the dependencies of saccade output on stimulation strength. Vector averaging and vector summation algorithms produces different predictions when decoding two simultaneous populations at varying levels of induced activity. As a result, we evoke behavioral results that can be matched to the predictions of each model in order to elucidate the proper mechanism needed to account for observed behavioral trends. Furthermore, in a subset to the study we expand on the interpretation of our results by performing an additional experiment, in which induced reflexive blinks are combined with stimulation-evoked movements. The blink reflex is believed to modulate inhibitory influences on the saccadic system (Goossens and Van Opstal 2000b; Schultz et al. 2010). Working under this premise, we show that the incorporation of the blink reflex provides a component that can further differentiate the predictions of each model, and therefore, offers an opportunity to further examine the decoding schemes. In the final study, we look to probe how the sequence of events involved in

generating saccades can affect motor control. In order to produce accurate eye movements, the saccadic system incorporates two required criteria. The first, which was assessed in the prior studies, is a neural mechanism that deciphers a population response of the SC. The second is an exponential transformation that converts saccade vectors, coded on a logarithmic topography, into visual coordinates. The order of these two criteria can be employed differently, in which each procedure generates different behavioral results. By establishing the proper order, we gain insight on system processing in the saccadic system, whereby the role and emerging properties of structures involved in producing saccades are better defined.

1.4 APPLICATIONS FOR MOTOR CONTROL

The intent of this thesis work was to probe aspects of neural signal processing in motor control. We gauged the topic through investigating the motor processes of the oculomotor system, specifically through neural stimulation in the SC. The laminar structure, topographical map, and direct role in motor control of the SC provide a highly constrained model system, in which processes and mechanisms of motor control can be understood with limited complexity. Although the results of each study are specific to the morphology of the SC and the processing of the oculomotor system, the underlying concepts revealed in this investigation align well with motor decoding concepts proposed in other subcortical and cortical areas (e.g., motor cortex, visual cortex, olfactory process; Carandini and Heeger 1994; Georgopoulos et al. 1986; Papadopoulou et al. 2011a). Overall, the work contributes towards the general understanding of the effective influence of microstimulation on evoked behavior and the neural mechanisms involved in motor control, both of which have significant implications towards improving quality of life. Advancements of hardware and software in modern day technology far surpass any conceivable implementation of the technology for biomedical application. To reach a level in which capability and usability can be in harmony, we must continue to pursue the understanding of the central nervous system in motor control. For example, assistive brain-machine interface devices, for individuals who have little to no motor function due to damage or disease of the central nervous system, rely on algorithms that decipher population activity in premotor and

motor cortex. In comprehending the encoding and decoding of motor activity, these algorithms can be optimized to extract information and improve device function. Furthermore, the next step in improving neuroprosthetics is integrating microstimulation to relay feedback information, an improvement that relies on understanding the effective influence of microstimulation in the brain. Another prosthetic example, to which this thesis may have the greatest implication, is visual prosthetics. Although the assistive device is progressing to the end goal of restoring vision, a limitation to the technology has stemmed through the inability to redirect vision to different areas of the visual scene. Understanding how the saccadic system accomplishes such a task may provide concepts that can translate to improve prosthetic function and generate a more natural experience. The final example I will mention comes from deep brain stimulation, in which continuous high-frequency stimulation is used in sub-cortical areas to alleviate motor disorders. Although effective, the technique can disrupt the neural function of areas not associated with motor disorder and cause adverse side effects. Furthermore, the longevity of the treatment is hindered by high power consumption. In order to remedy these barriers, the therapeutic treatment relies on understanding both the normal and disease state processing of motor control in order to optimize patterns of microstimulation to cause proper activation and restore neural function. In doing so, the treatment can maximize benefit while minimizing adverse effects and energy consumption.

2.0 THE RELATIVE IMPACT OF MICROSTIMULATION PARAMETERS ON MOVEMENT GENERATION

2.1 INTRODUCTION

Microstimulation in different brain structures has become a widely used technique to report causality between stimulation-induced modulation and resulting behavior. Microstimulation experimentation encompasses studies on motor control, cognition, neuroprostheses, and more (for reviews, see Cohen and Newsome 2004; Gandhi and Katnani 2011; Histed et al. 2012; Rebesco and Miller 2011). Such causal links have facilitated the transition of stimulation into the clinical setting as a therapeutic treatment to restore or suppress motor and/or psychiatric function in patients with different types of neuro-degenerative diseases (Holtzheimer and Mayberg 2011; Perlmutter and Mink 2006). As a result of microstimulation's ability to generate responses similar to natural physiological behavior, the methodology has become an accepted means to gauge brain function. The two stimulation parameters most often varied are current intensity and frequency. For example, skeletomotor studies have utilized ranges of current intensity and frequency to understand motor cortex signals (Graziano et al. 2002). On the other hand, deep brain stimulation varies both parameters to understand parkinsonian symptoms (Moro et al. 2002). Despite the ability of microstimulation to manipulate behavior, the efficacy of stimulation parameter settings has not been thoroughly evaluated.

We asked whether the relative impact of current intensity versus frequency on behavioral output could be assessed by testing the sensitivity of the superior colliculus (SC) with different patterns of microstimulation. The SC plays a critical role in the generation of saccades. Movements are preceded by a high frequency burst across an ensemble of neurons, where the

locus of the response dictates the desired vector and the vigor of the burst contributes to the speed of the movement (Sparks and Mays 1990). The sub-cortical brain structure serves as a promising candidate site in which to test different patterns of current intensity and frequency since stimulation of the SC evokes saccades whose metrics and kinematics are related analogously to the site and parameters (Groh 2011; Stanford et al. 1996; Van Opstal et al. 1990). Furthermore, the laminar structure, topographical map, and direct role in motor control of the SC provide a highly constrained model system, in which the impact and interactions of stimulation, to yield output, can be understood with limited complexity. With well-defined spatial and temporal population responses that reflect sensitivity to differential changes in stimulation, the impact of each parameter may be discriminated well by the oculomotor system.

We systematically varied both current intensity and frequency within a large range, from sub-threshold to supra-threshold levels, and correlated the different input combinations to resulting behavioral properties in order to obtain well-defined response surfaces. We examined saccade features under two conditions: (i) one stimulation parameter was fixed while the other varied, or (ii) both parameters varied but the total charge input was held constant. Our results demonstrated that frequency was more influential in inducing optimal behavioral properties, while current intensity was less effective and produced more gradual changes. Nevertheless, we found that by preserving total charge, different combinations of current intensity and frequency generated similar outputs, thus providing a sense of interchangeability. Overall, the evaluation on the relative impact of different regions of parameter space on evoked behavioral properties provides a useful measure for scientific and clinical work, where stimulation parameters are customized in order to achieve desired behavioral responses within specified boundaries.

2.2 METHODS

All procedures were approved by the Institutional Animal Care and Use Committee at the University of Pittsburgh and complied with the guidelines of the Public Health Service policy on Humane Care and Use of Laboratory Animals.

2.2.1 Subjects and Surgical Procedures

Two juvenile, male rhesus monkeys (*Macaca mulatta*) underwent one or more surgeries in a sterile environment and under isoflurane anesthesia. The initial procedure consisted of placing a Teflon-coated stainless steel wire (Baird Industries, Hohokus, NJ) under the conjunctiva of one eye and securing a head-restraint post to the skull. In the second procedure, one cylinder was cemented over a craniotomy. The chamber was placed stereotactically on the skull, slanted posteriorly at an angle of 38° in the sagittal plane. This approach allowed access to both colliculi and permitted electrode penetrations normal to the SC surface. After each surgery, the monkey was returned to its home cage and allowed to fully recover from surgery. Post-operatively, antibiotics and analgesics were administered as indicated in the protocol.

2.2.2 Experimental Procedures and Behavioral Tasks

Visual stimuli, behavioral control, and data acquisition were controlled by a custom-built program that uses LabVIEW architecture on a real-time operating system supported by National Instrument (Bryant and Gandhi 2005). Each animal was trained to sit in a primate chair with its head restrained and a sipper tube was placed near the mouth for reward delivery. The animal sat inside a dome surrounded by two alternating magnetic fields which induced voltages in the eye coil and thus permitted measurement of horizontal and vertical eye position (Robinson 1963). The animal fixated targets that were projected onto a circular mirror, which rear reflects onto the isoluminant wall of the dome. Anti-warping software obtained from Paul Bourke, University of Western Australia, allowed reflections from the mirror to appear undistorted and for distances to be properly transferred onto a curved surface. The monkey sat in the center of the dome which has a radius of 1m and spans ± 150° horizontally and ± 30° vertically of the visual field. A photodetector, positioned outside the animal's field of view, detected the actual time of appearance of visual objects, which was then used to correct for time shifts induced by the projector's refresh rate.

Both animals were trained to perform the oculomotor gap task. Every trial began with directing the line of sight to a fixation point for 300-500 ms before it was extinguished. The

fixation point was always at the straight-ahead location and was always kept constant across all trials for each stimulation site. Following a 200-400 ms "gap" interval, during which the animal was required to maintain the same eye position, another stimulus was illuminated in a random location in the visual periphery. Incorporation of the gap interval permitted fixation to become disengaged from a visual stimulus prior to saccade preparation, allowing the oculomotor system to be more responsive to incoming visual and/or stimulation input (Sparks and Mays 1983). Each animal was permitted 500 ms to redirect its visual axis on the saccade target and hold gaze steady for 300-500 ms to earn a liquid reward. As the animal performed this task, a platinum iridium microelectrode (1.0-1.5 MΩ; MicroProbes for Life Science, Inc., Gaithesburg, MD) was advanced with a hydraulic microdrive (Narashigie, Tokyo, Japan). The superficial layer of the SC was first identified by the presence of distinctive bursting of background activity associated with flashes of room lights. The electrode was then driven deeper into the SC until saccadic motor bursts were identified. At this stage, stimulation (40μA, 400Hz) was delivered during the gap interval, 100 ms after fixation offset, to determine the vector coordinates. The depth of the electrode was then minimally adjusted to obtain the shortest possible latency of the stimulation evoked saccade (20 - 40 ms). Train duration was manually set (range: 100-300ms) and always long enough to allow for completion of the stimulation evoked movements. Moreover, the peripheral saccade target was illuminated only after stimulation offset. Stimulation was delivered through the electrode on 20% of trials.

2.2.2.1 Microstimulation Permutation

The objective of the experiment was to assess the effects of a large range of stimulation parameters on the elicited behavioral response. Thus, both current intensity and frequency were incremented within a substantial range at each stimulation site. The minimum of the range was set to either evoke a very small movement or no movement (never lower than 10 μA and 100 Hz), and the maximum was always set in the supra-threshold range (never higher than 70 μA and 700 Hz). Differences in the chosen parameter ranges for each site could be attributed to factors such as depth of electrode and/or electrode tip distance from neurons and fibers (Ranck 1975; Tehovnik 1996). The sampling increment for each range was typically 5 μA and 50 Hz or 10 μA and 100 Hz, but was always chosen such that data sets had a total of 25, 36 or 49 possible combinations of current intensity and frequency (~5 trials of each combination was collected).

Example parameter ranges consisted of current intensity (20, 30, … 60, 70 μA) and frequency (200, 300, … 600, 700 Hz) or current intensity (10, 15, … 45, 50 μA) and frequency (100, 150, … 450, 500 Hz). Note that the parameters were intentionally set to be tenfold apart from one another. The intuition behind this design was to collect two types of conditions: one in which only one parameter varied relative to the other, and the other in which both parameter varied but the total charge input was held constant (i.e., 10 μA x 200 Hz = 20 μA x 100 Hz). Total charge, computed from different combination of the parameters, allowed for a better definition of the relative impact of current intensity versus frequency on behavioral output.

2.2.3 Electrical Stimulation

Constant current stimulation trains were generated using a Grass S88X stimulator in combination with Grass PSIU6 isolation units. Trains consist of cathodic phase leading, symmetric biphasic pulses (0.25 ms). Frequency and current intensity were dictated by each experimental design, typically spanning in the range of 10-70 μA and 100-700 Hz. In all cases, stimulation duration was always long enough to ensure that it outlasted the eye movement.

2.3 DATA ANALYSIS

Each trial was digitized and stored for off-line analysis. We used a combination of in-house software and Matlab 7.10.0 (R2011a). Horizontal and vertical eye position along with onset and offset times of the stimulation train were stored with a resolution of 1 ms. Component velocities were obtained by differentiating the eye position signal. Onset and offset of stimulation evoked saccades were then detected using a standard 30°/s velocity criteria, respectively.

2.3.1 Response Surface Methodology

Response surface methodology utilizes multivariate regression to model and analyze the relationships between a response and the variables that influence that response. Evoked movement properties (amplitude, peak velocity and latency) were defined as a function of current intensity and frequency and quantified with a regressed quadratic model:

$$Z(x,y) = ax^2 + by^2 + cxy + dx + ey + f \qquad \text{(Eq 1)}$$

where Z is either saccade amplitude or peak velocity; x is the current intensity predictor; y is the frequency predictor; a and d denote the coefficients describing the quadratic and linear effects attributed to current intensity, respectively; b and e denote the coefficients describing the quadratic and linear effects attributed to frequency, respectively; c denotes the coefficient for the interaction effect; f denotes the intercept coefficient.

We found that the response surface for saccade latency (stimulation onset to movement onset) was better approximated by an inverse multi-linear model. Therefore, we took the inverse of latency values to approximate the data with a simple multi-linear model:

$$Z(x,y) = cxy + dx + ey + f \qquad \text{(Eq 2)}$$

where Z is the inverse of saccade latency. All other terms are as described above with the quadratic terms set to zero ($a = b = 0$).

The optimal number of parameters for multivariate regression were determined by using the F-test, the coefficients were determined using a non-linear least squares optimization routine (Levenberg-Marquardt algorithm), the significance of each coefficient was determined by a t-score, and the coefficient of determination (R^2) was used to assess goodness-of-fit.

2.3.2 Canonical Analysis of Quadratic Model

Canonical analysis was a technique used to examine fitted quadratic models by assessing 2nd order equations (Eq 1) in canonical or standard form:

$$Z - Z_s = \lambda_1 E_1^2 + \lambda_2 E_2^2 \quad \text{(Eq 3)}$$

where Z_s is a stationary point that describes a region of parameter space in which little change occurs in response to changing the controllable factors; λ_1 and λ_2 are eigenvalues that describe the shape of the modeled surface; and E_1 and E_2 are eigenvectors or principal axes that convey the direction of change in yield for the modeled surface. *Eq 3* may be interpreted as follows. Instead of measuring the effects of each factor from the origin and in the direction of the original axes (*x* and *y*; Eq 1), the effects are measured from the stationary point and in the direction of the principal axes (E_1 and E_2; Eq 3). Therefore, a change in yield when moving away from the stationary point is defined by the expression on the right-hand side of *Eq 3*. The magnitude of the coefficients, λ_1 and λ_2, defines the amount of change in yield in the direction of E_1 and E_2, respectively. Moreover, the sign of the eigenvalues describes the nature of the stationary point, in which all negative defines a maximum, all positive defines a minimum, and mixed defines a saddle point. For example, if both λ_1 and λ_2 are negative, the stationary point is a maximum. This can be better interpreted by rewriting *Eq 3* as $Z = Z_s - \lambda_1 E_1^2 - \lambda_2 E_2^2$, which shows that any point chosen in the new coordinate system (E_1,E_2) will result in a loss of yield from Z_s. Therefore, the stationary point is a maximum with λ_1 and λ_2 measuring the falloff in yield in the direction of E_1 and E_2, respectively.

To derive the components of *Eq 3*, all second-order equations (Eq 1) were rewritten using matrix notation:

$$Z(x,y) = b_o + b_1 w + w' B w \quad \text{(Eq 4)}$$

where b_1 denotes a vector of the 1st order parameter estimates; *w* denotes a vector of the controllable factors; and *B* denotes a matrix of the 2nd order parameter estimates (note the off-

diagonal elements of *B* equal half the interaction coefficient). Equating the partial derivatives (d*Z*/d*x* and d*Z*/d*y*) of *Eq 4* to zero and solving the resulting system of equations, provided values for *w* used to reevaluate the equation and solve for a stationary point. The eigenvalues and corresponding eigenvectors were determined by eigen-decomposition of matrix *B.* For a full account of the usage and mathematics behind canonical analysis on surface responses see (Box 1954; Box et al. 1953).

2.3.3 Calculating Total Charge

The total charge (TC) elicited by different combinations of current intensity and frequency was calculated using the following equation:

$$TC = \mu A \cdot \tau \cdot \frac{duration}{T \cdot 1000} \qquad \text{(Eq 5)}$$

where μA is the set current intensity, τ is the set pulse width, and T is the set period of pulses (1/Hz) in the stimulation train. In biphasic pulsing the first phase, also known as the stimulation phase, has been shown to elicit the physiological effect and primarily influences activation, while the second phase, also known as the reversal phase, is used to reverse electrochemical reactions to minimize extracellular tissue damage, and is believed to have minimal effect on activation (for review, see Merrill et al. 2005). As a result, only the phase leading pulse was used for TC calculation.

The allotted duration used to calculate TC was chosen as a period of time when stimulation was significantly contributing to the saccade feature being analyzed. When analyzing radial amplitude and peak velocity, duration was chosen to be 20 milliseconds before saccade onset until saccade offset (Goossens and Van Opstal 2006; Munoz and Wurtz 1995; Ottes et al. 1986). When analyzing movement latency, duration was chosen to be the time from stimulation onset to saccade onset. We note that additional to the TC equation above, when calculating TC for latency the equation was further divided by duration in order to compute the TC relative to the rate of incoming pulses. The calculation stems from the notion that the rate of incoming charge is significant to the initiation of a movement (Carpenter et al. 2009; Hanes and Schall 1996).

2.4 RESULTS

We report on a total of 30 microstimulation sites from two monkeys (monkey 1 and 2: 13 and 17 sites, respectively), sampling a range of the SC motor map that spanned approximately 3^o to 40^o in amplitude and approximately -75^o to 50^o in direction. Twenty seven of the thirty sites were 6X6 permutation sets, two were 5X5 sets, and one was a 7X7 set.

2.4.1 Defining Response Surface Characteristics

Figure 3A illustrates a response surface that describes stimulation-evoked movement amplitude as a function of current intensity and frequency. Qualitative assessment was obtained by generating a surface that connected the mean behavioral response for each current intensity and frequency combination. The surface highlights a concave structure in which amplitude increases monotonically from a minimum to an apex. The individual slices that constitute the surface plot are shown in Figure 3, B and C, where qualitative differences can be observed when varying frequency versus current intensity. Variation in frequency seems to generate non-linear effects as opposed to the linear-like changes seen when varying current intensity. A similar relationship is observed with peak velocity (not shown). Latency, in contrast, is high and more

variable at low stimulation parameters and asymptotes to a minimum with supra-threshold stimulation (not shown). To implement conformity in the structure of multivariate regressions, we correlated the inverse of latency values to current intensity and frequency, seen in Figure 3D. In this representation, the inverse of latency also increased monotonically, however, the overall shape of the data was much more linear. This can be better appreciated in the individual slices of the surface shown in Figure 3, E and F. A qualitative assessment suggests that variation in frequency seems to cause much steeper slopes than variation in current intensity.

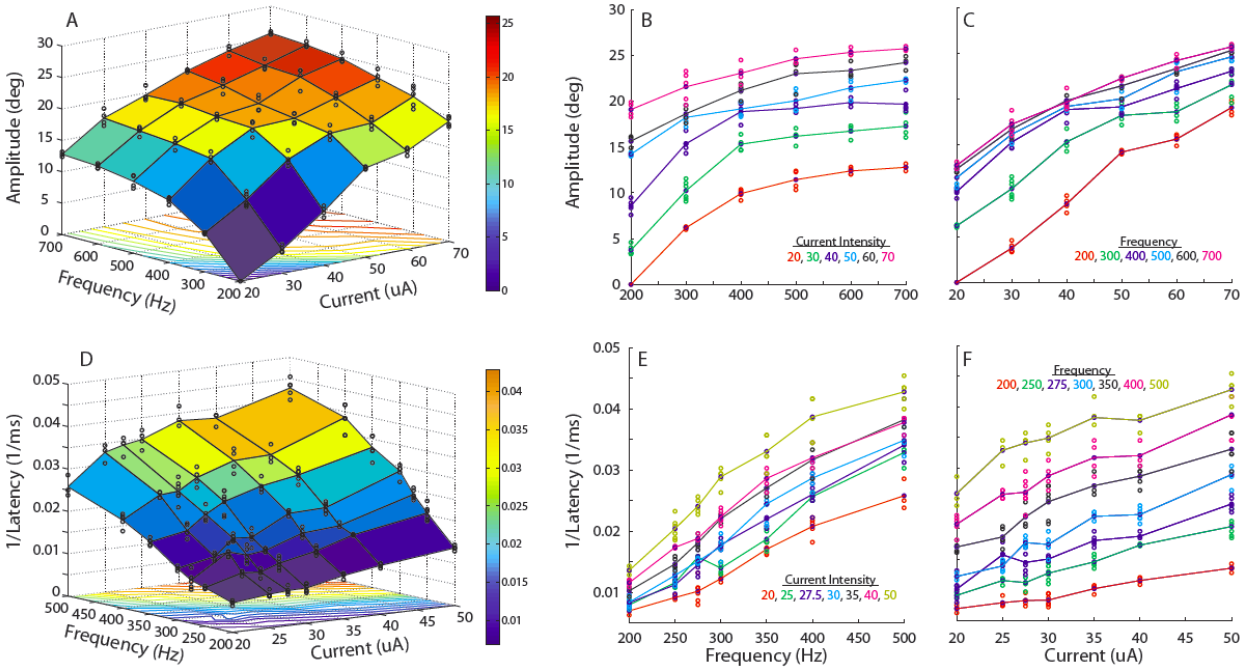

Figure 3. Example of behavioral property response surfaces
(A, D) Stimulation-evoked movement amplitude (top) and inverse of latency (bottom) as a function of current intensity (x-axis) and frequency (y-axis). Blue circles represent the distribution of evoked values collected for each combination of current intensity and frequency; mesh surface connects the mean of collected distributions; contour lines of the mesh surface are presented on the xy-axis; color bar conveys scale of saccade amplitude (top) and inverse of latency (bottom). **(B, E)** Slices taken across the surface in *A* and *D* along the y-axis; the lines connect the mean of the amplitude (top) and inverse of latency (bottom) distribution evoked at each frequency; the color of each slice indicates the level of fixed current intensity. **(C, F)** Slices taken across the surface in *A* and *D* along the x-axis; the lines connect the mean of the distribution evoked at each current intensity; the color of each slice indicates the level of fixed frequency.

Response surface methodology was used to quantify the surface features across all stimulation sites (see Methods). Each data set was first normalized in all three dimension (x, y, and z-axis were each divided by their respective maximum) in order to make comparisons across predictors and data sets, and then fit with a multivariate model. Figure 4, A and B, illustrates fits

for radial amplitude and peak velocity from the same stimulation site used in Figure 3A. As above, the concave structure and monotonic increase in output variables as a function of stimulation parameters are preserved. A quadratic model provided the proper approximation of the surface characteristics (Eq 1). The F-statistic revealed that 48 of the 60 surface fits were significantly ($p < 0.05$) improved when fitted with a quadratic rather than multi-linear model. Figure 4C illustrates a multi-linear model fit to the surface characteristics of the inverse of latency (Eq 3). The F-statistic revealed that only 1 of the 30 surface fits were significantly ($p < 0.05$) improved by using a quadratic model. Figure 4D illustrates a bar graph of the coefficients of determination (R^2) derived from all three behavioral output surface fits. Note, R^2 values are always higher then 0.75, with the majority greater than 0.85, demonstrating that the regressed models are significantly capturing the characteristics within the behavioral response data.

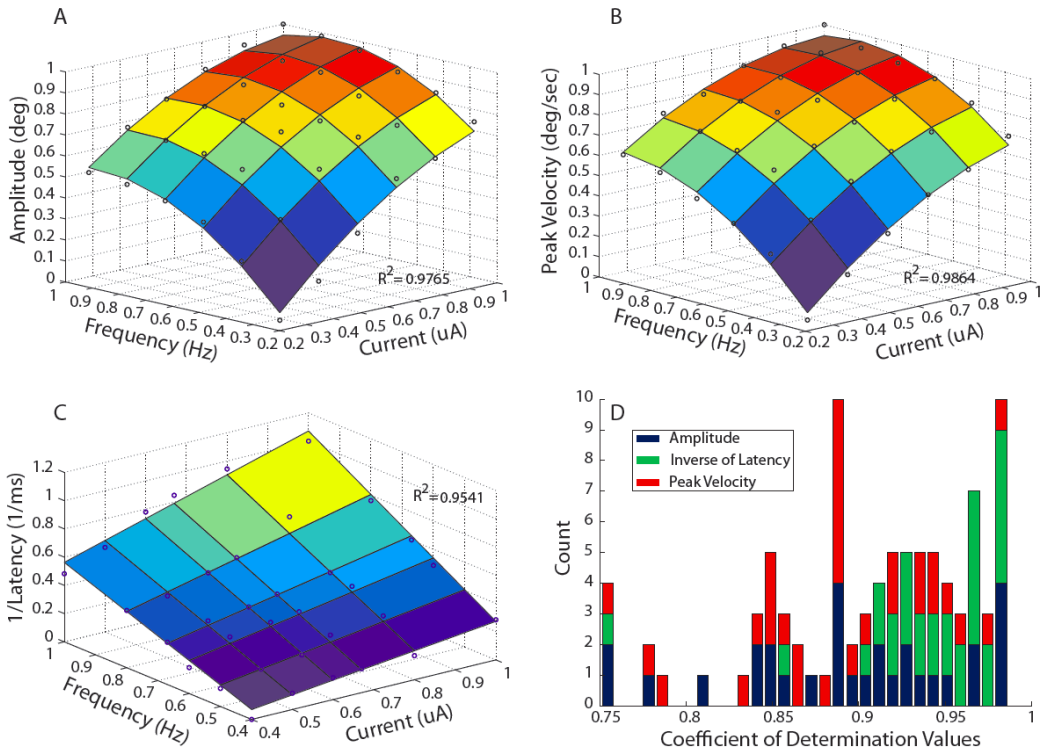

Figure 4. Example multivariate regression surfaces
(A,B) Quadratic model surface for normalized amplitude and peak velocity as a function of normalized current intensity and frequency. Blue circles represent sample mean across trials collected for each parameter combination; coefficient of determination (R^2) value reports goodness of fit for each surface. **(C)** Multi-linear model surface for normalized inverse of latency as a function of normalized current intensity and frequency. Blue circles represent sample mean across trials collected for each parameter combination; R^2 value reports goodness of fit for surface. **(D)** Bar graph of the coefficients of determination for all behavioral output surface fits from all stimulation sites (n = 30). Bar portions in blue represent values derived from amplitude fits, green derived from inverse of latency fits, and red derived from peak velocity fits.

In order to summarize the response surface shape across all stimulation sites and assess how each stimulation parameter contributed to the shape, we examined the coefficients derived from the multivariate regressions. Figure 5A illustrates the resulting distributions for each coefficient across all response surfaces. Note that all quadratic terms were found to be significant (t-score, $p < 0.05$) and negative, signifying a common concave shape for all amplitude and peak velocity surfaces. All linear terms were found to be significant (t-score, $p < 0.05$) and positive, signifying a common monotonically increasing direction across all responses surfaces. To better visualize the relative magnitude of the derived effects, we compare the coefficient associated with the current intensity and frequency terms. Figure 5, B and C, demonstrates that almost all quadratic and linear coefficients derived from radial amplitude (black) and peak velocity (light gray) lie above the line of unity. The same trend exists for linear coefficients derived from inverse of latency (Fig. 5D). Overall, the comparisons signify that the frequency predictor is the more prominent factor in contributing to the shape of a behavioral response surface.

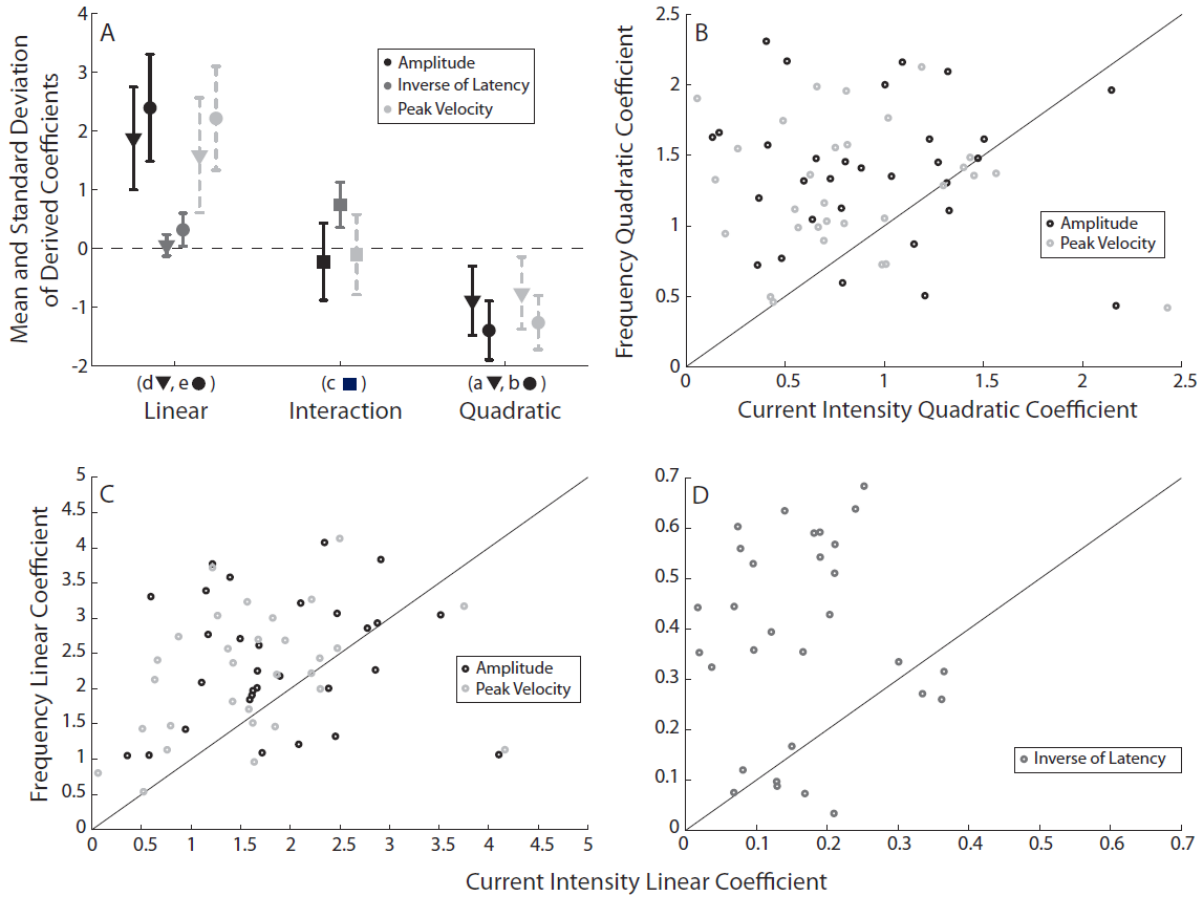

Figure 5. Comparison of optimized model coefficients
(A) Distribution (+/- one standard deviation from mean) of coefficients from all stimulation sites (n = 30). Mean of quadratic and linear effects associated with current intensity and frequency are shown as triangles and dots, respectively; mean of interaction effect shown as squares. Coefficients derived from amplitude fits shown in black, inverse of latency, gray, and peak velocity, dashed light gray. Association of the symbols to the coefficients of equation 1 and 2 (a, b, c, d, e) shown on x-axis. **(B)** Comparison of the absolute magnitude of the quadratic coefficients associated with the current intensity (x-axis) and frequency (y-axis); black circles represent values derived from amplitude fits; light gray circles represent values derived from peak velocity fits. **(C,D)** Comparison of the absolute magnitude of the linear coefficients associated with current intensity (x-axis) and frequency (y-axis); black circles represent values derived from amplitude fits; light gray circles represent values derived from peak velocity fits; gray circles represent values derived from inverse of latency fits.

The interaction term for each model was also assessed. For amplitude and peak velocity analyses, the interaction coefficient in the quadratic model was statistically significant (t-score, $p < 0.05$); however, Figure 5A illustrates that values derived for the coefficient were close to zero. Consistent with this result, there was no significant (F-test, $p < 0.05$) difference when fitting response surfaces for amplitude or peak velocity with a pure quadratic (no interaction term) versus full quadratic model. In contrast, the interaction effect derived from inverse of latency

surfaces was both significant (t-score, $p < 0.05$) and large in magnitude (Fig. 5A). In addition, all interaction coefficients were positive, implying a synergistic effect of the two predictors on latency.

2.4.2 Relative Impact of Stimulation Parameters

To evaluate how each stimulation parameter specifically affected behavioral output properties, the total charge (TC) of each parameter combination in a data set was calculated (see Methods). A noteworthy piece of information for performing such a calculation is that it allows a three-dimensional response surface to be collapsed into two-dimensions by scaling current intensity and frequency into common units (μA / msec), allowing for a better definition of the relative effects of each parameter. Total charge values were parsed into two groups: current series, calculated from combinations that have the same frequency but different current intensities, and frequency series, calculated from combinations that have the same current intensity but different frequencies. As a result, each series contained slices of the three-dimensional response surface that encompassed how variation in one parameter affected behavioral output while the other remained fixed. Slices derived from radial amplitude and peak velocity surfaces were regressed with a one phase exponential ($1-e^{-x\beta}$; β: slope coefficient) while slices from inverse of latency surfaces were fit with a linear equation ($\beta_1 x + \beta_2$; β_1 and β_2: slope and intercept coefficient). Any regression resulting in a coefficient of determination lower than 0.6 was removed from analysis (<10% of data removed).

Figure 6A illustrates a histogram of the exponential slope coefficients derived from current series (blue) and frequency series (red) taken from radial amplitude surfaces. The distribution is a result of regression across all stimulation sites. Note that the time constant for a one phase exponential function is inversely proportional to the regressed slope; therefore, the results demonstrate that variation in frequency generates significantly (Wilcoxon, $p < 0.001$) larger slopes or shorter risetimes in behavior when compared to variation in current intensity. To visualize the impact of having different time constants, Figure 6, B and C, illustrates slices from a frequency series (left) and current series (right) taken from one stimulation site. The color of a slice indicates the different level at which the non-iterating parameter was fixed while each slice

is a result of the iterating parameter. We observed that within the frequency series the iteration of frequency causes concave non-linearity by quickly driving the behavioral output to a plateau (hence the shorter risetimes). In contrast, within the current series the iteration of current intensity causes more gradual linear-like effects. The same analyses performed on peak velocity surfaces produced the same comparable result (not shown).

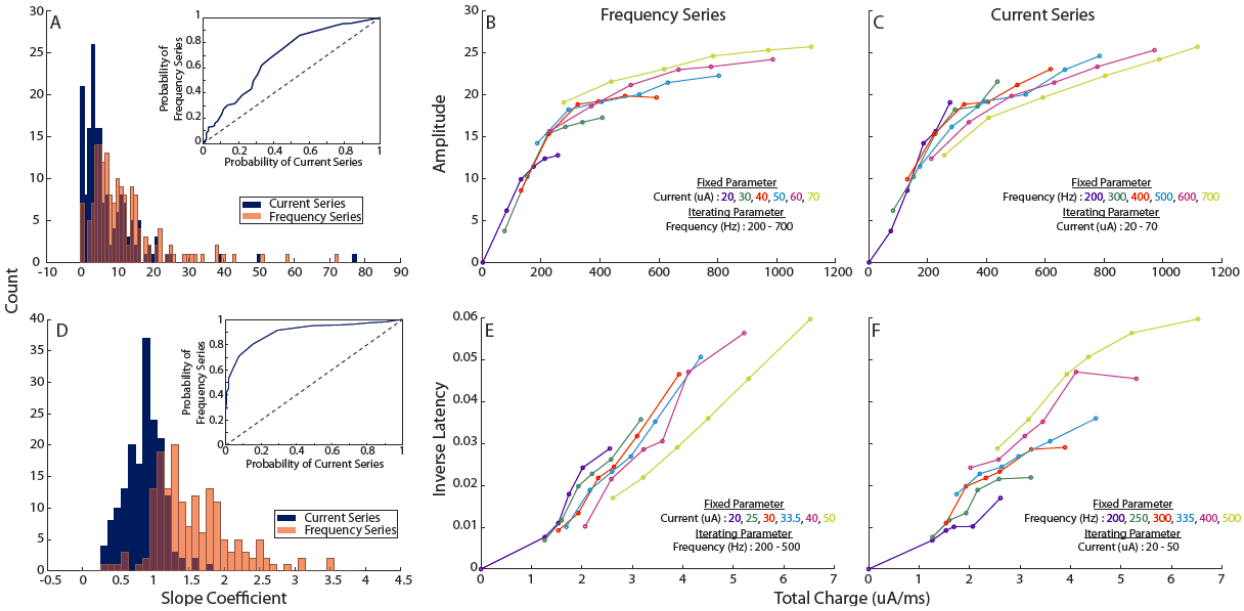

Figure 6. Total charge regression on amplitude and inverse of latency surfaces
(A, D) Histogram of the exponential slope coefficients derived from current series (blue) and frequency series (red) taken from all radial amplitude (top) and inverse of latency (bottom) surfaces. *Inset:* Receiver operator characteristic analysis comparing probability of attaining values from the current series versus the frequency series distribution when moving right to left on the x-axis of the histogram plot. **(B, E)** An example of frequency series slices calculated from one amplitude (top) and one inverse of latency (bottom) surface. Total charge values of each slice calculated from fixed current intensity levels (indicated by slice color) combine with iterating frequency values **(C, F)** Current series slices. Total charge values of each slice calculated from fixed frequency levels (indicated by slice color) combined with iterating current intensity values.

Figure 6D illustrates a histogram of the linear slope coefficient derived from current series (blue) and frequency series (red) taken from inverse of latency surfaces. The results demonstrate that variation in frequency generates significantly (Wilcoxon, $p < 0.001$) larger slopes than variation in current intensity. Figure 6, E and F, illustrates slices from a frequency series (left) and current series (right) taken from one stimulation site. The slopes of slices in the frequency series are noticeably steeper, indicating frequency as the more prominent factor in dictating the onset of movements.

2.4.3 Canonical Analysis

The characteristics captured in fitted quadratic models (amplitude and peak velocity) were further interpreted by assessing their canonical form, where the effects of varying current intensity and frequency were measured from a stationary point and in the direction of the derived principal axes of each modeled surface (see Methods). We demonstrate an example of this analysis in Figure 7A, which plots the contours of the example response surface in Figure 3A. The color bar of Figure 7A conveys normalized saccade amplitude, indicating that the maximum of the surface is in the top right corner of the figure and the minimum in the bottom left. Superimposed atop the contours are the derived principal axes. Traditionally, the axes are centered at the stationary point, but for a better visualization of the results we arbitrarily shifted them to the center of the figure. The relative magnitude of the eigenvalues is illustrated by the thick blue portions on each axis. The eigenvalues were both found to be negative (λ_1 = -1.16, λ_2 = -0.51), as were the eigenvalues obtained across all stimulation sites (λ_1 - amplitude: mean = -1.64, median = -1.65, std = 0.44; λ_2: mean = -0.68, median = -0.64, std = 0.40; λ_1 - peak velocity: mean = -1.50, median = -1.46, std = 0.48; λ_2: mean = -0.59, median = -0.61, std = 0.34). As interpreted from *Eq 3* (see Methods), negative eigenvalues define the stationary point as a maximum. Therefore, any direction taken from the stationary point will result in a loss of yield, with the falloff being greatest in the direction of the principal axis corresponding to the largest eigenvalue. Since λ_1 is greater than λ_2 in the example, we find that moving across the surface (right to left) in the direction of the first principal axis (E_1) results in a rapid loss in yield (as seen by the change of color in contour ridges); in contrast, moving across the surface in the direction of the second principal axis (E_2) results in considerably less change in yield. This result was consistent across all surfaces as the magnitude of the first eigenvalue was always found to be greater than the second ($\lambda_1 > \lambda_2$). The slope (ratio of frequency divided by current intensity components) of the principal axes E_1 and E_2 was also assessed to gauge how much each stimulation parameter contributed to the directions of the axes. For the first principal axis, E_1, in Figure 7A, the ratio (0.57 / 0.82) indicates that current intensity contributes most to the direction, signifying that changes in the level of current intensity are associated with greater changes in yield. Accordingly, frequency contributed more to the direction of the orthogonal axis, E_2 (slope = 0.82 / 0.57), signifying that changes in the level of frequency are associated with smaller

changes in yield. These results were consistent as current intensity was always found to contribute most to the direction of the first principal axis (across all site, ratio < 1; amplitude: mean = 0.47, median = 0.45, std = 0.29; peak velocity: mean = 0.61, median = 0.71, std = 0.29), and frequency to the second principal axis (across all sites, ratio > 1; amplitude: mean = 4.53, median = 2.25, std = 5.32; peak velocity: mean = 2.47, median = 1.39, std = 2.56).

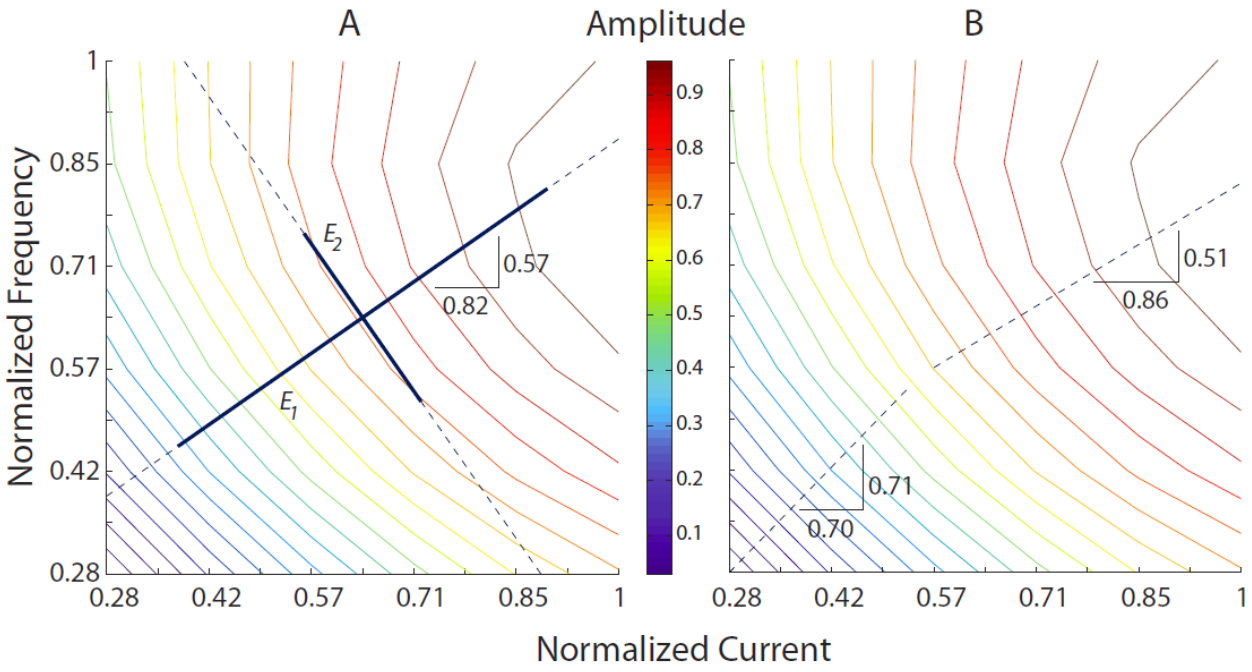

Figure 7. Example of canonical analysis
(A) Contour lines of the amplitude surface shown in figure 3. Color bar conveys normalized amplitude. E1 and E2 (dashed lines) represent the eigenvectors derived from the surface; solid blue portions convey the relative magnitude of the eigenvalues corresponding to each vector. Gradient of E1 reported on figure as: 0.57 / 0.82. **(B)** Eigenvectors corresponding to the largest eigenvalue derived from a low and high region of the amplitude surface. The gradient of each vector is reported as: low region: 0.71 / 0.70, high region: 0.51 / 0.86.

In addition, we arbitrarily divided each contour response into a low and high region and reevaluated how each parameter dictated the direction of the principal axes in each sub-region. Figure 7B illustrates the principal axes corresponding to the largest eigenvalue derived from the low and high region of the example surface. The reevaluation demonstrates that in lower parameter space the ratio of frequency divided by current intensity is far more equivalent (slope = 0.71 / 0.70), indicating similar effects on yield. It is not until higher parameter space that the ratio shifts in favor of current intensity (slope = 0.51 / 0.86), thus demonstrating the same result as the canonical analysis above. Current intensity contributing more to the change in yield at

higher levels agrees well with the longer time constants derived from regression of current series slices versus frequency series (see **Relative impact of stimulation parameter**).

2.4.4 Interchangeability of Stimulation Parameters

Having established the different effects of current intensity and frequency on behavioral output properties, we next assessed whether the stimulation parameters had compensatory effects. Observing contour responses like that in Figure 7, we find that a wide range of stimulation parameters correspond to each iso-amplitude ridge. Therefore, as a first level approximation we can appreciate that the parameters compensate for one another in the sense that departure from one ridge, by changing one stimulation parameter, can be compensated for by suitably changing the other parameter (returning to that ridge). Figure 8, A and B, illustrate a qualitative assessment of the contours from another example radial amplitude surface and an inverse of latency surface. The arrows in each figure demonstrate examples of how each factor must change in order to return to a previously departed ridge. A qualitative assessment of this manner can be made across the entire contour response, where the direction of the ridges indicates the amount of change that will be needed for one parameter to compensate for the other. Accordingly, we find that the direction of ridges for radial amplitude is sensitive to the region of parameter space (see **Canonical analysis** above); therefore, the amount of change for one parameter to compensate for the other varies. In contrast, the direction of ridges for the inverse of latency is consistently dictated by frequency; therefore, to compensate for small changes in frequency, there must always be large changes in current intensity.

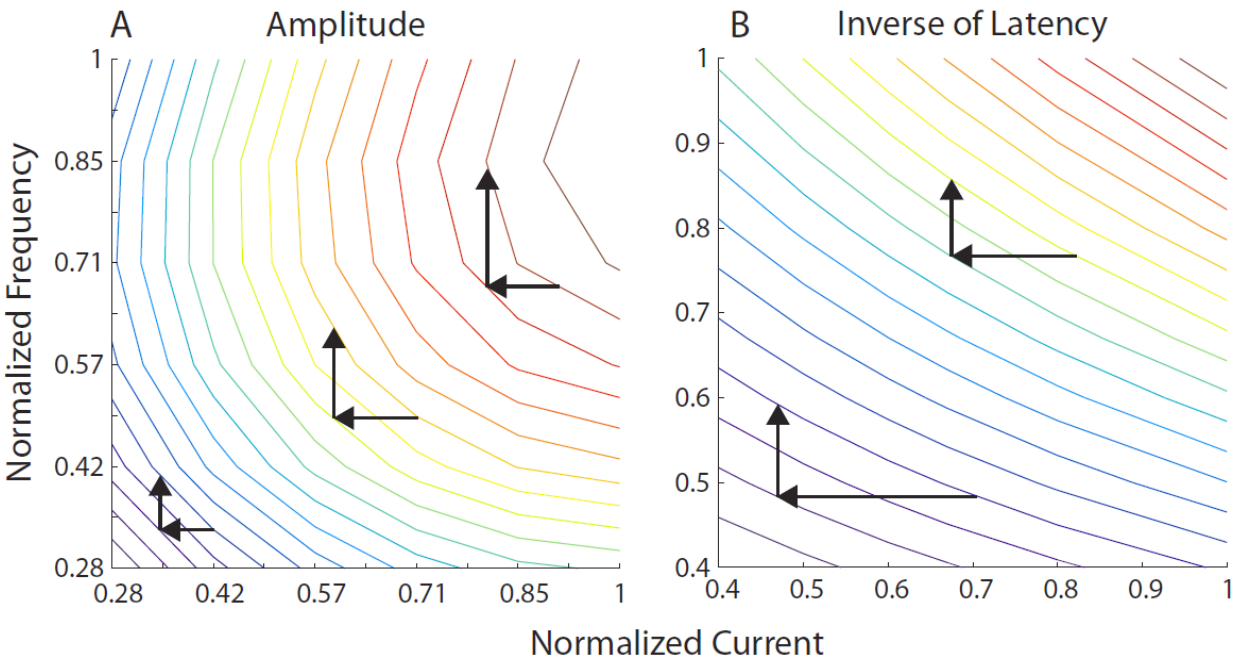

Figure 8. Assessing compensatory effects
Contour lines of an amplitude **(A)** and inverse latency **(B)** surface as a function of normalized current intensity and frequency. Arrows provide a qualitative assessment of how departure from a contour line, by reducing current intensity, can be compensated for, returning to the contour line, by increasing frequency.

Along with qualitatively assessing the contours of surfaces for compensatory sensitivity, we also wanted to quantify whether current intensity and frequency were interchangeable factors. Interchangeability was gauged by matching total charge (TC) values within each data set that were not significantly (Wilcoxon, $p > 0.05$) different, and then correlating the generated behavioral outputs from each matched pair. Figure 9, A and B, illustrates the correspondence of paired radial amplitude and paired peak velocity outputs. Within each pair, the output evoked by TC calculated from parameter combinations where frequency (divided by ten) was greater than current intensity was always plotted on the x-axis; combinations in which current intensity was greater than frequency (divided by ten) was always plotted on the y-axis. Comparing paired outputs in this manner provided a better evaluation of the relative impact of each parameter. Correlation was assessed by linear regression in which the slope and correlation coefficient for each output distribution was: slope = 1.06, R^2 = 0.965 and slope = 0.941, R^2 = 0.899, respectively. To quantify the amount of shift from perfect correspondence we calculated the residual error (Euclidean distance from orthogonal projection) of each data point from the line of

unity. The inset of each figure illustrates a histogram of the magnitude of error (radial amplitude: median = 0.001, std = 0.039; peak velocity: median = -0.006, std = 0.043). Each distribution was not significantly (Wilcoxon, $p > 0.05$) different from a distribution centered at zero. Overall, the insignificant shift from unity and high degree of correlation demonstrates that the relative impact of current intensity and frequency are comparable when TC is preserved. Despite the different relative impact observed when one parameter is fixed and the other varied, the result conveys a strong sense of interchangeability, in which the parameters can compensate for different relative effects as long as the TC remains constant. In contrast, current intensity and frequency did not show the same interchangeability for paired latency outputs. Figure 9C illustrates the correspondence of paired inverse of latency outputs. Linear regression of the distribution derived a slope of 0.804 and correlation coefficient of 0.899, while the distribution of residual error (median = -0.06, std = 0.065) was found to be significantly (Wilcoxon, $p < 0.05$) different from a distribution centered zero. The relatively shallow slope and significant shift below the line of unity demonstrates that in preserving TC the relative impact of frequency, on driving the onset of behavior, is greater than current intensity.

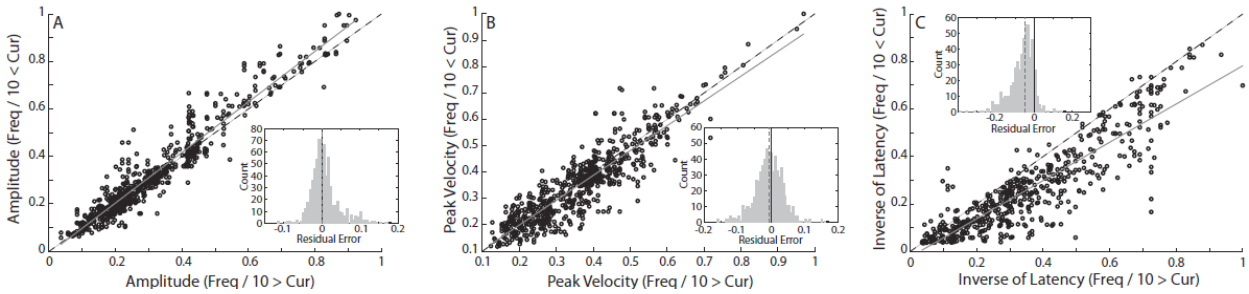

Figure 9. Gauging interchangeability

Amplitude **(A)**, peak velocity **(B)**, and inverse latency **(C)** values (black circles) paired by matching the total charge that evoked the properties within each data set (n = 30). Within each pair, the values evoked by total charge calculated from parameter combinations where frequency (divided by ten) was greater than current intensity was plotted on the x-axis; current intensity greater than frequency (divided by ten) was plotted on the y-axis. A linear regression line (gray) was fitted to each distribution; dashed black line represents line of unity. Inset: Distribution of residual error from the line of unity. Dashed gray line illustrates the median of the error distribution (light gray); black line centered at zero. Residual error was computed as the Euclidean distance between each point and its projection on the line of unity.

2.5 DISCUSSION

We examined the relative impact of current intensity and frequency on the behavioral properties of saccades evoked by microstimulation of the SC. Our results demonstrate that activity induced for motor control in the saccadic system reflects a different sensitivity to each parameter. We found that the rate of incoming pulses was the more prominent factor in generating optimal responses. Varying frequency from low to high levels caused rapid saturation in saccade amplitude and peak velocity, and steep reduction in reaction time. In contrast, saccade properties displayed more gradual, linear-like trends as current intensity increased. Interestingly, despite the different effects of each parameter, high correlations were conveyed when amplitude and peak velocity properties were paired by matching total charge values. The result demonstrates that different combinations of current intensity and frequency can generate similar output properties provided the total charge, inducing the activity, is equivalent. No such result, however, was found when pairing latency values as frequency was always the strongest factor in dictating the onset of movements.

2.5.1 Neural Mechanisms of Action

Prior to generating visually-guided saccades, low-level discharge in an ensemble of collicular neurons accumulates gradually toward an activation threshold, at which point it transitions abruptly into a high-frequency burst to initiate a saccade. The population of active neurons can be envisioned as a Gaussian mound, whereby the metrics and kinematics encoded in the activity are defined by the spatiotemporal features (Sparks et al. 1976). It is generally assumed that SC microstimulation also activates a Gaussian distribution as a result of (supra-threshold) stimulation-evoked saccades being nearly equivalent to visually-guided movements (Van Opstal et al. 1990). However, previous studies have demonstrated that sub-optimal microstimulation can attenuate both kinematics and metrics (Groh 2011; Katnani et al. 2012; Stanford et al. 1996; Van Opstal et al. 1990); moreover, our current study provides a systematic investigation of the differential effects of current intensity and frequency on movement-evoked properties. In this section, we explain our results by speculating on the spatiotemporal features of

the overall activity produced during microstimulation. With frequency and current intensity defining the rate and magnitude of incoming pulses, respectively, and being the major factors that constitute the total extracellular current flux to which neural elements respond, we will discuss the collicular networks responsive nature to each factor, reflected through the evoked behavioral trends.

Typically, a very small number of neural elements are directly activated with each pulse delivered through the microelectrode (Histed et al. 2009), and a substantially larger fraction of the population response is recruited through synaptic activation (McIlwain 1982). The frequency of microstimulation contributes to the ensemble response predominantly by driving the temporal integration of action potentials, while current intensity regulates mainly spatial summation (Ranck 1975; Tehovnik 1996; Vokoun et al. 2010). During the epoch of time when microstimulation induces activity to trigger a movement, our data demonstrates (Fig. 6) that saccade initiation is determined primarily by frequency. Consistent with the framework that activity must meet a threshold to trigger a movement (Hanes and Schall 1996) temporal summation could be the key integrative mechanism that accumulates the population activity toward that threshold. Once threshold is attained, the low-level discharge transitions to a high-frequency burst, which we suspect is driven by biophysical properties and/or intracollicular interactions (Isa and Hall 2009). Due to the non-linear scaling and quick saturation of amplitude and peak velocity with stimulation frequency, we speculate that frequency provides the temporal precision for the kinetics and interactions, excitation and inhibition of the collicular network, to operate in a manner that allows for the production of the high-frequency burst mode needed during a movement. In contrast, we expect that the collicular network is less responsive to current intensity. One interpretation is that spatial recruitment of collicular neurons scales approximately linearly with current intensity. A smaller distribution of activity could weaken the intracollicular network and therefore reduce the duration for which the high-frequency burst can be sustained. Alternatively, the weaker drive from the SC to the burst generator could prematurely resume omnipause neuron activity, which inhibits the saccadic system. Either or both of these mechanisms could account for the gradual linear-like trends generated across different levels of current intensity.

Further insight on the relative impact of current intensity and frequency is provided when assessing the compensatory effects between parameters. Our results demonstrate that different

combinations of current intensity and frequency delivered during the intrasaccadic period can produce similar amplitudes and peak velocities on average. Given that each parameter is thought to influence neural activity differently, this result might not be expected. However, the finding supports the idea that past the point of triggering a movement, spatial and temporal patterns of activity can begin to compensate for one another, where the degree of compensation to produce similar patterns of depolarization is dependent on how responsive the neural system is to each parameter.

Additional microstimulation parameters can be manipulated to influence neural activation and perhaps behavior. Aside from current intensity and frequency, the pulse width, shape of pulse train, and interphase delay of biphasic pulsing, can be systematically varied. These factors were not incorporated in our investigation, as every additional component causes a significant increase in the number of permutations. Large permutation sets are difficult to obtain due to electrode longevity, animal fatigue, and the desire to preserve tissue health. Nevertheless, we speculate from the relationships quantified in this investigation that, similar to our interpretation of varying current intensity and frequency, the responsive nature of the kinetics and interaction connections in the neural network can explain the differential effects of microstimulation parameters on behavior. Increasing or decreasing the width of a pulse or interphase interval, which can effectively trigger a movement, is essentially equivalent to respectively decreasing or increasing the frequency of pulses. Therefore, we expect the manipulation of these parameters to influence temporal activity patterns in a manner that will generate behavioral trends similar to what was observed when varying frequency (Fig. 5 and Fig. 6). However, the impact of scaling these trends (equivalent to shifting the red distribution in Fig. 5A and Fig. 6A) may differ depending on the ability of each parameter to engage the neural network with a more natural/physiological temporal activation pattern (Kimmel and Moore 2007). Modeling efforts have demonstrated that the spatial selectivity (proximity from electrode tip) of neurons (Grill and Mortimer 1995) along with selectivity of cell bodies versus axons (McIntyre and Grill 2000) can be affected by pulse width. Thus, manipulating the parameter can impact the activation pattern of distributed neural activity in different ways. However, the models generally use a lattice arrangement with an organized layout of fibers and cell bodies, making it difficult to interpret how different activation patterns would truly influence behavior. A systematic study of pulse width or interphase delay on evoked behavior would be an interesting area for future research.

Finally, we show that saccade kinematics evoked from the SC is nonlinearly correlated with stimulation frequency. In contrast, stimulation in the pontine and reticular formations produces movements that continue for the duration of the stimulation (until biomechanical limits). In addition, the kinematics of these movements has been shown to linearly scale with frequency (Cohen and Komatsuzaki 1972; Gandhi et al. 2008; Quessy and Freedman 2004). This discrepancy in stimulation effects suggest a general neural network property, in which direct or indirect recruitment of neurons within a topographically organized structure activates a network level response that can dominate the stimulation-induced activation, while the network level response is weaker or nonexistent in regions that operate primarily with a rate code. Importantly, a suggestion of this nature is not unique to the SC, as recurrent microcircuit architectures have been found in other areas of the brain (Keller 1993). Furthermore, recent work has demonstrated network level responses in cortex (Logothetis et al. 2010). Therefore, the effective influence of microstimulation in the SC may generalize to other cortical and sub-cortical regions.

2.5.2 Significance in the Scientific Setting

Microstimulation is a pillar in neuroscience. The technique has been quintessential in testing hypotheses, revealing emerging properties, and defining brain function. A primary motivation behind this study was to provide a robust evaluation of the different factors in stimulation in order to help solidify the methodology and extend the experimental capability. Understanding the relative impact of varying current intensity versus frequency can help to appropriately select the parameter space necessary to achieve desired behavior. Data of this nature can be beneficial when designing an experiment to test specific properties of a neural system or to test the predictions of a neural model. For example, within the oculomotor field, the input to output relationship characterized in this investigation provides a resource to challenge existing concepts and models that describe spatiotemporal motor decoding in the superior colliculus (Groh 2001; Katnani et al. 2012). In addition, a well-developed neural field model of the collicular network trained on these microstimulation results could reveal emerging properties in the SC and provide insightful information on the mechanisms underlying saccade generation.

Nevertheless, the characterized relationship goes beyond the oculomotor system and provides insight on the general understanding of properties in neural coding. Although effects of stimulation can be specific to the morphology of a neural network (i.e., type of neurons, density of ion channels, etc.), the underlying concepts revealed in this investigation align well with converging evidence in other subcortical and cortical areas that demonstrate an overall higher sensitivity to the temporal component of microstimulation (Butovas and Schwarz 2003; Kimmel and Moore 2007). Furthermore, as a result of tissue impedance and fiber structure being variable across brain region, we propose a unifying dimension of total charge, in which the impact of current intensity and frequency, as a first level approximation, can generalize to other areas of the brain.

2.5.3 Significance in the Clinical Setting

Therapeutic stimulation in the central nervous system looks to customize parameters in order to optimize benefit while minimizing side effects and power consumption. Our results provide a useful measure to achieving these goals by demonstrating the effectiveness of current intensity and frequency within different regions of parameter space. For example, trends like those shown in Figure 7 and 8 provide a first level assessment of the trade-off between desired yield and power consumption. The data demonstrates that when varying current intensity or frequency behavioral effects occur within two regimes: low parameter space, in which the effectiveness of current and frequency are comparable, and high parameter space, in which variation in frequency, in contrast to current intensity, generates steady optimal yield (this may be better visualized by observing the saturation effects at high levels of frequency illustrated in the slices of Fig. 3B and 6B). As a result, we can conclude that frequency has the potential to generate more stable response output. In correspondence to optimize therapeutic stimulation, it may seem suitable then to fix frequency at high levels in order to stabilize desired clinical effects, and then vary current intensity to minimize observed side effects or meet specified design constraints.

The work from this investigation also draws many parallels to mechanisms of action involved in deep brain stimulation (DBS). Note that a majority of DBS experimentation utilizes

constant voltage stimulation, where varying voltage is analogous to varying current intensity. Previous work in the DBS field has demonstrated that lowering voltage, as opposed to frequency, causes a steep fall off in alleviating symptoms of neurological disorders (Moro et al. 2002). In parallel we have shown that lowering current intensity causes a rapid drop off in output properties (see **Canonical analysis**); therefore, similar to current intensity, the relative impact of voltage may be explained by the less responsive nature of neural networks to the parameter. Nevertheless, the impact of voltage on symptom alleviation is confounding. Modeling work has demonstrated that even at low levels of voltage, neural elements are still stimulus driven by the set frequency (Hashimoto et al. 2003; McIntyre et al. 2004). Being that parkinsonian symptoms are believed to occur due to corrupted temporal firing patterns within relay loops (Guo et al. 2008), one would not expect the impact of voltage to be very critical. Nevertheless, as discussed above (see **Neural mechanisms of action**) induced temporal activity may be constrained by spatial recruitment, in which frequency may be critical in defining the proper neural command to drive a system but current intensity impacts the strength of that command. Therefore, in context to DBS, frequency may be able to effectively drive relay loops in a stable fashion, but the fidelity of that signal is ineffective until the strength is appropriately set, thus alleviating symptoms.

3.0 A TEST OF SPATIAL TEMPORAL DECODING MECHANISMS IN THE SUPERIOR COLLICULUS

3.1 INTRODUCTION

With external environments rich in stimuli that continuously bombard our sensory systems, neural structures have the ability to store distributions of information that can be decoded by lower-level structures in order to execute motor behavior. The saccadic system is well studied in this respect; specifically, research efforts have focused on motor control of saccadic eye movements to study ensemble activity in the superior colliculus (SC) (for a review, see Gandhi and Katnani 2011). In the visual domain, every potential target recruits a population of activity in the SC and the distribution of information is somehow decoded to direct the line of sight to a desired object. As a result, studies have focused on target selection revealing that reorientation towards a specific target can be probabilistic, depending on factors like saliency (McPeek and Keller 2002) and relative priority (Kim and Basso 2010; Mysore and Knudsen 2011). Once a population has been selected, however, the next crucial step is to transform the ensemble of collicular activity into a proper motor command for saccade generation. Insights into such decoding computations have been facilitated, in part, by the laminar layout of the SC and the topographical organization of saccade vectors. Recordings have indicated that the neural population of saccade-related cells in the motor map is well described by a Gaussian mound, in which neurons at the center fire maximally for the executed saccade vector, while cells away from the center exhibit lower firing rates (Ottes et al. 1986; Sparks et al. 1976). This investigation focuses specifically on how population firing patterns in the SC can be decoded to specify a saccadic command.

Different computational schemes have been proposed as potential mechanisms for decoding SC activity into a saccade vector: vector summation (VS) (Badler and Keller 2002; Brecht et al. 2004; Van Gisbergen et al. 1987), vector averaging (VA) (Brecht et al. 2004; Lee et al. 1988; Walton et al. 2005), and vector summation with saturation (VSS) (Goossens and Van Opstal 2006; Groh 2001). In all three models, the central premise is that each recruited cell, *n*, in the population contributes to the saccade by combining two factors: its activity, a_n, (which could be the cell's mean or peak firing rate, or the number of spikes in the burst), and its fixed efferent connection strengths to the horizontal and vertical brainstem burst generators, $\vec{m}_n$, which are solely determined by the cell's location in the motor map. The SC population then determines the saccade vector $\vec{S}$ by summing all weighted cell contributions:

$$\vec{S} = \gamma \cdot f\left[\sum_{n=1}^{N} a_n \cdot \vec{m}_n\right] \qquad (1)$$

with N the number of active cells, γ a scaling factor, and *f[x]* the effective input-output characteristic of the brainstem. The three models differ in the way in which the scaling and the input-output function are implemented. In the VS and VA models the latter is simply the identity (*f[x] = x*), whereas in the VSS model it is a sigmoid. In the VS and VSS models the scaling parameter is a constant, while in the VA model it normalizes the total population activity (Lee et al. 1988): $\gamma = 1/\sum_{n=1}^{N} a_n$

Vector averaging has garnered success by accounting for the findings from simultaneous supra-threshold microstimulation of two sites in the SC (Katnani and Gandhi 2011; Robinson 1972), and from local inactivation of the SC motor map (Lee et al. 1988). However, the VA scheme does not account for the observed relationship between the level of SC activity and saccade velocity (Berthoz et al. 1986; Goossens and Van Opstal 2000b), nor for the decrease in saccade amplitude with decreasing microstimulation strength (Groh 2011; Katnani and Gandhi 2010; Van Opstal et al. 1990). Moreover, it is not obvious how to implement the normalization factor physiologically (Groh 2001). In contrast, the VS model does not need an intricate nonlinear scaling mechanism to explain saccade decoding, and readily accounts for the decrease of saccade amplitude with micro-stimulation strength. However, it cannot yield weighted vector averaging, which has been shown by dual microstimulation experiments; nor does it generate fixed-vector saccades for suprathreshold microstimulation. By including output saturation,

however, the VS model becomes the VSS scheme, which accounts for suprathreshold single- and dual-stimulation results, as well as for the results of local inactivation (Goossens and Van Opstal 2006; Groh 2001). So far, the VSS model has largely been tested for a single SC population. Since the environment typically provides multiple objects of interest, it is of importance to test the SC decoding mechanism with more challenging situations. The purpose of this investigation is to study the effects on saccades by inducing and manipulating two active populations in the SC with different stimulation strengths (Groh, 2001).

Figure 10 illustrates the hypothetical results of a VSS model tested with dual microstimulation. Figure 10A provides a temporal layout of a summation with saturation output for single (red and green) and dual (blue) microstimulation at different levels of activity. The figure illustrates that when VSS is operating at high levels of activity, summation is constrained by saturation and as result dual microstimulation resembles a weighted vector average. Figure 10B illustrates the spatial representation of a prediction that corresponds with outputs from dashed gray box B. Nevertheless, when VSS is operating at low levels of activity, summation is not constrained by saturation, and as a result dual microstimulation resembles vector summation. Figure 10C illustrates the spatial representation of a prediction that corresponds with outputs from dashed gray box C. Thus, the model predicts a transition from resembling vector summation at low levels activity to resembling vector averaging at high levels of activity.

In contrast to the VSS predictions, we found that at both high and low stimulation strengths the movement elicited by dual-site microstimulation always resembled a weighted vector average of the movements evoked by the same level of activity at each site individually. This trend persisted even when low-level stimulation at one site co-occurred with activity for a visual-evoked saccade at another site. Thus, the output from two synchronous populations in the SC does not result from the independent summed contributions of the individual sites. Collectively, our results indicate that the VSS model, although appealing in its simplicity, does not explain the decoding of multiple active populations. We propose that extending the model with intracollicular interactions could account for the data observed in this study.

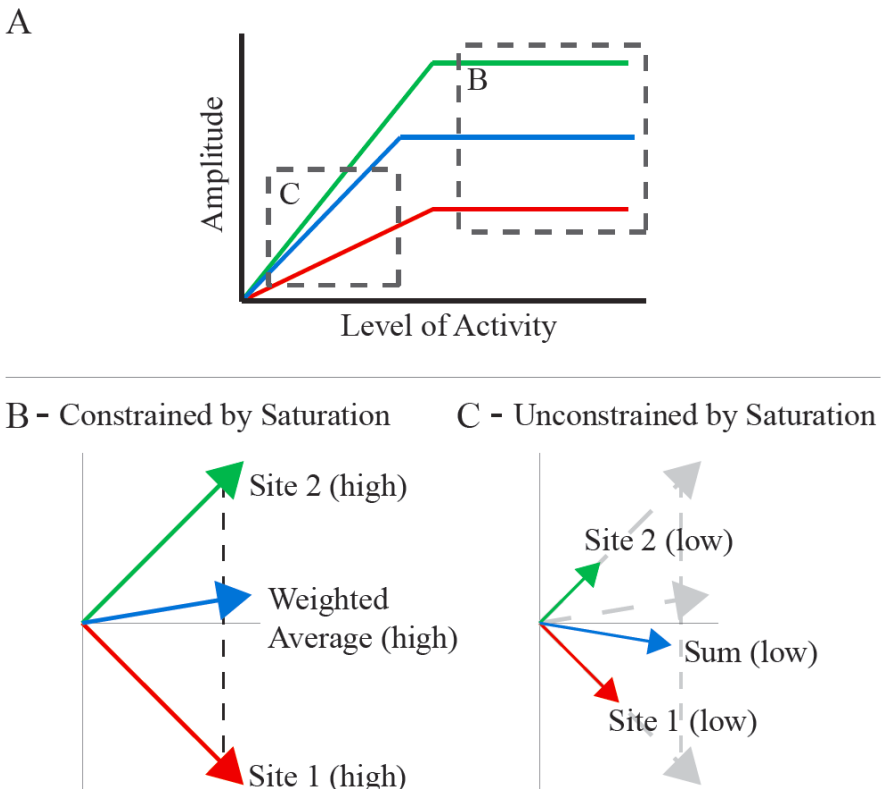

Figure 10. Vector summation with saturation predictions for stimulation-evoked vectors **(A)** provides a temporal layout of the VSS predictions (adapted from Groh 2001). The red and green lines illustrate the result of stimulation at each individual site; the cyan line illustrates the output with dual microstimulation; the dashed gray boxes illustrates the level of activity at which the model is operating to generate the predictions in *B and C*. **(B,C)** Spatial representation of a prediction that corresponds with outputs from dashed gray boxes in *A*. Site 1 and site 2 (high/low) represent individual site-specific vectors evoked by high/low stimulation parameters and are shown as red and green lines, respectively. Simultaneous stimulation of the two sites produces the cyan vector [Weighted Average (high)/Sum (low)]. Dashed black line in *B*, represents all possible weighted average locations between the two site-specific vectors.

3.2 METHODS

All procedures were approved by the Institutional Animal Care and Use Committee at the University of Pittsburgh and complied with the guidelines of the Public Health Service policy on Humane Care and Use of Laboratory Animals.

3.2.1 Subjects and Surgical Procedures

Two juvenile, male rhesus monkeys (*Macaca mulatta*) underwent one or more surgeries in a sterile environment and under isoflurane anesthesia. The initial procedure consisted of placing a Teflon-coated stainless steel wire (Baird Industries, Hohokus, NJ) under the conjunctiva of one eye and securing a head-restraint post to the skull. In the second procedure, one cylinder was cemented over a craniotomy. The chamber was placed stereotactically on the skull, slanted posteriorly at an angle of 38° in the sagittal plane. This approach allowed access to both colliculi and permitted electrode penetrations normal to the SC surface. After each surgery, the monkey was returned to its home cage and allowed to fully recover from surgery. Post-operatively, antibiotics and analgesics were administered as indicated in the protocol.

3.2.2 Experimental Procedures and Behavioral Tasks

Visual stimuli, behavioral control, and data acquisition were controlled by a custom-built program that uses LabVIEW architecture on a real-time operating system supported by National Instrument (Bryant and Gandhi 2005). Each animal was trained to sit in a primate chair with its head restrained and a sipper tube was placed near the mouth for reward delivery. The animal sat inside a dome surrounded by two alternating magnetic fields which induced voltages in the eye coil and thus permitted measurement of horizontal and vertical eye position (Robinson 1963). The animal fixated targets that were projected onto a circular mirror, which rear reflects onto the isoluminant wall of the dome. Anti-warping software obtained from Paul Bourke, University of Western Australia, allowed reflections from the mirror to appear undistorted and for distances to be properly transferred onto a curved surface. The monkey sat in the center of the dome which has a radius of 1m and spans ± 150° horizontally and ± 30° vertically of the visual field. A photodetector, positioned outside the animal's field of view, detected the actual time of appearance of visual objects, which was then used to correct for time shifts induced by the projector's refresh rate.

Both animals were trained to perform the oculomotor gap task. Every trial began with directing the line of sight to a fixation point for 300-500 ms before it was extinguished.

Following a 200-400 ms "gap" interval, during which the animal was required to maintain the same eye position, another stimulus was illuminated in a random location in the visual periphery. Incorporation of the gap interval permitted fixation to become disengaged prior to saccade preparation, allowing the oculomotor system to be more responsive to incoming visual and/or stimulation input (Sparks and Mays 1983). Each animal was permitted 500 ms to redirect its visual axis on the saccade target and hold gaze steady for 300-500 ms to earn a liquid reward. As the animal performed this task, two platinum iridium microelectrodes (1.0-1.5 MΩ; MicroProbes for Life Science, Inc., Gaithesburg, MD) were individually advanced with independent hydraulic microdrives (Narashigie, Tokyo, Japan). The superficial layer of the SC was first identified by the presence of distinctive bursting of background activity associated with flashes of room lights. The electrode was then driven deeper into the SC until saccadic motor bursts were identified. At this stage, stimulation (40μA, 400Hz) was delivered during the gap interval to determine the vector coordinates. The depth of the electrode was then minimally adjusted to obtain the shortest possible latency of the stimulation evoked saccade (20 - 40 ms). Train duration was manually set (range: 100-300ms) and always long enough to allow for completion of the stimulation evoked movements.

3.2.2.1 Experiment 1: Dual Microstimulation

The objective of the first experiment was to assess the decoding mechanism based on saccades evoked by simultaneous stimulation of two SC sites. As illustrated in Figure 11A, microstimulation was delivered 100 ms after fixation offset. Following stimulation offset, a visual stimulus was presented in a random location in the periphery, to which the animal directed its visual axis to obtain a reward. Stimulation was delivered through either one electrode (10% of the trials per electrode) or through both electrodes (another 10% of trials). Initially, the stimulation parameters were supra-threshold (always set to 40μA, 400Hz, 100-300 ms, biphasic pulses). The current intensity and/or frequency through both electrodes were then reduced to a level which yielded non-optimal saccades from each stimulation site. Table 1 lists the sub-optimal parameters used for each paired site. Such saccades typically exhibit lower peak velocities and reduced amplitudes (Van Opstal et al. 1990), even with prolonged stimulation durations (Groh 2011; Guillaume and Pélisson 2001; Katnani and Gandhi 2010). The remaining

70% of control (non-stimulation) trials was pooled together to establish a data base of visually guided saccades that were used for comparison with stimulation-evoked saccades.

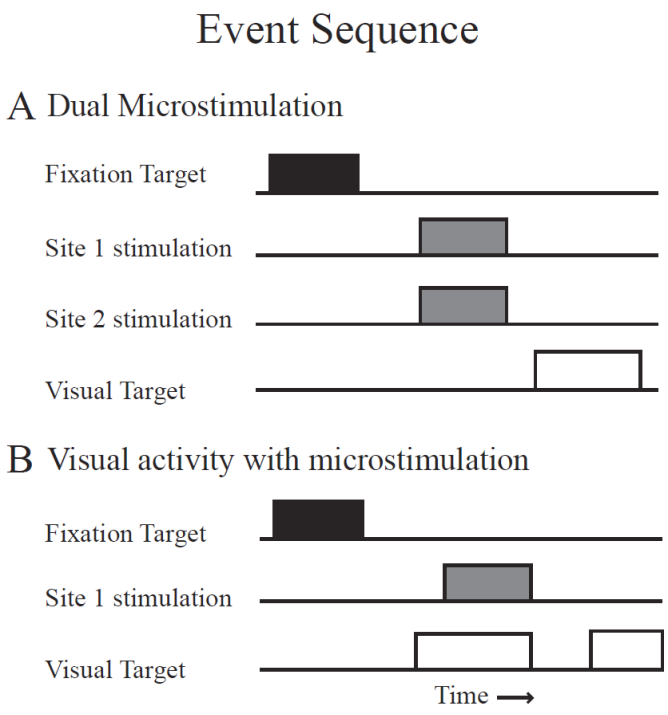

Figure 11. Sequence of events for two experimental paradigms
Timeline of events for **(A)** dual microstimulation, **(B)** visual activity with microstimulation. The onset, duration, and offset of each component in both paradigms is represented by blocked regions of different shades (fixation target, black; site stimulation, gray; peripheral target, white).

3.2.2.2 Experiment 2: Visually Induced Activity with Microstimulation

Next, we examined the effect of microstimulation on visually-guided saccades. On 20% of gap saccade trials, microstimulation was delivered to one SC site during the presentation of a visual target (Fig. 11B), not during the gap period as above. More specifically, the onset of the stimulation-evoked movement was timed to coincide with the typical saccade reaction time to the visual target. Following a 200 ms blank period after stimulation offset, another visual target was presented in a random location in the visual periphery, which the monkey had to fixate to obtain a liquid reward. On another 10% of trials, however, stimulation was delivered to the electrode during the gap period (see Fig. 11A) to collect the saccade vector associated with the site and stimulation parameters.

The location of the visual target presented in relation to the evoked stimulation vector was loosely chosen to achieve similar distributions of distances in SC coordinates as was collected in Experiment 1. Stimulation-evoked saccades that interacted with the visual target showed no obvious signs of curvature (saccades directed first toward one target and then towards the other in midflight; Arai et al. 2004; Port and Wurtz 2003) and reflected a weighted combination of the visual and stimulation-evoked saccades; only this subset of movements was analyzed for the purpose of this study. Saccades observed on other trials clearly resembled pure stimulation movements (stimulation onset occurred well before the visually guided saccade), curved saccades (stimulation onset occurred during the visually guided saccade), or pure visual movements (stimulation onset occurred after the visually guided saccade) (McPeek et al. 2003; Noto and Gnadt 2009), and were excluded from additional analyses. We note that movement of this nature were rarely observed during each session (<1% of data removed) as the stimulation onset spanned a narrow temporal range. As before, the experiment was first performed with supra-threshold stimulation parameters and then again repeated with stimulation settings that evoked reduced amplitude saccades.

3.2.3 Electrical Stimulation

Constant current stimulation trains were generated using a Grass S88X stimulator in combination with Grass PSIU6 isolation units. Trains consisted of anodal phase leading, biphasic pulses (0.25 ms). For high or supra-threshold stimulation conditions, current intensity and frequency were fixed at 40 μA and 400 Hz. The lower parameter space could be as low as 10 μA and 100 Hz, and differed for each data set in order to evoke reduced amplitude saccades (see Table 1). Low stimulation settings were determined by selecting current intensities, frequencies, or both that reliably produced movements (>90% probability of evoking movement) but also significantly reduced the amplitude of the movements (~15% or more change in amplitude). Only one set of high and low stimulation-evoked saccades was collected for each data set, as the dual-stimulation protocol was only a small part of a larger stimulation study to systematically analyze the relationship between stimulation parameters and saccade features (Katnani and

Gandhi 2010; Katnani and Gandhi 2011). In all cases, stimulation duration was always long enough to ensure that it outlasted the eye movement.

Table 1. Suboptimal parameters used for each paired site

Vector Pair	Site-specific amplitude (Site 1/Site 2/Dual site)	Lower stimulation setting (Site 1/Site 2)	Reduced amplitude (Site 1/Site 2/Dual Site)
1	13.3 / 14.4 / 11.3	40uA, 200Hz / 40uA, 200Hz	10.1 / 10.4 / 7.5
2	13.2 / 7 / 6.9	40uA, 300Hz / 40uA, 200Hz	9 / 4.1 / 4
3	8.5 / 19.5 / 8.4	40uA, 125Hz / 40uA, 125Hz	5.2 / 8.2 / 5
4	3.9 / 12.5 / 5.8	10uA, 400Hz / 10uA, 400Hz	2.4 / 6.6 / 3
5	20 / 3.5 / 6.3	20uA, 400Hz / 20uA, 400Hz	13.5 / 2.5 / 3
6	7.7 / 8.2 / 7.7	15uA, 400Hz / 15uA, 400Hz	6.4 / 5.4 / 5.7
7	22.3 / 10.7 / 13.5	10uA, 400Hz / 10uA, 400Hz	12.9 / 2.5 / 3.6
8	31.9 / 25.2 / 29.3	10uA, 400Hz / 30uA, 400Hz	11.8 / 14.6 / 13.7
9	16.5 / 26.4 / 20.6	15uA, 400Hz / 17uA, 400Hz	11.2 / 9.6 / 9.2
10	27.5 / 14.1 / 12.1	30uA, 400Hz / 25uA, 400Hz	12.6 / 6.3 / 6.9
11	13.1 / 21.3 / 16.3	12uA, 400Hz / 13uA, 400Hz	5.2 / 6 / 11.1
12	17.7 / 19 / 17.4	12uA, 400Hz / 18uA, 400Hz	12.2 / 6.1 / 8.1
13	40.2 / 33.4 / 38.5	20uA, 400Hz / 15uA, 400Hz	25.4 / 27 / 27.4
14	12.6 / 26 / 11.4	32uA, 400Hz / 28uA, 400Hz	9.2 / 10.7 / 7.9
15	17.6 / 14.4 / 11.6	25uA, 400Hz / 20uA, 400Hz	15.5 / 8.9 / 7.5
16	40 / 14.4 / 21.4	10uA, 400Hz / 12uA, 400Hz	27.9 / 10 / 12.9
17	7.9 / 7.1 / 7.7	11uA, 400Hz / 15uA, 400Hz	5.3 / 4.3 / 4.7
18	17.2 / 10.8 / 11.3	20uA, 375Hz / 20uA, 200Hz	10.2 / 8.3 / 7.9
19	27 / 5.9 / 9.1	20uA, 220Hz / 20uA, 200Hz	18 / 4.4 / 9
20	4.3 / 12.1 / 7.9	20uA, 200Hz / 20uA, 200Hz	2.8 / 10.6 / 5
21	13.1 / 43 / 21.4	39uA, 235Hz / 17uA, 180Hz	9.6 / 36.1 / 11.4
22	16.8 / 18.1 / 15.9	20uA, 400Hz / 20uA, 400Hz	13.6 / 15.4 / 12.7
23	9.1 / 9.4 / 10.4	20uA, 150Hz / 25uA, 175Hz	6.5 / 6.6 / 6.4
24	15.9 / 8.6 / 9.7	35uA, 250Hz / 25uA, 150Hz	7.9 / 5.9 / 6.4
25	18.1 / 13 / 15.6	20uA, 150Hz / 18uA, 150Hz	10.1 / 8.5 / 9.5
26	7.9 / 23.4 / 16.1	25uA, 130Hz / 20uA, 100Hz	5.4 / 19.7 / 7
27	11.1 / 7.3 / 8.8	20uA, 400Hz / 20uA, 400Hz	8.7 / 5.5 / 5.9
28	32.9 / 10.2 / 13.1	40uA, 100Hz / 40uA, 100Hz	24.7 / 5.8 / 14.6
29	23.5 / 8.3 / 16.3	15uA, 400Hz / 33uA, 400Hz	14.7 / 5.9 / 8
30	22.6 / 4.9 / 7.4	18uA, 400Hz / 12uA, 400Hz	13.3 / 3.6 / 7.3

3.3 DATA ANALYSIS

Each trial was digitized and stored for off-line analysis. We used a combination of in-house software and Matlab 7.10.0 (R2010a). Horizontal and vertical eye position along with onset and offset times of the stimulation train were stored with a resolution of 1 ms. Component velocities were obtained by differentiating the eye position signal. Onset and offset of stimulation evoked saccades were then detected using a standard 30°/s velocity criteria, respectively.

Eye movements evoked during simultaneous stimulation or during stimulation with visual stimuli were quantified using two techniques. The first analysis uses a straightforward Euclidean metric. We compared the predictions of the VSS computation to actual data by simply calculating the magnitude of each elicited vector and the magnitude of the respective vector addition prediction.

The second analysis used a multi-linear regression:

$$V_3 = A \cdot V_1 + B \cdot V_2 \qquad (2)$$

The analysis was performed for each vector pair elicited by high and low stimulation settings. The two coefficients A and B define the single site vector (V_1 and V_2) contribution to the output (V_3). The sum of the coefficients describes where the vector falls in relation to the single site vectors. For example, coefficients that sum to 1 identify a weighted vector averaging response, while a sum of 2 indicates vector summation. Two pieces of information are noteworthy about the regression technique. First, a coefficient sum of 1 does not imply that each site contributes half its vector (coefficients equaling .5) as averaging movements can be rotated due to the weight/contribution from each site being different. Second, during simultaneous stimulation we do not know how the single site vectors interact to contribute to the elicited averaging movements. Therefore, we must assume that these independent vectors are conveyed by the single site stimulation trials collected under each parameter setting. To ensure that each of the individual vectors was well-characterized we bootstrapped the single site endpoint distributions, with replacement, and averaged across them.

3.4 RESULTS

3.4.1 Analysis of Microstimulation Elicited Saccade Features

Here we provide a robust characterization of saccades evoked by low stimulation parameters. We demonstrate that using low versus high stimulation parameters produces significant and reliable changes in saccade properties that help to assess if such movements can be accommodated for by decoding models.

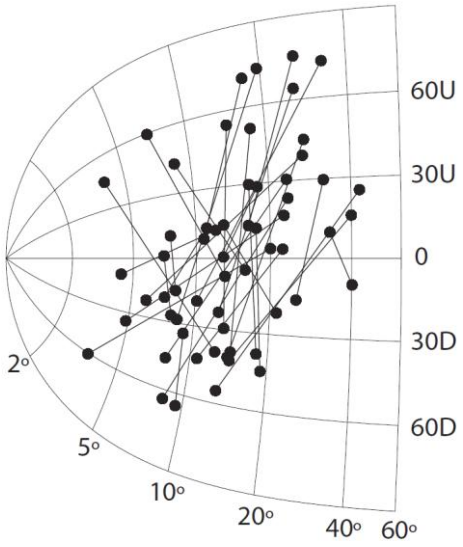

Figure 12. Distribution of paired-stimulation sites
The vector evoked by each site is shown by a black dot and the pair is connected by a line. All 30 paired sites are represented on the SC saccade motor map. Numbers spanning from left to right indicate saccade amplitude. Vertically aligned text (right) denotes saccade direction: U, up; D, down.

We report on a total of 30 stimulation induced saccade-vector pairs obtained from two monkeys, sampling a range of the SC motor map that spanned approximately 2^o to 45^o in amplitude and approximately -80^o to 80^o in direction (Fig. 12). The vector pairs exhibited radial amplitude differences between 0^o to 28^o and directional differences between 20^o to 100^o. In order to reduce the amplitude of saccade vectors, current intensity (18 sites), frequency (4 sites), or both (8 sites) were lowered at each electrode. We found that regardless of the stimulation parameter lowered, we could reliably produce a smaller-then-optimal saccade vector for single or dual stimulation sites in the SC (see Table 1). Furthermore, the saccade always completed within

the train duration. Figure 13 illustrates the radial amplitude and radial velocity of saccades produced by high (40 µA) and low (20 µA) current intensities from single (left) and dual (right) stimulation sites. The figure provides insight towards the differences generated in saccade features when stimulating at high and low levels. One can observe a reduction in amplitude, a significant shift in response latency, and more variability in the amplitude and velocity traces.

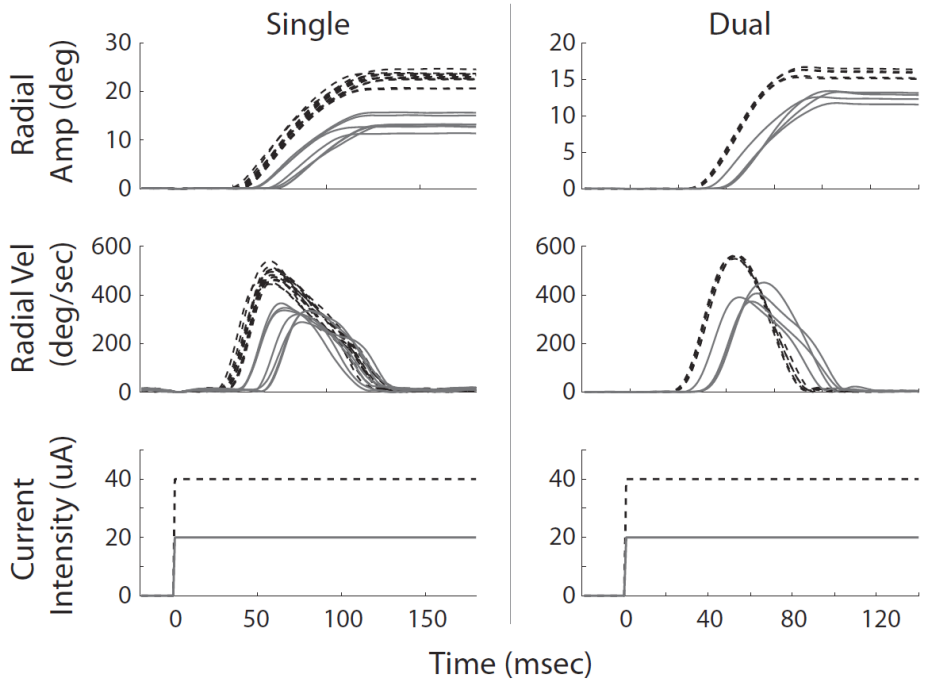

Figure 13. Traces of stimulation-evoked saccades
Left: Radial amplitude (top) and radial velocity (middle) for saccades evoked by high (black dashed traces) and low (solid gray traces) stimulation parameters for a single site in the superior colliculus (SC). Bottom row illustrates the different current intensity used to generate each distribution of traces. **Right**: The same as the left panel, but for saccades generated by simultaneous stimulation of two sites in the SC.

To characterize these differences across all stimulation evoked saccade vectors (single and dual stimulation sites), we categorized each data set into a high or low group based on the stimulation parameters that evoked them. Figure 14A illustrates the radial amplitude of saccades in the high versus low groups (site 1: red, site 2: green, dual site: cyan) using a log-log plot. Almost all points are below the line of unity demonstrating a significant reduction in amplitude (paired t-test, $p < 0.001$). To assess variability, vector distributions of radial amplitude and peak velocity were normalized by their respective mean values obtained from the same site and with the same stimulation parameters. The normalized distributions across all data sets were then

pooled together and the high and low group were compared. Figures 14, B and C, illustrate the normalized distributions pooled across all sites of radial amplitude and peak velocity, respectively, generated by high stimulation parameters versus those generated by low stimulation parameters; notice the larger variability introduced by lower stimulation parameters. Observing that the data distribution is nearly Gaussian, we performed F-tests to assess whether dual site stimulation at high or low levels produced less variability in the different saccade distributions than those generated by single-site stimulation. We found no significant differences in the distributions produced by high level stimulation. Distributions for low-level stimulation were always more variable then those produced by high level stimulation. Interestingly, however, dual-site stimulation at low levels generated significantly less variability in radial amplitude and radial velocity when compared to single-site stimulation (radial amplitude: F-test, $p < 0.05$, radial velocity: F-test, $p < 0.05$).

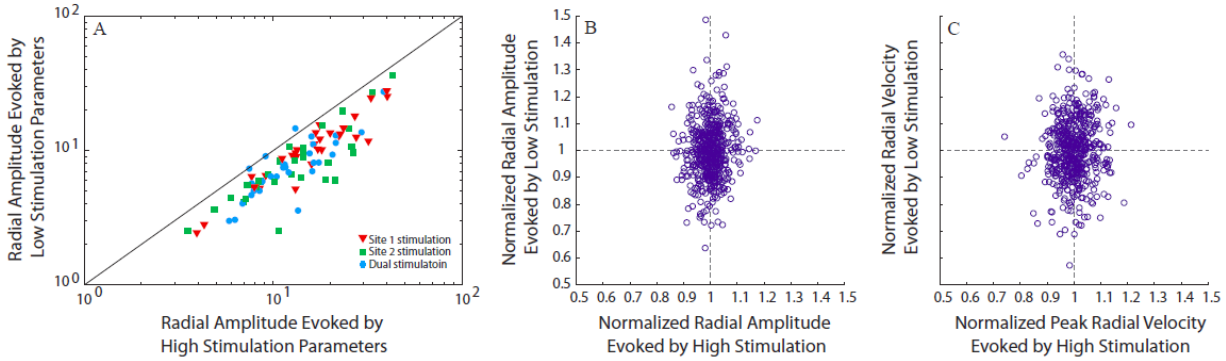

Figure 14. Saccade features of stimulation-evoked movements
(A) Correspondence of mean radial amplitude between saccades evoked by high versus low stimulation parameters. Filled red triangles and green squares represent the mean radial amplitude of saccades evoked by single site stimulation (site 1 and site 2); cyan dots represent the mean radial amplitude of saccades evoked by dual site stimulation. **(B)** Normalized radial amplitudes evoked by high versus low stimulation parameters. **(C)** Normalized radial velocities evoked by high versus low stimulation parameters. Note the larger spread of data points along the y-axis in *B* and *C* demonstrates that saccade features evoked by low stimulation parameters have greater variability.

To characterize the kinematics of saccades produced by low stimulation parameters we illustrate the main sequence properties (Fig. 15, A and B) and the skewness of the velocity profiles, compared to visually guided saccades. Panels A and B of Figure 15 demonstrates that lower stimulation parameters generate slower and longer-duration saccades, even when elicited by dual-site stimulation (site 1: red triangles, site 2: green squares, dual site: cyan circles). All peak velocity and duration distributions generated by low stimulation parameters (single and

dual site) were significantly different from visually guided distributions (peak velocity: KS-test, $p < 0.001$, duration: KS-test, $p < 0.001$); furthermore, distributions generated by dual site stimulation were not significantly different from those generated by single site stimulation (peak velocity: KS-test, $p > 0.11$, duration: KS-test, $p > 0.34$). Neither the peak velocity nor duration of saccades produced by high stimulation parameters was significantly different from visually guided saccades (KS-test, $p > 0.4$; data not shown).

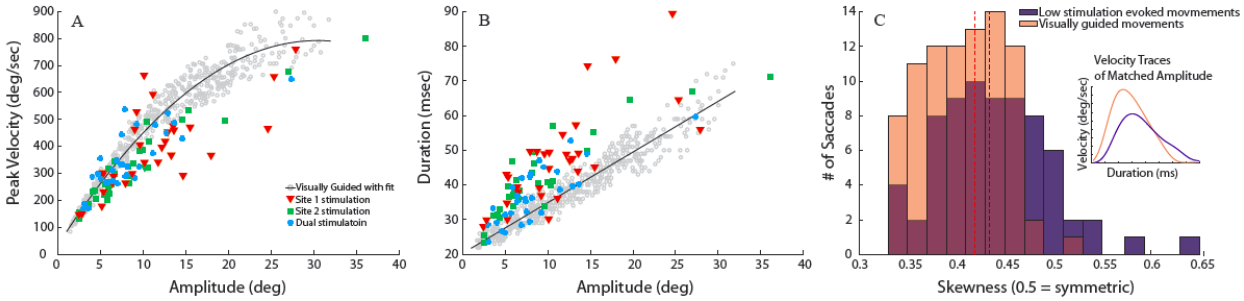

Figure 15. Kinematics of saccades produced by low stimulation parameters
Mean radial amplitude versus mean peak velocity **(A)** and mean duration **(B)**. Filled red triangles and green squares represent main sequence properties for saccades evoked by low stimulation parameters at a single site; cyan dots represent properties for saccades evoked by dual site stimulation; gray circles and solid black line in A and B represents sequence properties and fit for visually guided saccades. **(C)** Histogram comparison of the skewness values calculated for visually-evoked (transparent red) and stimulation-evoked (blue) movements that fall within an amplitude bin that ranges from 2^o to 16^o; dashed lines indicated the median for the color matched distribution. Inset: example velocity trace for a visually guided (transparent red) and stimulation-evoked (blue) movement of similar amplitude (~19^o).

As can be seen in figure 15, A and B, the majority of stimulation points fall within an amplitude bin that ranges from 2^o to 16^o. We calculated and compared the skewness of all stimulation-evoked and visual evoked saccades within this range (Fig. 15C). The velocity profiles generated from low stimulation conveyed the typical positive skewness (time to peak velocity divided by total saccade duration is usually less than 0.5; (Van Opstal and Van Gisbergen 1987)) seen in visually guided saccades. However, the inset of figure 15C provides an example of how low stimulation parameters tend to generate broader peaks as a result of lower peak velocities and longer durations. Figure 15C summarizes the result by comparing the distributions of skewness for eye movements evoked by low stimulation (blue) and those generated by visual stimuli (red). Note that values equal to 0.5 signify symmetry, greater than 0.5 signify positive skewness, and less than 0.5 signify negative skewness. The median of blue

distribution (0.44; blue dashed line) was significantly different (rank sum, $p < 0.01$) from red distribution (0.41; red dashed line) indicating more symmetric velocity profiles.

3.4.2 Simultaneous Dual Microstimulation

Having shown that lower stimulation parameters reliably reduces the radial amplitude of evoked saccades, we can now utilize different levels of microstimulation as a tool to explicitly test the predictions of collicular decoding schemes.

Figure 16A illustrates results of high and low stimulation for one vector pair. Open symbols represent high or supra-threshold stimulation endpoints (40 µA, 400 Hz). The dashed red and green traces denote the spatial trajectories elicited at each site in the vector pair; the dashed cyan lines are the result of dual site stimulation with the same supra-threshold parameters. The dashed black line connecting the single site endpoint distributions represents all possible weighted average locations between the two vectors. Note that the dual-stimulation endpoints lie close to the vector-average line. When the experiment was repeated with lower stimulation parameters at each electrode (40 µA, 200Hz), the endpoints generated by single site stimulation, as well as by dual stimulation, scaled back together (filled endpoints). The solid black line, connecting the single site endpoints, represents all weighted average locations between the two reduced amplitude vectors. Thus, Figure 16A shows that at both high and low stimulation settings, dual site stimulation produced movements that resembled a weighted vector average.

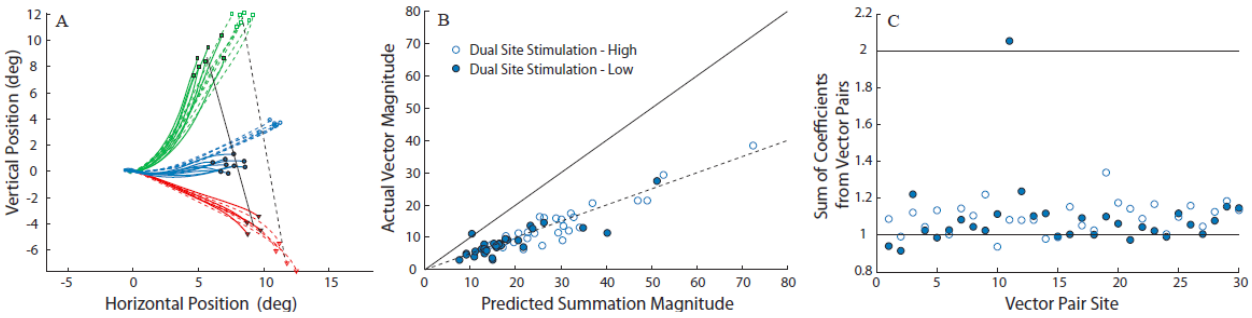

Figure 16. Simultaneous dual microstimulation results
(A) Dashed red and green trajectories represent the individual site-specific vectors elicited by high stimulation parameters (40μA, 400Hz) and are shown with their corresponding endpoint distributions, open red triangles and open green squares. Simultaneous stimulation of the two sites produced the dashed cyan trajectories, cyan circle endpoints. Solid red and green trajectories represent the reduced amplitude vectors elicited at each individual site by low stimulation parameters (40μA, 200Hz) and are shown with their corresponding endpoint distributions, filled red triangles and filled green squares. Simultaneous stimulation of the two sites with low stimulation parameters produces the solid cyan trajectories, cyan dot endpoints. Dashed line between the two site specific-vectors, and solid line between the two individual reduced amplitude vectors represent all possible weighted average locations. **(B)** Comparison of mean radial amplitudes elicited by dual site stimulation versus the summed amplitude of paired site-specific movements. Solid black line represents perfect correspondence between predicted summation and actual response; dashed black line represents perfect correspondence between predicted averaging and actual response. **(C)** Collected vector pairs versus sum of multi-linear regression coefficients. Solid line at 1 indicates averaging responses; solid line at 2 indicates summation responses. **(B, C)** Open cyan circles represents mean amplitude or coefficient sums evoked by high stimulation parameters; filled cyan circles represents mean amplitude or coefficient sums evoked by low stimulation parameters.

To summarize the results for all vector pairs (n = 30 paired sites), we plotted (Fig. 16B) the magnitude of the sum of paired site specific movements, at both high (open circles) and low (filled circles) stimulation, versus the actual magnitude of the movement elicited by dual-site stimulation. The figure illustrates that the majority of points fall below the unity line, and lie close to the half slope of the line (dashed line) confirming an absence of linear addition and showing a dominant averaging response. The consistency of the results across all high and low stimulation parameters highlights the insensitivity of the mechanism to the chosen stimulation settings. We also performed multi-linear regression, in which the sum of coefficients derived from the regression of each vector pair (see methods) quantifies where movements elicited by dual stimulation fall within the spectrum of averaging (sum of coefficients equals one) to linear summation (sum equals two). Figure 16C illustrates that the summed parameters values for almost all low (filled circles; mean=1.09, std = 0.19) and high stimulation strengths (open circles; mean=1.09, std = 0.08) were about 10% larger than 1. The parameter distributions

generated by high and low stimulation strengths were not significantly different from one another (t-test, $p = 0.91$).

In an attempt to observe any trends that could provide insight into the dominant averaging response, the sum of coefficients generated from each vector pair was correlated to spatial and temporal saccade features (i.e., directional separation between saccade vectors, location on the SC motor map, radial amplitude differences, and latency differences). Due to the minimal variability generated in the distribution of coefficient sums, the analysis revealed no trends. Notice, however, that a single vector pair did exhibited vector summation (coefficient sum = 2.05). Unfortunately, the saccade features for the data set did not differ from all other vector pairs that conveyed averaging responses.

3.4.3 Interactions of Visually-guided and Stimulation-evoked Saccades

When testing the VSS model with dual microstimulation we observed that the evoked saccades did not meet the linear predictions of the model. Furthermore, we found that the kinematics of movements elicited by lower stimulation parameters did not match those generated by visually guided saccades. Being that it is unclear how microstimulation induced activity to generate such saccades, it might be argued that the observed averaging outcome is a result of an inadequate drive provided by dual microstimulation. Therefore, we replaced one of the two loci with visual-target-driven activity to observe if any changes occur when part of the total SC population is generated by natural activation.

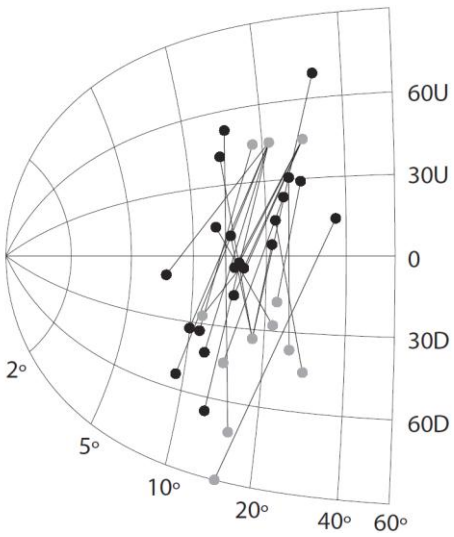

Figure 17. Distribution of paired-visual and stimulation sites
Each vector evoked by stimulation is shown by a black dot; each vector evoked by the presentation of visual target is shown by a gray dot. The pair is connected by a line. All 22 paired sites are represented on the SC saccade motor map. Numbers spanning from left to right indicate saccade amplitude. Vertically aligned text (right) denotes saccade direction: U, up; D, down.

We studied a total of 22 vector pairs, sampling a portion of the SC saccade-vector map that spanned approximately 7^o to 36^o in amplitude and approximately -90^o to 70^o in direction (Fig. 17; gray dots: visual targets, black dots: stimulation sites). The visually guided movements and stimulation induced movements exhibited radial amplitude differences anywhere between 0^o to 21^o and directional differences between 22^o to 123^o. We found that stimulation onset coinciding just before the onset of the saccade to the visual target generated a straight trajectory whose amplitude and direction were influenced by both the visual target and the stimulation evoked movement (Note: for simplicity we will call these movements, VE saccades). Accordingly, the addition of the mean stimulation site latency (high parameter setting: 29 ms, std = 9 ms; low parameter setting: 90 ms, std = 30 ms) to the onset of stimulation relative to the presentation of the visual target (high parameter setting: 171 ms, std = 27 ms; low parameter setting: 116 ms, std = 45 ms) approximately equaled the mean reaction time of the visually guided saccades (212 ms, std = 33 ms).

We reduced the evoked amplitudes for single stimulation sites by varying current intensity (12 sites), frequency (2 sites), or both (8 sites). Figure 18A illustrates VE saccades (cyan trajectories) produced at both high (40 µA, 400 Hz; open circles) and low (15 µA, 400 Hz; filled circles) stimulation parameters for a single vector pair. The red trajectories correspond to

the single site stimulation at high (open triangles) and low (filled triangles) parameter settings, while the green trajectories represent saccades made to the visual target. As with the dual stimulation results, the endpoints of the VE saccades, evoked by either high or low stimulation parameters, more closely resembled weighted vector averaging responses than linear vector summation, although responses were systematically larger than the weighted average for both stimulation strengths. Figure 18B illustrates a summary of the results across all vector pairs by comparing the magnitude of the summation prediction to the magnitude of the movement elicited by stimulation.

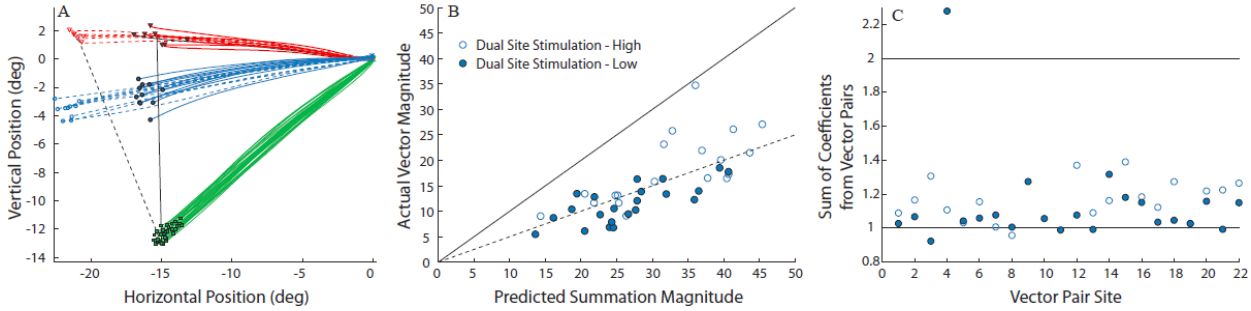

Figure 18. Visually induced activity with microstimulation results
(A) Dashed red lines and open red triangles represent the trajectories and endpoints elicited by high stimulation parameters (40μA, 400Hz); solid green lines and squares represent trajectories and endpoints made to the presented visual target; dashed cyan lines and open cyan circles represent trajectories and endpoints of VE saccades evoked with visual activity and high stimulation parameters. Solid red lines and triangles represent trajectories and endpoints elicited by low stimulation parameters (15μA, 200Hz); solid cyan lines and dots represent trajectories and endpoints of VE saccades evoked with visual activity and low stimulation parameters. Dashed line between the site specific-vectors and visual target, and solid line between reduced amplitude vector and visual target represent all possible weighted average locations. **(B)** Comparison of mean radial amplitudes for VE saccades versus the summed amplitude of paired site-specific movements. Solid black line represents perfect correspondence between predicted summation and actual response; dashed black line represents perfect correspondence between predicted averaging and actual response. **(C)** Collected vector pairs versus sum of multi-linear regression coefficients. Solid line at 1 indicates averaging responses; solid line at 2 indicates summation responses. **(B, C)** Open cyan circles represents mean amplitude or coefficient sums evoked by visual activity with high stimulation parameters; filled cyan circles represents mean amplitude or coefficient sums evoked by visual activity with low stimulation parameters.

Regardless of the stimulation settings, high (open circles) or low (filled circles), nearly all points fall below the solid unity line and close to the half slope of the line (dashed line). In addition, multi-linear regression (Fig. 18C) revealed that almost all low (filled circles; mean = 1.13, std = 0.27) and high stimulation values (open circles; mean = 1.16, std = 0.12) were about 14% larger than one. The distributions were not significantly different from one another (t-test, p = 0.63). We note that again one vector pair exhibited summation like results (coefficient sum = 2.27) with

no distinct differences to provide insight to outlying result. Furthermore, we compared the saccade features of the vector pair to dual site microstimulation pair that also conveyed summation. No similarities were found as the two pairs were different in amplitudes, directions, amount of amplitude reduction, and vector separation.

The main sequence of VE saccades (Fig. 19; red triangles) were not significantly different (KS-test: $p = 0.869$) from those evoked by simultaneous stimulation of two sites with low stimulation parameters (Fig. 19; cyan dots). The peak velocities and durations of VE saccades were significantly smaller and longer than those of visually guided movements (Fig. 19, black traces; peak velocity: KS-test < 0.001, duration: KS-test < 0.001). Furthermore, the skewness of VE saccades was also similar to the dual stimulation results, exhibiting broader peaks as a result of lower peak velocities and longer durations (data not shown).

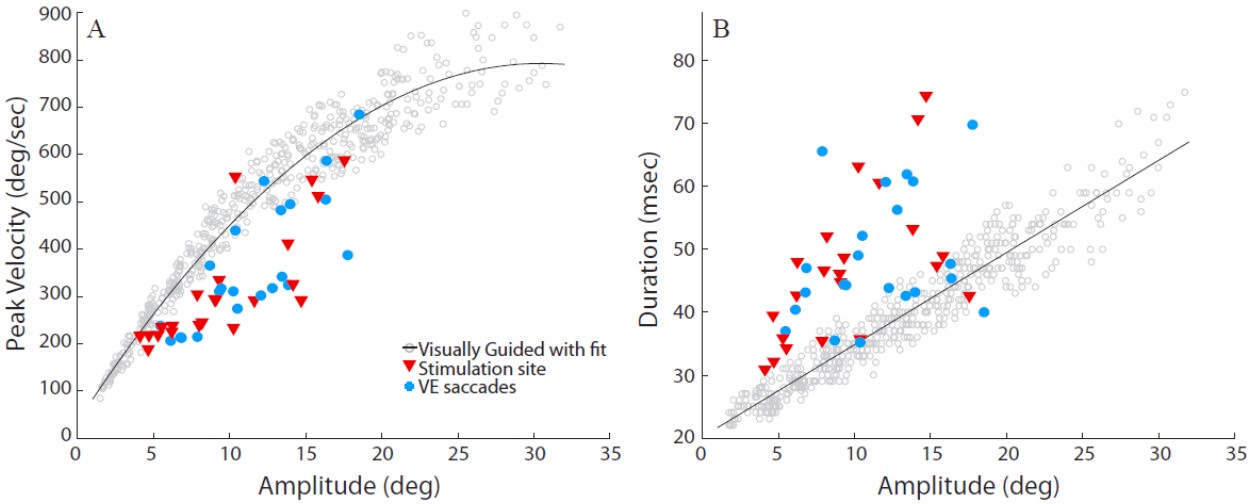

Figure 19. Kinematics of stimulation-evoked saccades and VE saccades
Mean radial amplitude versus mean peak velocity **(A)** and mean duration **(B)**. Filled red triangles represent main sequence properties for saccades evoked by low stimulation parameters at a single site; filled cyan circles represent properties for VE saccades; the solid black line in *A* and *B* represents a fit of the main sequence properties for visually guided saccades (gray circles).

3.5 DISCUSSION

Vector summation with saturation (VSS) makes an experimentally testable prediction for low versus high levels of activity at two simultaneous populations in the SC motor map.

Specifically, the model predicts that the low-level activities generate a vector that resembles the linear addition of the two single-site vectors, whereas the result of high activity at each site resembles the weighted vector average of the two single-site saccades (Fig. 10; (Groh 2001)). We found that at both high and low stimulation levels the evoked movements always resembled a weighted vector average of the two individual saccade vectors (Fig. 16). As a result, we conclude that the VSS decoding scheme in its simplest form is insufficient to properly describe spatiotemporal decoding of multiple populations of activity in the oculomotor system.

3.5.1 Interpreting Microstimulation

Microstimulation is arguably a crude technique that requires further study to understand how stimulation parameters (i.e., current intensity and frequency, neural circuitry) relate to evoked behavior (Katnani and Gandhi 2010). Yet, stimulation studies using supra-threshold parameters have yielded saccades with metrics that closely matched the movement fields of nearby cells recorded with the same electrode and kinematics that were indistinguishable from visually guided saccades of the same amplitude. At lower current intensities (Van Opstal et al. 1990) or frequencies (Stanford et al. 1996) evoked saccades have smaller amplitudes, and velocities that fall below the normal main sequence. These findings can in principle be explained by different mechanisms. For example, microstimulation might induce an electric field around the electrode tip that results in a Gaussian activation pattern, the size and height of which depend on the stimulation parameters. Supra-threshold microstimulation then produces neural activity that resembles the activity for normal visually guided saccades. Lowering current intensity reduces the passive spread of the electric field (Ranck 1975; Stoney et al. 1968)), while lowering the pulse-train frequency reduces the local strength of the electric field (Ranck 1975; Tehovnik 1996). Both manipulations decrease the total input strength to the cells, leading to a smaller population response and thus slower and smaller saccades. An alternative explanation could be that only a few cells near the electrode tip are directly activated by the electric field (Histed et al. 2009), and that the total population response results from synaptic transmission through the local intracollicular network (McIlwain 1982). The effectiveness of this transmission could then systematically depend on both the current intensity and frequency (stimulation strength).

Either assumption can explain the dependencies of the population (and resulting saccade) output on microstimulation parameters. Importantly, the high similarities between electrically and visually elicited movements strongly suggest that SC population responses are decoded in the same manner, regardless their cause. Thus, we can utilize microstimulation to manipulate the stereotypical responses generated by the oculomotor system in order to gain more insight on spatiotemporal decoding mechanisms.

3.5.2 Interpreting an Absence of Linear Addition

Contrary to the prediction of the VSS model, we did not observe linear addition when simultaneously stimulating two sites in the SC with low stimulation parameters. Here we discuss whether such a result is evidence against a summation mechanism, or due to the methodology. We consider two potential issues that could mask linear addition.

First, reduced amplitude saccades evoked by single and dual site stimulation could be the result from truncation due to insufficient pulse-train duration (Van Opstal et al. 1990). Stanford et al (1996) demonstrated that when using low-frequency pulse trains, stimulation duration had to be increased to yield the same saccade. However, closer examination of their results suggests that low stimulation frequencies could produce changes in saccade amplitude at all applied train durations. A recent study by Groh (2011) also demonstrated a reduction in saccade amplitude at lower stimulation frequencies (and initial eye-in-head position). Our data are in agreement with this finding, as smaller amplitude saccades evoked by low current and/or frequency were always completed well before the stimulation offset. Therefore, we consider it unlikely that a lack of linear addition would result from insufficient train duration.

Second, could averaging be an artifact of dual microstimulation? Low current intensity and/or frequency might induce population profiles that result in weak excitation. Previous research suggested a balance between local excitation and global inhibition during the execution of normometric saccades (Hikosaka and Wurtz 1985a, b). Therefore, total motor activity induced by low stimulation parameters may drive the balance between excitation and inhibition in an inadequate fashion; this potentially could mask the true intent of decoding. To account for this possibility we performed an additional experiment in which one of the two stimulation sites was

replaced with a visual target. The introduction of visually induced activity would allow the preparation of a normal motor command that should correspond to the natural excitation-inhibition dynamics of the system. We reasoned that the visually guided movement will always drive the system close to saturation, and therefore, the combination of the movement with either high or low stimulation parameters should evoke saccade amplitudes constrained by saturation. Contrary to this prediction, low-level stimulation evoked responses with smaller amplitudes than the visual saccades as a result of being the weighted average between the visual target and the reduced stimulation vector (see Fig. 18). Furthermore, the velocity profiles of the evoked movements exhibited lower peak velocities and longer durations, similar to saccades evoked by dual-site microstimulation. Therefore, it is unlikely that the observed averaging result is an artifact of dual microstimulation.

3.5.3 Decoding Mechanisms

Three decoding mechanisms have been proposed in literature to explain spatiotemporal decoding in the oculomotor system: vector averaging (VA), vector summation (VS), and vector summation with saturation (VSS). In this section we will discuss how each mechanism relates to the data obtained in experiments 1 and 2.

As explained in the Introduction, the VA scheme in its strictest sense depends only on the stimulation site and therefore does not produce smaller saccade amplitudes and has no mechanism to influence saccade kinematics. Therefore, although the outcome of our data exhibits vector averaging (Fig. 16B and Fig. 18B), the VA model would not predict a difference in amplitude, or kinematics, when changing from high to low levels of stimulation. To account for these findings, two mechanisms have been added to the VA model: (i) firing rates in the brainstem burst generator co-vary with SC activity levels (Nichols and Sparks 1996; Sparks and Mays 1990), and (ii) a change in the normalization factor (Eqn. 1) to $\gamma = 1/(K + \sum_{n=1}^{N} a_n)$ allows the averaging scheme to yield reduced amplitude saccades (Van Gisbergen et al. 1987; Van Opstal and Goossens 2008). In this way, the vigor of activity in the SC influences the gain of the brainstem burst generator, and the addition of K as a constant in the normalization (in spikes/s) can influence the amplitude of decoded saccades. For example, if the total population activity in

the SC is low, K can dominate the denominator to reduce the amplitude of the saccade. The scheme then resembles the vector summation model (see Eqn. 1, where $\gamma = 1/K$). If the population activity is high, K becomes negligible and the computation approaches vector averaging. However, by extending the VA computation in such a manner the model becomes a VSS scheme (generating the same prediction), in which saturation is implemented at high levels of activity through normalization (equivalent to reaching a threshold level).

A recent proposal of vector summation (Goossens and Van Opstal 2006) states that the saccade goal is computed by the summation of mini-vectors elicited by each spike of active cells in a population. The SC motor map thus specifies the desired saccade trajectory, including its kinematics. As a result, saccade vectors now depend strongly on activity level. This allows the model to predict differences in saccade metrics and kinematics when tested with high versus low activity for one motor command. However, the VS model assumes that SC cells are independent units and that weighting occurs entirely downstream of the motor map; therefore, the model cannot account for multiple population decoding (i.e., experiment 1 and 2) and needs an additional criterion to constrain eye movements.

Vector summation with saturation establishes a decoding mechanism that can define how much of the total activity from the SC motor map actually contributes to a movement. However, neurons in the SC are still assumed to be independent units and the summation of their spikes is only constraining once a threshold is reached (Goossens and Van Opstal 2006; Groh 2001). As a result, the model predicts linear addition at low levels of activity when the threshold is not met, but this prediction was not confirmed by our data. To account for the findings in this investigation we speculate that excitatory and inhibitory interactions in the motor map are critical for limiting a summation mechanism. Evidence suggests that lateral interactions are involved in shaping stimulation induced activity (see **Interpreting microstimulation** section above); therefore, the addition of intracollicular interactions (Lee and Hall 2006; Meredith and Ramoa 1998; Munoz and Istvan 1998; Pettit et al. 1999) would allow the model to account for the possibility that multiple sites within the SC motor map compete through lateral inhibitory connections. Under these circumstances, both sites would have reduced firing rates (and hence lead to slower saccades), resulting in a reduction of the total number of spikes. Therefore, the interactions provide a method in which the summation of spikes could be constrained at both high and low activity levels. Further evidence is needed to corroborate interactions as a

constraining mechanism. Nevertheless, naturally evoked saccades have been shown to land in intermediate location relative to multiple visual stimuli (‘global effect’) (Coren and Hoenig 1972; Godijn and Theeuwes 2002). An experiment that utilizes two-site recording in the SC to correlate naturally induced neural activity to global effect behavior could potential validate the interaction mechanism. Previous experimentation in the SC (Edelman and Keller 1998; McPeek et al. 2003; Port and Wurtz 2003; Van Opstal and Van Gisbergen 1990) would provide a foundation for the significance of such work.

Finally, we speculate that intracollicular interactions need not be the definitive mechanism to constrain summation. For example, interactions between concurrent motor commands can occur at other nodes of the oculomotor neuraxis (e.g., frontal eye fields, basal ganglia). Also, the gating of the saccadic system by the pontine omnipause neurons (OPNs) is a function of saccadic velocity (Yoshida et al. 1999). Since eye velocity is attenuated for low-frequency stimulation, the OPNs may resume earlier, thus limiting the magnitude of the stimulation-evoked movement. Additional studies are required to probe the potential contributions of these mechanisms.

4.0 ANALYSIS OF STIMULATION-EVOKED SACCADES PERTURBED BY BLINKS

4.1 INTRODUCTION

Microstimulation in the intermediate and deeper layers of the superior colliculus (SC) produces fast eye movements (saccades) whose amplitude and direction depend on the site of stimulation within the topographical vector map of the SC (Gandhi and Katnani 2011; Ottes et al. 1986; Robinson 1972). As illustrated in a simplified schematic in Figure 20, the SC output drives the brainstem burst generator (BG) to produce the saccade (Scudder et al. 2002). This oculomotor drive also inhibits the brainstem omnipause neurons (OPNs), which discharge at a tonic rate during fixation and become quiescent during saccades. Intracellular and local field recordings show that the OPNs are hyperpolarized during saccades, and the temporal profile of the membrane potential is the reciprocal of the saccade velocity waveform (Van Horn et al. 2010; Yoshida et al. 1999). The local feedback loop that operates on the BG ensures that the desired saccade command from the SC is produced.

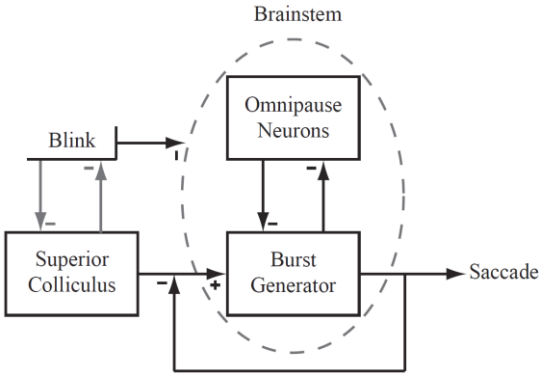

Figure 20. Simplified conceptual scheme of saccade generation
Excitatory projections from the superior colliculus (SC) drive the saccadic burst generator (BG) in the brainstem. Activity from the BG is regulated by a feedback loop to preserve saccade accuracy. Within the brainstem a mutual inhibitory network exists between the omnipause neurons (OPNs) and the BG. Blinks have been shown to affect the brainstem in a manner that suppresses OPN activity. In addition, we incorporate mutual inhibitory effects between the blink and the SC in order to comment on the behavioral correlations seen within our data. Evidence supports the existence of such interaction, although the exact neural correlate is unknown.

However, previous studies have demonstrated that the site-specific amplitude of saccades can be reduced, as well as the kinematics attenuated, when the SC is electrically stimulated with sub-optimal levels of current intensity and frequency (Groh 2011; Katnani et al. 2012; Stanford et al. 1996; Van Opstal et al. 1990). We speculate that slower and smaller saccades induced by sub-optimal stimulation could potentially reflect a weaker inhibition on the OPNs, which will enable them to resume prematurely and inhibit the BG. Effectively, the feedback loop will be over-ridden and the saccade amplitude reduced.

Based on this conceptual framework, prolonged cessation of the OPNs during ongoing sub-optimal stimulation of the SC would lead to an increase in saccade amplitude. We investigated this hypothesis by perturbing stimulation-evoked saccades with air-puff induced blinks. The eye movement associated with blinks causes modulations in the brainstem (Fig. 20) in a manner that has been linked to cessation of OPN activity (Schultz et al. 2010). Thus, an air-puff delivered to one eye at randomly selected times during low level stimulation could serve to test our hypothesis. Our results demonstrate that the amplitude of saccades can increase when coinciding with a blink. In addition, the effect had an inverse relationship (anti-correlated) with the peak velocity of the blink perturbation seen across animals: a larger increase in evoked saccade amplitude was more likely to occur with a weaker blink perturbation. As a result, we

interpret our findings in terms of potential blink related effects on the colliculus as part of a mutual inhibitory network (Fig. 20; gray arrows).

4.2 METHODS AND DATA ANALYSIS

All procedures were approved by the Institutional Animal Care and Use Committee at the University of Pittsburgh and complied with the guidelines of the Public Health Service policy on Humane Care and Use of Laboratory Animals. Four juvenile, male rhesus monkeys (*Macaca mulatta*) underwent one or more surgeries in a sterile environment and under isoflurane anesthesia. The initial procedure consisted of placing a Teflon-coated stainless steel wire (Baird Industries, Hohokus, NJ) under the conjunctiva of one eye and securing a head-restraint post to the skull. In the second procedure, one cylinder was cemented over a craniotomy. The chamber was placed stereotactically on the skull, slanted posteriorly at an angle of 38° in the sagittal plane. This approach allowed access to both colliculi and permitted electrode penetrations normal to the SC surface. After each surgery, the monkey was returned to its home cage and allowed to fully recover. Post-operatively, antibiotics and analgesics were administered as indicated in the protocol.

Behavioral paradigms as well as stimulation and reflex-blink procedures were similar to those described in previous papers (Bryant and Gandhi 2005; Gandhi and Bonadonna 2005; Katnani et al. 2012). Briefly, all animals were trained to perform the oculomotor gap task. Every trial began with directing the line of sight to a fixation point for 300-500 ms before it was extinguished. Following a 200-400 ms "gap" interval, during which the animal was required to maintain the same eye position, another stimulus was illuminated in the visual periphery. Each animal was permitted 500 ms to redirect its visual axis on the saccade target and hold gaze steady for 300-500 ms to earn a liquid reward. As the animal performed this task, a platinum iridium microelectrode (1.0-1.5 MΩ; MicroProbes for Life Science, Inc., Gaithesburg, MD) was advanced with a hydraulic microdrive (Narashigie, Tokyo, Japan). The electrode was driven deeper into the SC until saccadic motor bursts were identified. At this stage, supra-threshold stimulation (40μA, 400Hz) was delivered during the gap interval to determine the site-specific

vector coordinates. The depth of the electrode was then minimally adjusted to obtain the shortest possible latency of the stimulation evoked saccade (20 - 40 ms). Train duration was manually set (range: 100-300ms) and always long enough to allow for completion of the stimulation-evoked movements.

Microstimulation was delivered during the gap period on 20% of the trials. Supra-threshold and sub-optimal stimulation parameters were delivered in separate blocks. Constant current stimulation trains were generated using a Grass S88X stimulator in combination with Grass PSIU6 isolation units. Trains consisted of cathodic phase leading, biphasic pulses (0.25 ms). For high or supra-threshold stimulation conditions, current intensity and frequency were fixed at 40 μA and 400 Hz. The lower or sub-optimal parameter space could be as low as 10 μA and 100 Hz, and differed for each data set in order to evoke reduced amplitude saccades. Low stimulation settings were determined by selecting current intensities, frequencies, or both that reliably produced movements (>90% probability of evoking movement) but also significantly reduced the amplitude of the movements (~15% or more change in amplitude). Only one set of high and low stimulation-evoked saccades was collected for each data set. In all cases, stimulation duration was always long enough to ensure that it outlasted the eye movement.

The protocol for the experiment was to investigate the effects of blinks on stimulation-evoked saccades, in which the objective was to have OPN inhibition outlast the typical duration of stimulation-evoked movements. To achieve this, the trigeminal blink reflex was evoked during stimulation on 20% of the gap trials. A puff of air was delivered at random times just before or during stimulation. Approximately 200 ms after stimulation offset, a target was presented in the visual periphery, which the animal fixated to receive a liquid reward. Furthermore, on 10% of non-stimulation trials only the puff was administered during the gap period. These puff-only trials generated consistent eye movements that accompanied the blink (blink related eye movements or BREMs) and were used to assess the behavioral characteristics produced by inducing the trigeminal blink reflex. Eyelid movements were recorded using a small Teflon-coated stainless steel wire that was taped to the eyelid of the eye not implanted with the scleral coil. The eyelid coil signal, maintained in arbitrary units, was amplified in software to clearly identify eye closure as deflections in the vertical channel.

The air-puff data were collected during both supra-threshold and sub-optimal microstimulation at 42 sites. The analyses focus only on movements evoked by sub-optimal

parameters as air puffs yielded blinks over 90% of the time during stimulation with low current intensities (14 sites), low pulse-train frequencies (6 sites), or both (22 sites). During supra-threshold stimulation air-puffs were completely ineffective in producing blinks for 16 of the 42 sites. For the remaining sites air-puffs yielded blinks less than 10% of the time therefore producing an insufficient amount of data. The result is consistent with a previous study that reported the inability to evoke blinks with supra-threshold stimulation (Gnadt et al. 1997).

Each trial was digitized and stored on the computer's hard disk for off-line analysis. We used a combination of in-house software and Matlab 7.10.0 (R2011a). Horizontal eye position and vertical eye and eyelid position along with onset and offset times of the stimulation train were stored with a resolution of 1 ms. Component velocities were obtained by differentiating the eye and eyelid position signals. Onset and offset of stimulation-evoked saccades and blink-related eye movements were then detected using a standard 30°/s velocity criteria, respectively.

4.3 RESULTS

Effects of the trigeminal-blink reflex on saccades evoked by sub-optimal microstimulation were tested on 42 SC sites in four animals (monkey 1: 17, monkey 2: 7, monkey 3: 10, monkey 4: 8). The site-specific vectors spanned approximately 8^o to 40^o in amplitude and approximately -70^o to 40^o in direction. Figure 21 shows representative examples of spatial trajectories of stimulation-only evoked movements (SoMs, blue trajectories) and stimulation with blink evoked movements (SwBMs, green, cyan, red, and gray trajectories) observed at four sites, one from each animal. All traces are aligned and shifted to start at stimulation onset and at the origin, respectively. The black diamonds superimposed on the SwBMs trajectories indicate the eye position at the time of blink onset. The trajectories shown in the left column illustrate examples in which SBMs clearly exhibit larger radial amplitudes then SoMs. In contrast, the trajectories in the right column identify sites that showed either minimal or no increase in saccade amplitude.

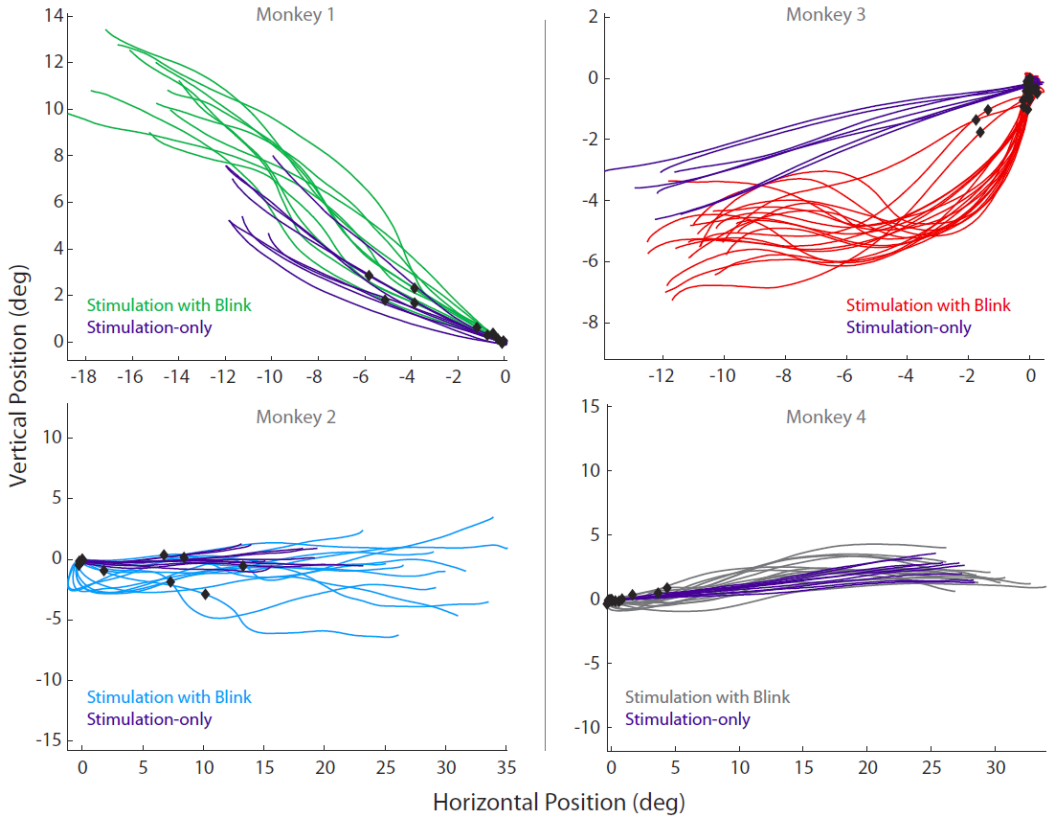

Figure 21. Microstimulation with blink examples
Representative examples of spatial trajectories (horizontal vs. vertical eye positions) shown from the four animals evoked by sub-optimal microstimulation. In all plots, the blue trajectories represent stimulation-evoked reduced amplitude saccades without blinks. Note: mean metrics (horizontal, vertical) evoked by suprathreshold stimulation for monkey 1 (-20.6, 8.5), monkey 2 (29.9, 0), monkey 3 (-23.2, -4.5), monkey 4 (34.8, 5.3). The traces in the other colors represent movements evoked when stimulation was combined with a puff-evoked blink. All traces are offset to the origin with each trace being plotted from stimulation onset to movement offset. Note: Black diamonds superimposed on the trajectories indicate where the blink occurred relative to stimulation onset.

We next wanted to verify that blink duration overlapped saccade duration, and that the offset of the typical blink-related eye movement (BREM), and presumably the associated cessation of OPN activity (Schultz et al. 2010), outlasted the offset of the SoM. In principle, this computation requires the properties of BREMs that occur during stimulation with puff trials. As a result of not having access to these properties, we utilized the properties of BREMs collected during puff-only trials. To gauge the validity of the substitution we assessed positional traces of the eyelid during blinks. Figure 22 shows that the eyelid traces of blinks produced during puff-only (green) and stimulation with puff (blue) trials were qualitatively similar. Furthermore, a statistical comparison of the eyelid peak velocities revealed no significant (paired t-test, $p > 0.05$)

differences. We note that although we do not know if and how the properties of BREMs change when combined with stimulation, the similarity in the eyelid profiles supports the assumption that the BREMs were similar in the two conditions. Therefore, we used BREM properties evoked during puff-only trials to assess blink related effects on stimulation-evoked saccades. As a result, we found that BREM duration, on average, always outlasted the offset of SoMs (Monkey 1: mean = 33 ms, std = 17, Monkey 2: mean = 62 ms, std = 27, Monkey 3: mean = 15 ms, std = 32, Monkey 4: mean = 36 ms, std = 22).

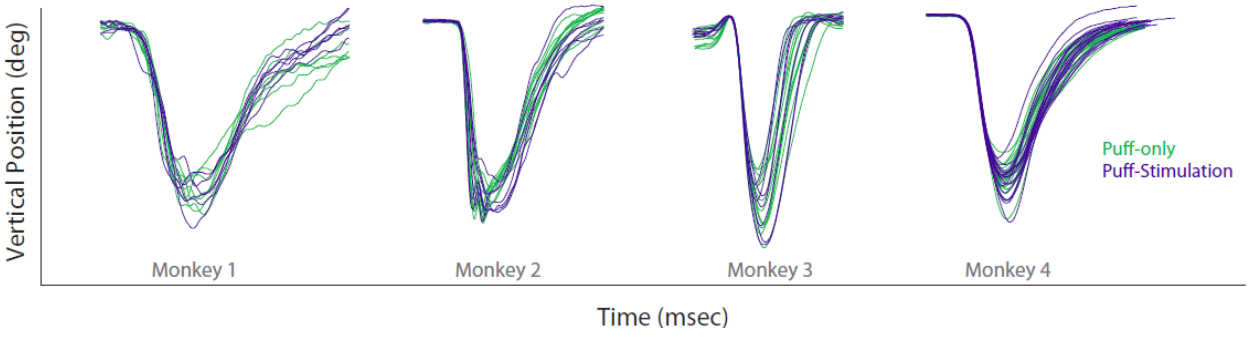

Figure 22. Examples of compared eye-lid deflections
Comparison of the vertical eye lid position for blinks evoked during puff-only trials (green) and puff with stimulation trials (blue). All traces are aligned on movement onset and taken from one data set for each monkey.

To quantify the blink-induced change in amplitude, we compared, on a site-by-site basis, the mean radial amplitudes of SoMs and SwBMs (Fig. 23). The radial amplitude was significantly larger for SwBMs across the entire dataset as well as for monkeys 1 and 2 (green and cyan dots; paired t-test, $p < 0.001$). However, the SwBM amplitude was not significantly larger for monkeys 3 and 4 (red and gray dots; paired t-test, $p > 0.05$). We wondered whether the significant hypermetria observed for monkeys 1 and 2 could have been simply due to a linear superposition of the BREM contribution. To test for this, we subtracted the maximum horizontal and vertical excursions of BREMs collected during puff-only trials (see Methods) from the endpoints of SwBMs. While this step naturally reduces the amplitude of the movements, shifting them closer to the amplitudes of the SoMs (equivalently a downward shift closer to the line of unity in figure 23, data not shown), the hypermetria in monkeys 1 and 2 remained statistically significant (paired t-test, $p < 0.001$). Therefore, the large radial amplitudes of SwBMs for monkeys 1 and 2 were not just the result of an added BREM contribution.

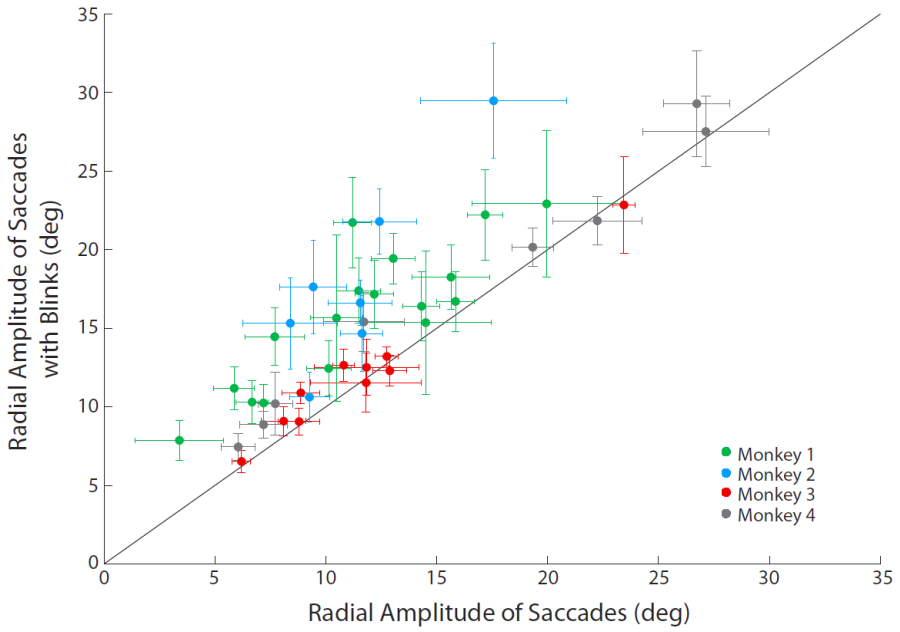

Figure 23. Comparison of radial amplitude

Comparison of mean radial amplitudes for stimulation-evoked saccades without and with a puff-evoked blink. Green dots represent values from monkey 1; cyan, monkey 2; red, monkey 3; gray, monkey 4. Error bars represent one standard deviation from the mean; solid line marks unity slope. The majority of stimulation sites lie above the unity line, indicating an increase of saccade amplitude due to the blink-saccade interaction.

We next tested whether the change in amplitude was in the direction of the stimulation-evoked vector, as opposed to a direction mediated by the BREM. We note that the absolute values of endpoints were used in this analysis in order to standardize alignment for movements in opposing directions. We subtracted the mean endpoint of the SoMs from the endpoint of each SwBM endpoint for each data set. As a result, the SwBM endpoints were plotted relative to the mean endpoint of SoMs for the corresponding stimulation site (Fig. 24; monkeys 1, 2, 3, and 4: green squares, cyan triangles, red circles, and gray diamonds, respectively). The data demonstrate that the majority of SwBM endpoints, horizontal and vertical component, for monkeys 1 and 2 were significantly shifted away from zero (t-test: $p < 0.001$) and lie in the upper-right quadrant, verifying that the overshoot occurred in the direction of the stimulation-evoked saccade (this can also be appreciated from the examples in figure 21, left column). In contrast, the majority of endpoints for monkeys 3 and 4 were clustered around zero. However, the total distribution of SwBM endpoints, across all data sets for monkey 3 showed a significant (t-test: $p < 0.001$) overshoot in the vertical component when compared to the total distribution of

SOM endpoints. For monkey 4 we found a significant (t-test: $p < 0.001$) overshoot in the horizontal component. The observed vertical overshoot seen in monkey 3 corresponded with incomplete compensation seen in SwBMs, while a few sites for monkey 4 did exhibit a slight horizontal overshoot in the direction of the stimulation-evoked saccade. Both findings can be appreciated by the spatial trajectories shown in figure 21, right column; nevertheless, the number of points showing small vertical overshoot in monkey 3 and small horizontal overshoot in monkey 4, did not significantly contribute to the overall change in amplitude seen across all sites for each monkey (Fig. 23).

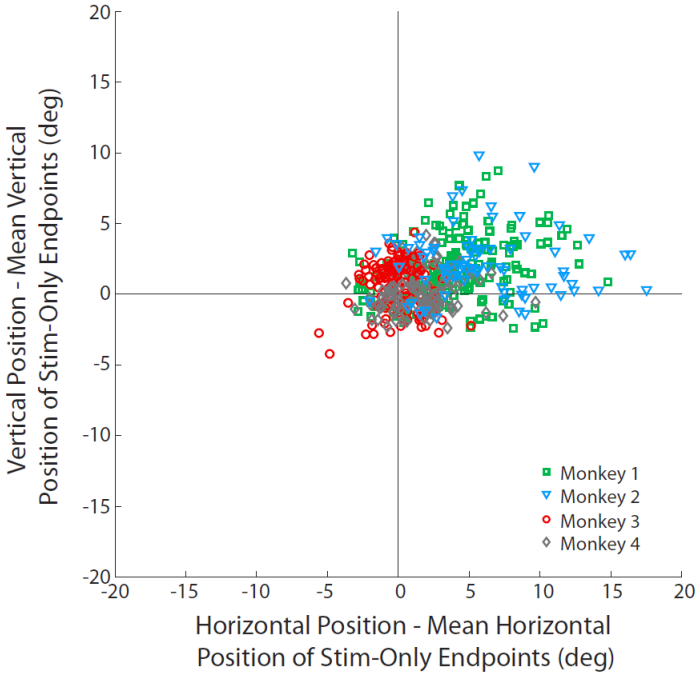

Figure 24. Alignment analysis

Alignment between stimulation-evoked saccades without and with a puff-evoked blink. Green squares represent data for monkey 1; cyan triangles, monkey 2; red circles, monkey 3; gray diamonds, monkey 4. Note that the absolute values of endpoints were used to standardize alignment for movements in opposing directions.

We next asked whether the different results seen across animals could somehow correlate to the characteristics of each animal's blink perturbation. The vigor of the premotor burst in the SC is correlated with the eye velocity. Given that blinks reduce saccade velocity we reasoned that blink-induced attenuation may interact with collicular activation and in turn influence whether prolonged stimulation could increase saccade amplitude. As a result, we focused on the

BREM dynamics elicited by each monkey during puff-only trials. We wondered whether the size of the blink perturbation, derived from BREM peak velocity, could reveal the potency of any potential combative interactions. We found that the peak velocity of the BREM was monkey specific; in other words, consistent within an animal (Gandhi 2012) but significantly different across animals (ANOVA: $p < 0.001$). Figure 25 illustrates the relationship between the maximum velocity of BREMs and the difference in radial amplitude between SoMs and SwBMs (monkey 1, 2, 3, and 4: green squares, cyan triangles, red circles, and gray diamonds, respectively). Note, the correlation for each animal seems to orient vertically and exhibits no distinguishable trend; however, when the data are pooled across animals the overall correlation demonstrates an inverse relationship (correlation coefficient = -0.6, $p < 0.001$), in which higher peak velocities of BREM significantly correlate to smaller differences between SoM and SwBM amplitude. Therefore, the size of the blink perturbation seems to indicate a potential level of impedance on induced activity, explaining the variable extent of increase across monkeys.

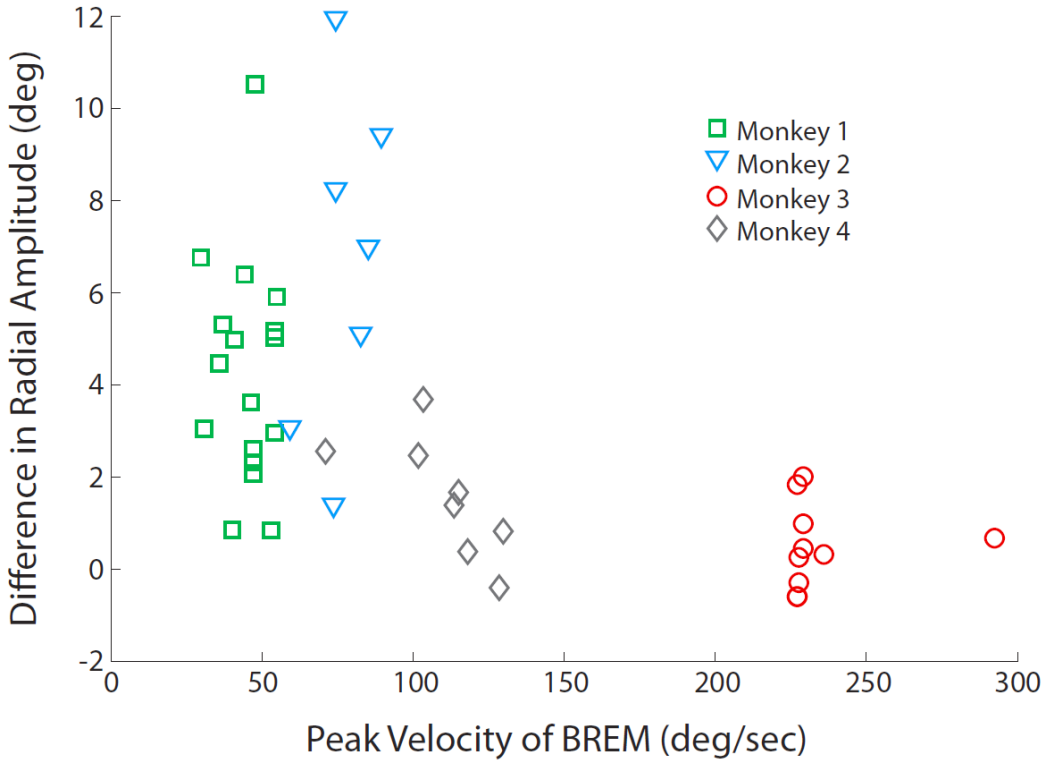

Figure 25. Correlation with BREM kinematics
The peak velocity of BREM movements versus the change in mean radial amplitude of stimulation-evoked saccades colliding with a puff-evoked blink. Green squares correspond to monkey 1; cyan triangles, monkey 2; red circles, monkey 3; gray diamonds, monkey 4.

In an attempt to identify additional trends that could account for the distribution of radial amplitude differences between SoMs and SwBMs, within an animal and across animals, we correlated the differences with numerous saccade features (i.e., peak velocity of movements, BREM onset and offset relative to stimulation onset and offset, location on the SC motor map, BREM duration, eye lid peak velocity, and latency differences), but found no statistically significant trends.

4.4 DISCUSSION

4.4.1 Neural Signatures of Saccade-blink Interactions

Brainstem OPNs are deeply inhibited during saccades, as their membrane potentials exhibit steep hyperpolarization that mirrors the eye-velocity waveform (Van Horn et al. 2010; Yoshida et al. 1999). The similarity in kinematics of visually-guided saccades and those evoked by supra-threshold stimulation of the SC suggests that OPN inhibition is comparable in the two situations. With weaker stimulation parameters, however, the eye velocity is attenuated, potentially indicating weak excitation of the saccadic BG and therefore weak inhibition of the OPNs (Fig. 20). This mechanism could then lead the OPNs to resume their discharge prematurely, thereby over-riding the operation of the BG feedback loop (Fig. 20) and truncating the stimulation-evoked saccade. We reasoned that delaying the resumption of OPN activity would grant the brainstem BG access to additional spikes induced by stimulation, which in turn would produce a larger movement. One means of suppressing OPN activity on a trial-by-trial basis was to invoke the trigeminal blink reflex. The rapid eyelid depression during a blink is accompanied by a loopy BREM, whereby the OPNs pause for the duration of this movement (Schultz et al. 2010). Thus, a blink that is induced during a stimulation-evoked saccade could potentially provide a larger window of OPN inactivity. Using this approach, we found a consistent increase in saccade amplitude in two animals, but a relatively weaker effect in the other two animals. We never observed a decrease of the stimulation-induced saccade amplitude. The results can therefore be interpreted in support of our hypothesis with the added caveat that

the complex influence of air-puff and/or blink on neural processes within the SC-OPN-BG network could potentially weaken the magnitude of this effect.

In a previous study air-puffs were shown to rarely evoke blinks when associated with supra-threshold stimulation (Gnadt et al. 1997). We interpret this result to support the concept that the vigor of SC output can control the likelihood of producing a blink, as blinks and saccades are part of a mutual inhibitory network. In accordance with this notion, naturally occurring blinks are less likely to accompany small-amplitude saccades (Gandhi 2012; Williamson et al. 2005) driven by high discharge rates in the rostral SC, compared to larger amplitude movements driven by low discharge rates in caudal regions (Anderson et al. 1998; Goossens and Van Opstal 2012; Goossens and Van Opstal 2006). Thus, there appears to be a direct correlation between the level of SC activity, whether generated in response to a stimulus or stimulation, and the probability of inhibiting a blink. We speculate that the results from this investigation also provide further evidence towards the reverse interaction between blinks and saccades, in which the potency of blinks can affect the probability of inhibiting SC activity. Saccade trajectories have been shown to be strongly perturbed by a blink (Goossens and Van Opstal 2000a), and the high-frequency discharge of saccade-related burst neurons in the SC is also markedly reduced during blinks (Goossens and Van Opstal 2000b). These findings in combination with our results indicate that the magnitude of attenuation in the collicular ensemble activity is directly correlated with the magnitude of the blink-induced perturbation. The attenuation need not be caused by the blink itself; a corollary discharge of the blink motor command, which could be triggered by the air-puff and/or a sensory response to the air-puff could be sufficient. Within this context, the suppressive effect of the blink interacts destructively with the population response generated by microstimulation. Therefore, a weak blink-related signal (for example, when BREM peak velocity is small; monkeys 1 and 2; Fig. 25) has a relatively minor inhibitory effect on the SC population response. As a result, continued stimulation coupled with prolonged OPN suppression will lead to a larger amplitude eye movement. On the other hand, a potent blink signal (i.e., when BREM peak velocity is high, as in monkeys 3 and 4) will significantly inhibit the population response associated with sub-optimal stimulation, such that the SC drive to the BG is effectively too weak to prolong the eye movement, even if the OPNs remain quiescent.

4.4.2 Significance to Motor Decoding in the Oculomotor System

Saccade generation requires the brainstem BG to decode population activity emanating from various oculomotor structures, including the superior colliculus. The vector summation with saturation (VSS) model proposes that the cumulative sum of the collicular output drives the BG until saturation constrains the sum and terminates the movement (Goossens and Van Opstal 2006; Groh 2001; Van Opstal and Goossens 2008). We recently concluded that the saturation function could be implemented in multiple ways, including intracollicular interactions and gating by the OPNs (Katnani et al. 2012). The blink manipulation in the present study explored this latter mechanism. Presumably, the blink prolongs the duration of OPN suppression, which would effectively allow the cumulative sum of SC activity to occur over a longer duration and generate a larger movement. Consistent with this prediction, we did observe larger amplitude movements when a blink coincided with stimulation, although suppressive effects of the blink on the saccadic drive may in turn have reduced the increase (Goossens and Van Opstal 2000b). The result would have been even more compelling if the evoked vector amplitude, in the presence of a blink, could have exceeded the site-specific saccade vector. Unfortunately, the inability to evoke blinks during supra-threshold stimulation, and suppressive effects of the blink on the saccadic drive, may have prevented this assessment.

A competing model is a decoding mechanism based on vector averaging (VA), and determines desired saccade metrics by normalizing the collicular ensemble activity to compute its center of mass (Lee et al. 1988). However, the VA model does not predict reduced amplitude saccade vectors and kinematics produced by sub-optimal stimulation parameters (Groh 2011; Katnani et al. 2012; Van Opstal et al. 1990), since the level of stimulation is irrelevant to the computation. However, if the attenuated velocity profile reflects a weaker SC output (see **Neural signatures of saccade-blink interactions**), then OPNs could prematurely resume and mask the metrics defined by the averaging mechanism. Therefore, the removal of OPN activity during stimulation could allow previously truncated movements to reach the true metrics defined by the VA computation. In this sense, the blink manipulation paired with SC microstimulation can make similar predictions for both VSS and VA schemes, and therefore may not be an appropriate test to differentiate the two mechanisms. However, if blinks could be induced during supra-threshold stimulation, one would expect different results dependent on the decoding mechanism.

For VA, the metrics of the movement should match the site-specific vector, or computed center of mass, regardless of prolonged OPN inactivity. On the other hand, for VSS the movement should exceed the site-specific vector as OPN suppression prolongs the occurrence of saturation. We conclude that our results in combination with other evidence, not related to the blink (Goossens and Van Opstal 2006; Groh 2001; Groh 2011; Katnani et al. 2012; Van Opstal and Goossens 2008), lend overall support for the VSS mechanism.

5.0 ORDER OF OPERATIONS FOR DECODING SUPERIOR COLLICULUS ACTIVITY FOR SACCADE GENERATION

5.1 INTRODUCTION

The superior colliculus (SC) is a critical, sub-cortical hub that plays a major role in converting sensory information into a motor command for saccade generation (Gandhi and Katnani 2011; Sparks 1986). Visual information in the SC is organized topographically in a logarithmic manner. A disproportionately large amount of SC tissue is allocated for (para-) foveal space and small-amplitude saccades, while a compressed region is attributed for the visual periphery and large-amplitude saccades (Cynader and Berman 1972; Robinson 1972). With the presentation of a stimulus, a population of neurons becomes active at a locus that represents the vector between the stimuli and line of sight (Wurtz and Goldberg 1972). Under ordinary circumstances, a comparable population discharges a high frequency premotor burst to produce a saccade of the appropriate displacement (Sparks et al. 1976). To make certain that the saccadic eye movement lands near the desired location, two critical operations must be performed. One, the population response must be decoded using standard decoding mechanisms like averaging or summation. Two, the SC output must undergo an exponential transformation to convert the saccade vector into visual coordinates (Ottes et al. 1986); the inverse transformation used to map visual space into SC coordinates. Studies have implemented the order of these two operations in different fashions. To the best of our knowledge, no attempt has been made to distinguish the order of these operations.

In one scheme, the exponential transformation is applied to each SC neuron's location to represent it in vector coordinates (equivalently, visual space). A decoding mechanism is then applied to the transformed population output to yield saccade vector metrics ("cyan path" in Fig.

26A). This study only considers the averaging decoding algorithm, and therefore, we'll refer to this sequence as a vector-averaging computation (or VA model). Research and computational models typically use this order of operations to decode saccade metrics (Van Opstal and Goossens 2008; Walton et al. 2005). In the other sequence, the decoding algorithm happens in collicular coordinates. It computes the optimal location of activity in units of millimeters using principles of center-of-mass or center-of-gravity. The optimal location then undergoes an exponential transformation to produce the saccade metric (CM model, "magenta path" in Fig. 26A). Studies associated with averaging saccades (Arai et al. 1994; Glimcher and Sparks 1993) and SC role in spatial feedback control (Anderson et al. 1998) have relied on this sequence to decode the saccade vector.

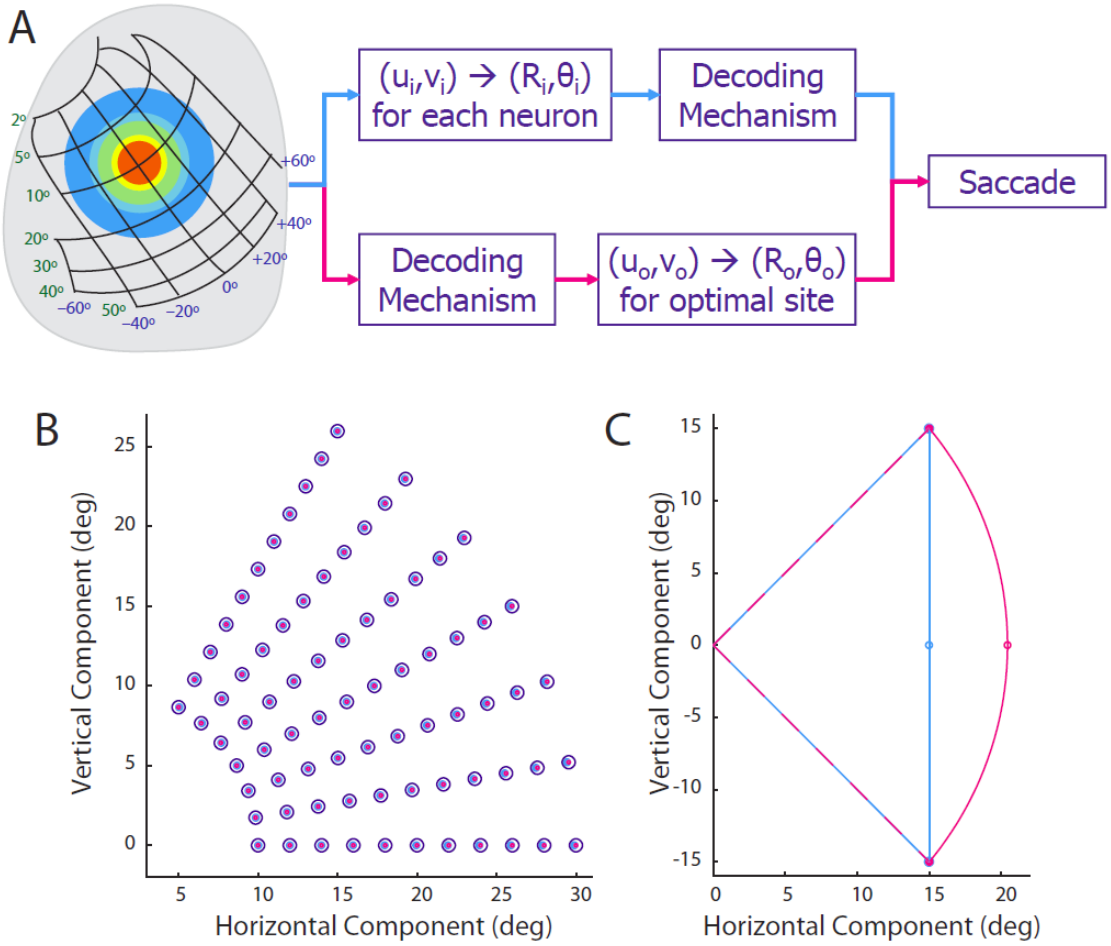

Figure 26. Representation and predictions based on the order of decoding operations **(A)** Order of operations for decoding population activity in the superior colliculus (SC) to generate saccades. Cyan path represents the sequence set by vector averaging (VA) model. The SC coordinates of neuron's (u_i,v_i) are first exponentially transformed into visual coordinates (R_i,Θ_i) and then a decoding mechanism is applied to the ensemble of neurons. Magenta path represents the sequence set by the center-of-mass (CM) model. The decoding mechanism determines the optimal location in SC coordinates (u_o,v_o), which then undergoes an exponential transformation to yield the saccade vector (R_o,Θ_o) in visual coordinates. **(B)** Saccade output (open magenta circles, CM output; cyan dots, VA output) of each path shown in *A* when tested with single target locations (open blue circles). **(C)** Saccade output of each path shown in *A* when tested with paired target locations [15°, 15°] and [15°,-15°]. Dashed magenta and cyan lines represent saccade vector response to each target separately; open magenta and cyan circles represent the saccade endpoint of each model when decoding simultaneous populations of equal strength; solid magenta and cyan lines represent saccade endpoint distribution when decoding simultaneous populations of varying strengths.

The primary objective of this study was to address the order in which the two operations are implemented. It should be emphasized that our focus is not to address the specific decoding algorithm. We recognize that vector summation (VS) is another prevalent algorithm used to decode SC activity (Goossens and Van Opstal 2006; Van Gisbergen et al. 1987). Previous

modeling has demonstrated that VA and VS can generate approximately equivalent decoding predictions ("cyan path" in Fig. 26A) despite accounting for two different decoding principles (Van Opstal and Van Gisbergen 1989). However, we concentrate on the comparison of VA and CM, due to their simple implementation and similar description of decoding that allows for a straightforward investigation pertaining to the order in which decoding and exponential transformation is implemented.

We first reconstructed and simulated the well-established VA and CM models that are often used or referred to in order to describe the sequences for decoding SC activity. Each was assessed by observing the response to a wide range of single target locations. Both produced nearly identical saccade endpoints (Figure 26B), yielding no clear distinction between the two algorithms. When the models were tested for their predictions of decoding two simultaneous populations, as during an averaging saccade task, a large separation between endpoints was observed. Importantly, when the strength of each population was varied in order to simulate a wide range of weighted averaging saccade endpoints, the VA model predicted endpoint distributions along a straight line (solid cyan trace; Figure 26C), while the CM model predicted distributions with curved geometry (solid magenta trace; Figure 26C). Next, we experimentally tested the VA and CM models by examining saccade endpoint distributions elicited from simultaneous and weighted microstimulation of two SC sites. We focused on matching the geometry of the collected distributions to the predictions of each model. We found that nearly every distribution showed a straight geometry in the visual field, a result consistent with the predictions of the VA model.

5.2 METHODS

All procedures were approved by the Institutional Animal Care and Use Committee at the University of Pittsburgh and complied with the guidelines of the Public Health Service policy on Humane Care and Use of Laboratory Animals.

5.2.1 Subjects and Surgical Procedures

Three juvenile, male rhesus monkeys (*Macaca mulatta*) underwent one or more surgeries in a sterile environment and under isoflurane anesthesia. The initial procedure consisted of placing a Teflon-coated stainless steel wire (Baird Industries, Hohokus, NJ) under the conjunctiva of one eye and securing a head-restraint post to the skull. In the second procedure, one cylinder was cemented over a craniotomy. The chamber was placed stereotactically on the skull, slanted posteriorly at an angle of 38° in the sagittal plane. This approach allowed access to both colliculi and permitted electrode penetrations normal to the SC surface. After each surgery, the monkey was returned to its home cage and allowed to fully recover from surgery. Post-operatively, antibiotics and analgesics were administered as indicated in the protocol.

5.2.2 Experimental Procedures and Behavioral Tasks

Visual stimuli, behavioral control, and data acquisition were controlled by a custom-built program that uses LabVIEW architecture on a real-time operating system supported by National Instrument (Bryant and Gandhi 2005). Each animal was trained to sit in a primate chair with its head restrained and a sipper tube was placed near the mouth for reward delivery. The animal was seated inside a dome surrounded by an alternating magnetic field which induces a voltage in the eye coil and thus permits measurement of eye position (Robinson 1963). The animal fixates targets that were projected onto a circular mirror which rear reflects onto the isoluminant wall of the dome. Anti-warping software obtained from Paul Bourke, University of Western Australia, allowed reflections from the mirror to appear undistorted and for distances to be properly transferred onto a curved surface. The monkey sat in the center of the dome which has a radius of 1m and spans ± 150° horizontally and ± 30° vertically of the visual field. A photodetector, positioned outside the animal's field of view, detected the actual time of appearance of visual objects, which was then used to correct for time shifts induced by the projector's refresh rate.

In each experimental session, the animal performed the oculomotor gap task (discussed below) as two platinum iridium microelectrodes (1.0-1.5 MΩ; MicroProbes for Life Science, Inc., Gaithesburg, MD), each inserted into separate guide tubes and mounted on independent X-

Y translation stages connected to hydraulic microdrives (Narashigie, Tokyo, Japan), were individually advanced to the SC. The superficial layer of the SC was first identified by the presence of distinctive bursting of background activity associated with flashes of room lights. The electrode was then driven deeper into the SC until saccadic motor bursts were identified. At this stage, stimulation (40μA, 400Hz) was delivered during the gap period of the oculomotor task to determine the vector coordinates. The depth of the electrode was then minimally adjusted to obtain the shortest possible latency of the stimulation evoked saccade (20 - 40 ms). Train duration was manually set (range: 100-300ms) and always long enough to allow for completion of the stimulation evoked movements. Supra-threshold stimulation parameters were intentionally chosen as weaker settings often yielded non-optimal saccades that exhibited slower velocities and reduced amplitudes (Van Opstal et al. 1990), even with prolonged stimulation durations (Groh 2011; Guillaume and Pélisson 2001; Katnani and Gandhi 2010).

During data collection the animal performed the oculomotor gap task. Each trial began with directing the line of sight to a fixation point for 300-500 ms before it is extinguished. Following a 200-400 ms "gap" interval, during which the animal was required to maintain the same eye position, another stimulus was illuminated in the visual periphery. Incorporation of the gap interval permits fixation to become disengaged prior to saccade preparation, allowing the oculomotor system to be more responsive to stimulation input. Stimulation was delivered during the gap period on a randomly selected 30% of the trials. For 20% of the trials, stimulation was delivered to each electrode individually, collecting site specific saccade vectors; for 10% of the trials stimulation was delivered simultaneously with no temporal shift between the pulses elicited from each electrode, producing a saccade whose amplitude and direction were influenced by the movement generated at each site independently. Stimulation onset occurred 100ms after the offset of the fixation target and, if necessary, presentation of the peripheral stimulus was delayed until after stimulation offset. The animal was required to saccade to this target to earn a liquid reward. Depending on the vector elicited each day, the initial fixation target was controlled to ensure that the evoked movements were not reduced by orbital position effects.

Simultaneous stimulation first occurred with supra-threshold stimulation parameters matched at both electrodes (40μA, 400Hz, 100-300 ms). Distributions spanning a significant portion between the two single site vectors were obtained by weighting the current intensity or frequency through one electrode in increments of 10 μA or 100 Hz while holding the parameters

at the other electrode constant. After incrementing through a sufficient range, the stimulation parameters were once again matched and the weighting was repeated for the second electrode.

5.2.3 Electrical Stimulation

Constant current stimulation trains were generated using a Grass S88X stimulator in combination with Grass PSIU6 isolation units. Trains consist of anodal phase leading, biphasic pulses (0.25 ms). Frequency and current intensity were dictated by each experimental design, typically spanning in the range of 40-80 μA and 400-800 Hz.

5.3 DATA ANALYSIS

Each trial was digitized and stored for off-line analysis. We used a combination of in-house software and Matlab 7.10.0 (R2010a). Horizontal and vertical eye position along with onset and offset times of the stimulation train were stored with a resolution of 1 ms. Component velocities were obtained by differentiating the eye position signal. Onset and offset of stimulation evoked saccades were then detected using a standard 30°/s velocity criteria, respectively.

Regression was used to best fit a straight line to the data and generate a coefficient of determination (R^2) to assess the goodness of fit. It is important to note that data sets that contain almost vertical or horizontal distributions yield R^2 values close to zero. This is a result of the regression analysis, which is not capable of estimating coefficients that can generate a line for distributions that have nearly constant dependent or independent variables. Therefore, the data were rotated in order to assess linearity. To verify that rotation did not affect our results, distributions were rotated systematically (in 5^o increments) and a linear regression was applied for each rotation. This exercise revealed that R^2 values remained relatively invariant to rotation until the distribution reached a purely vertical or horizontal direction. The maximum R^2 value from each distribution is used in the analyses.

5.3.1 Computational Models

The VA and CM schemes are found in literature as computations and/or verbal descriptions used to explain how collicular activity is decoded for saccade generation (Anderson et al. 1998; Van Opstal and Goossens 2008). We reconstructed each model to test their fundamental properties with specific protocols that produce predictions that can be experimentally validated.

The right SC was modeled as a single layer grid of homogeneously distributed cells in millimeter coordinates (u,v). Each cell's vector components (H,V) were defined by exponentially transforming the collicular grid using the equations (Ottes et al. 1986):

$$H = A \cdot e^{\frac{u}{B_u}} \cdot \cos\left(\frac{v}{B_v}\right) - A \qquad (1)$$

$$V = A \cdot e^{\frac{u}{B_u}} \cdot \sin\left(\frac{v}{B_v}\right) \qquad (2)$$

with constant parameters A = 3 deg, B_u = 1.4 mm, and B_v = 1.8 mm.

A population of activity (P) was generated in the SC using a standard bivariate Gaussian equation:

$$P = Fe^{\frac{-(u-u_o)^2+(v-v_o)^2}{2\sigma^2}} \qquad (3)$$

The strength and variance (F = 500 spikes/s and σ = .5 mm) of the population were set by the values reported in Van Gisbergen et al (1987). Outside a radius of 2σ, population activity was set to zero. The population was centered at cells (u_o,v_o), calculated using the horizontal (H_t) and vertical (V_t) component of the desired or input target location (Optican 1995; Ottes et al. 1986):

$$u_o = \frac{B_u}{2} \cdot \log\frac{(H_t+A)^2+V_t^2}{A^2} \qquad (4)$$

$$v_o = B_v \cdot \tan^{-1}\left(\frac{V_t}{H_t+A}\right) \qquad (5)$$

By repeating equations 3-5 another target location could also be incorporated to generate a second, simultaneously active population in the SC. In cases where a portion of each population shared millimeter coordinates, the overlapping activity was summed. If overlapping activity was averaged, as opposed to summed, we found minute differences in the decoded saccade vector (less than a tenth of a degree). Furthermore, neural recordings in the SC have demonstrated that the presence of competing populations can reduce the overall SC activity (Basso and Wurtz 1997; Li and Basso 2005); therefore, we also reduced the firing rate of our overall simulated activity profiles by 40%, in accordance with observations from neural recordings during saccades directed to two targets presented simultaneously (Edelman and Keller 1998). As a result, we observed that the predictions of each model did not change. In order to avoid border effects, all target locations (single or paired) were restricted to visual space that would generate populations completely confined within the SC. Generated populations were then decoded through two different algorithms:

5.3.1.1 CM Computation

$$CM(u_o, v_o) = \frac{\sum_{n=1}^{N} r_n \cdot C_n}{\sum_{n=1}^{N} r_n} \qquad (6)$$

Equation (6) performs an average in uniform millimeter space to find the center of the population that delineates the optimal saccade vector (r_n is the mean firing rate of cell n, and C_n denotes the spatial location (u,v) of each active cell in millimeters). The resulting coordinates (u_o,v_o) calculated from the equation were then exponentially transformed (eqn. 1 & 2) to obtain the saccade vector in visual coordinates.

5.3.1.2 VA Computation

$$\mathrm{VA(H,V)} = \frac{\sum_{n=1}^{N} r_n \cdot \eta \cdot R_n}{\sum_{n=1}^{N} r_n} \qquad (7)$$

Equation (7) first involves exponentially transforming all active cells (eqn. 1 & 2) in order to derive R_n, the vector components (H,V) encoded by active cell n. The weighted vector average of all contributions was then calculated in order to obtain the saccade vector in visual coordinates (Lee et al. 1988; Van Opstal and Goossens 2008).

In addition to weighing each vector contribution with mean firing rate, r_n, a fixed scaling constant, η, was also required. We found that the model yielded accurate responses to a target location of (12^o, 12^o) if η had a value of 0.9768. Once determined, η was fixed for all target locations.

5.3.1.3 Weighing Procedure

As observed in equations 6 and 7, each averaging computation involves a weight defined by the mean firing rate of each cell. In cases where paired target locations were input to each model, the mean firing rate could be manipulated by creating Gaussians with different population strengths. This was accomplished by increasing the strength (F_1) of one population while holding the strength (F_2) of the second population constant:

$$F_1 = w + F, \qquad F_2 = F \qquad (8)$$

where w is an allotted increment of spikes/s. Equation (8) is then repeated where F_2 is varied while F_1 is held constant. A procedure of this manner allows for the models to simulate a wide range of weighted averaging saccades between the input target locations.

5.4 RESULTS

5.4.1 Model Response to Single and Paired Target Locations

Each computational model was simulated with a wide range of single target locations in the first quadrant. The results of the simulations are shown in Figure 26B. Both models are shown to respond to each target location with high accuracy [CM – mean endpoint error 0.0019 degrees (SD: 0.001), VA – mean endpoint error 0.0342 degrees (SD: 0.0273)]. Thus, the saccade endpoints generated from single target locations does not distinguish between the two mechanisms.

Each computation was then performed using two simultaneous target locations. The example shown in Figure 26C illustrates the predictions for the target pair [15°, 15°] and [15°,-15°]. The VA (cyan circles) and CM (magenta circles) endpoint prediction when decoding two simultaneous populations of equal strength are shown to be separated by 5.45°. Next the strength of each population was varied (see methods) to generate a distribution of weighted vector predictions between the target locations. As observed in Figure 26C, the separation between predictions varies due to each model outputting distributions of different geometries. The VA generated a straight distribution (solid cyan) while the CM generated a curved distribution (solid magenta). The straight versus curved predictions were consistent across all input target pairs with the requirement of different directions.

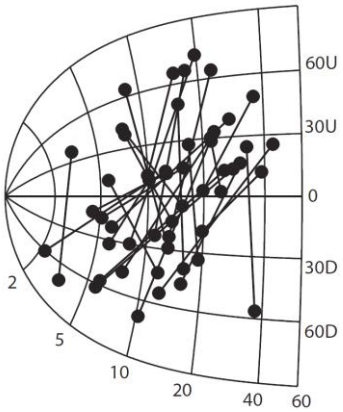

Figure 27. Distribution of paired-stimulation sites
The vector evoked by each site is shown by a black dot and the pair is connected by a line. All 26 paired sites are represented on the SC saccade motor map. Numbers spanning from left to right indicate saccade amplitude. Vertically aligned text (right) denotes saccade direction: U, up; D, down.

5.4.2 Analysis of Stimulation Induced Distributions

A total of 26 stimulation induced vector pairs (Fig. 27) were studied from three monkeys, sampling a portion of the SC vector map that spanned from approximately 2° to 40° in amplitude and approximately -70° to 70° in direction. Collectively, the vector pairs exhibited amplitude differences anywhere between 0° to 30° and directional differences between 25° to 105°. The distribution of endpoints were investigated by systematically varying current intensity (14 sites), frequency (5 sites), or both (7 sites; frequency was held constant while current was varied, and

vice versa), producing a total of 33 pairs for analysis. Two vector pair examples are shown in Figure 28, A and B. The distribution of saccade endpoints were obtained by varying current intensity (Fig. 28A) and frequency (Fig. 28B). We found that varying either parameter produced comparable distributions; therefore, all distributions generated by varying current intensity or frequency, were analyzed for the purposes of this investigation. Superimposed on top of the collected data are the VA and CM predictions simulated with the corresponding vector pairs (cyan and magenta line, respectively).

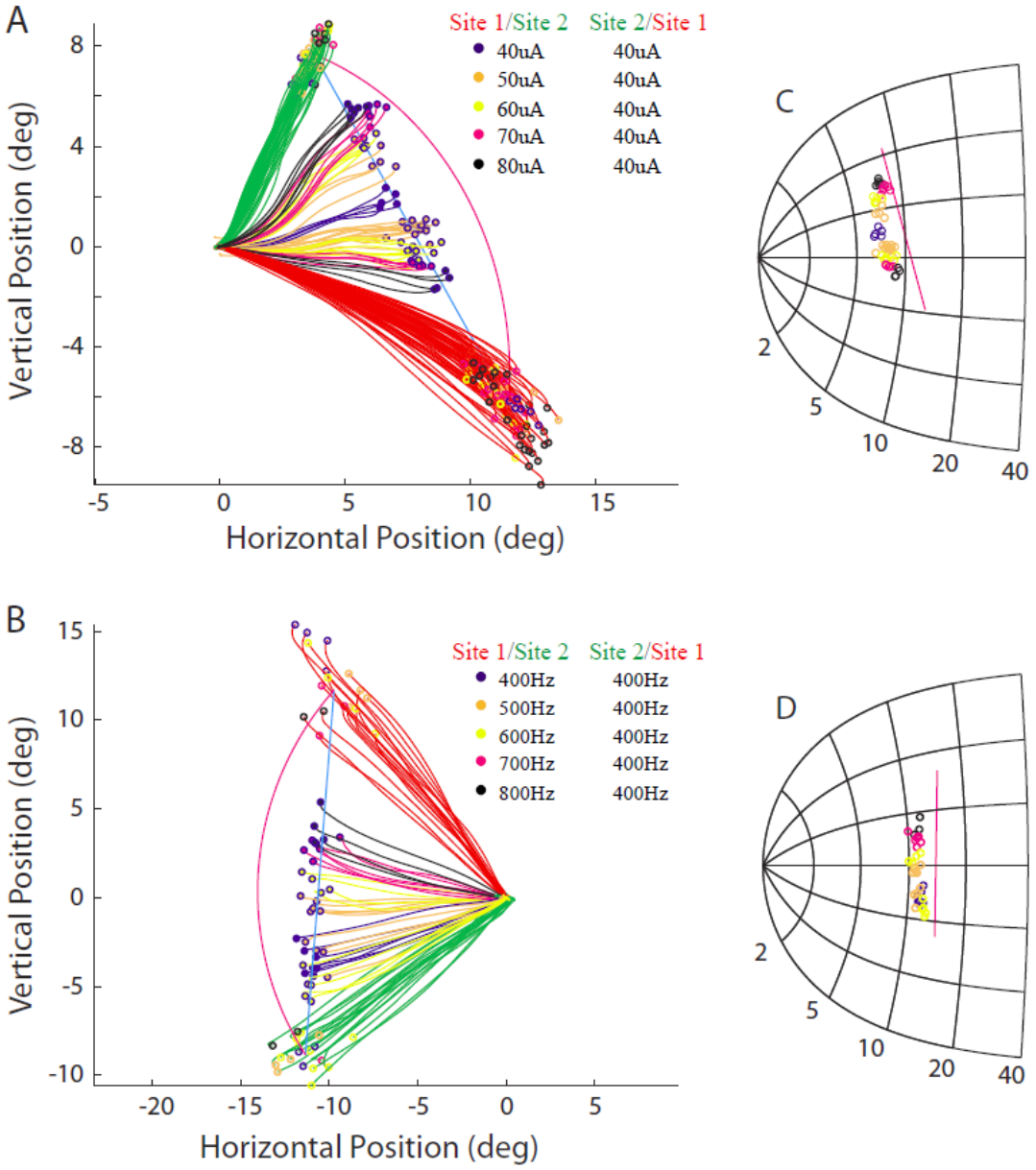

Figure 28. Family of saccades evoked by weighted, simultaneous stimulation of two SC sites **(A, B)** Red and green trajectories represent stimulation of each site separately; blue, orange, yellow, magenta, and black trajectories and endpoints correspond to the saccades generated by paired stimulation of different current intensities in *A* and frequencies in *B* (see key for stimulation parameter values); solid cyan and magenta line represent vector averaging (VA) and center-of-mass (CM) predictions, respectively, when simulated with the corresponding vector pair. *Key*: If the stimulation parameter of site one is being varied (left column) the stimulation parameters at site two are fixed (right column); this procedure is then repeated for site two. As a result, there is a reflection of repeated colors for the elicited saccade vectors when one site is weighed over the other. **(C, D)** Transformation of endpoint distributions into SC coordinates (open blue circle); solid magenta line represents the SC coordinates decoded in the CM model when simulated with the corresponding vector pair.

Figure 28, C and D, illustrates the logarithmic transformation (eqn. 4 & 5) of each collected endpoint into SC coordinates. By performing this transformation we observe the center of each active population in the SC that would generate such endpoints. For comparison, the geometry of the computed population centers decoded by the CM model when simulated with the corresponding vector pair is also shown in the figure (magenta line). Note, that when the strength of each population is varied within the CM model, the decoded population center shifts on a straight line between the two SC coordinates set by the input vector pair. Thus, the VA and CM models generate predictions on a straight line (cyan line in Fig. 28, A and B; magenta line in Fig. 28, C and D) in different domains (visual versus SC coordinates). To assess which decoding mechanism is more likely the candidate to produce the observed data, we performed a linear regression (see Methods) on the endpoint distribution in visual space (e.g., Fig. 28A) and on the same distribution transformed into SC coordinates (e.g., Fig. 28C). Figure 29 illustrates the comparison of R^2 values in each domain across all collected vector pairs. Almost all values lie above unity indicating a significantly (t-test, $p = 3.04e^{-4}$) better representation of linearity in visual space. The significance of the result suggests that averaging occurs within visual coordinates as almost all distributions had strong linear fits in visual space. Although a large portion of values also demonstrate good linear fits in SC coordinates, this does not detract from the fact that the geometry of the collected endpoint distributions showed little to no curvature in visual space (as would be predicted by a CM model).

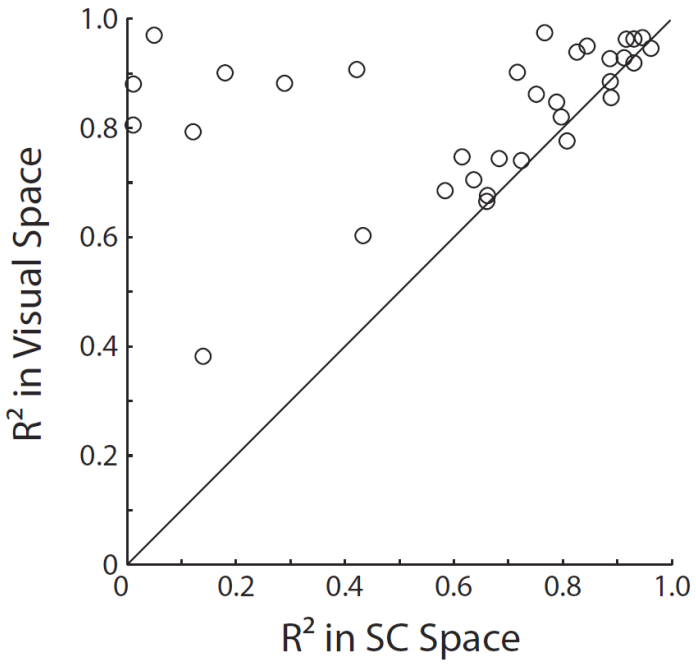

Figure 29. Comparison of endpoint distributions in visual and SC coordinates
R2 values (open circles) derived from linear regressions performed on saccade endpoint distributions in visual space (y-axis) and when transformed into SC coordinates (x-axis). Solid line represents unity line.

Visual assessment of the data in SC coordinates indicated the presence of curvature even for distributions with high R^2 values from the linear regression analysis. For example, the regression on the distribution shown in Figure 30A, resulted in an R^2 value of 0.9124; however, one can clearly observe curvature in the data. Therefore, we developed an index of curvature (IC) analysis to quantify any curvature within the distributions in visual space and when transformed into SC coordinates. The analysis involves performing a two-dimensional average on the distribution of points in order to obtain a description of its geometry (dashed black line; Fig. 30A). Points along the fit geometry were then projected onto a straight line that connected the ends of the overall distribution (line labeled *b*). The curvature of the data was then quantified by selecting the projection of maximum magnitude (line labeled *a*) and dividing it by the magnitude of *b*. A noteworthy piece of information is that the two-dimensional average did not generate perfect geometry descriptions due to noise in the data. Thus, distributions that show no curvature still generated non-zero IC values due to the geometric fit not perfectly overlapping with the straight line that connects the ends of the distribution. To ensure that projections signified actual deviation from straight geometries and were not just a result of noise in the data, all selected magnitudes were classified according to the variance of the data. Magnitudes that did

not exceed at least one standard deviation from the two-dimensional average fit were classified as insignificant. The amount of curvature recorded from each distribution when in visual space versus SC coordinates is shown in Figure 30B. The solid squares represent insignificant curvature values in both coordinate domains. The open circles represent insignificant curvature values in visual space, but significant curvature values in SC coordinates. Almost all values lie below the unity line demonstrating that a significant (t-test, $p = 2.13e^{-10}$) amount of curvature is introduced into the distribution when transformed into SC coordinates. Furthermore, all values are insignificant in visual coordinates, reinforcing that distributions in the visual field are relatively straight. A result of this manner contradicts the predictions of the CM model.

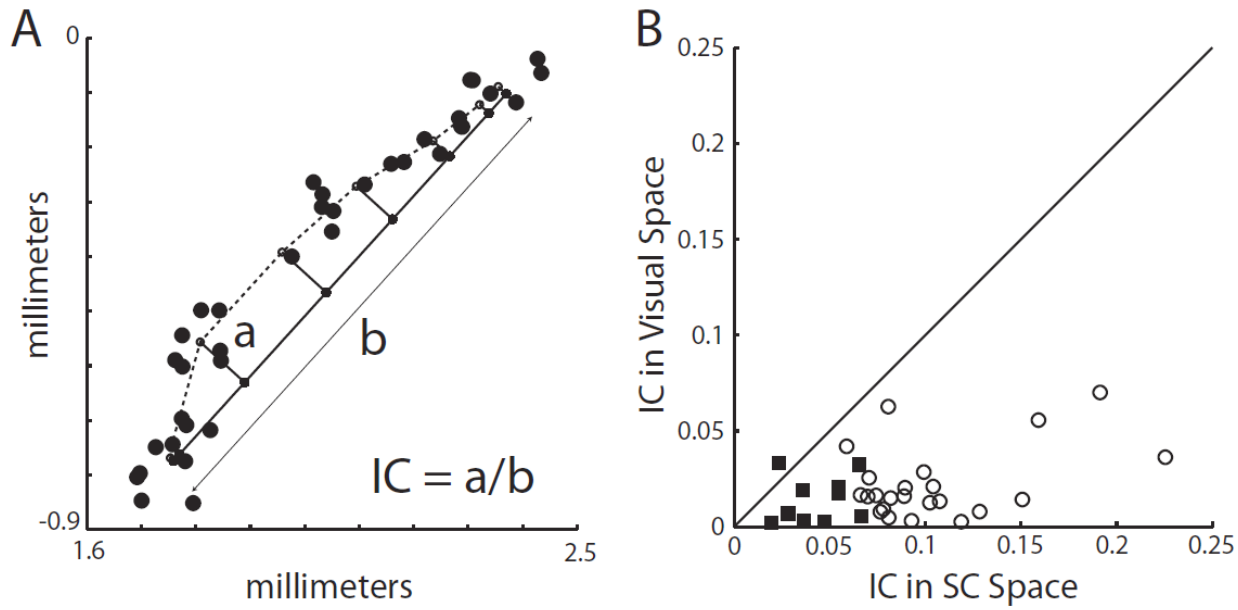

Figure 30. Comparison of index of curvature (IC) values in visual and SC coordinates
(A) Example of IC derivation on transformed endpoint distribution (large black dots) in SC coordinates. Dashed line represents geometry fit; solid line (b) represents straight path between the overall ends of the distribution; small black dots with connecting lines represents projections from the geometry fit to straight path. The IC value is computed as the maximum projection length (a) divided by (b). **(B)** IC values derived from analysis on saccade endpoint distributions in visual space (y-axis) and when transformed into SC coordinates (x-axis). Solid line represents unity line; solid squares represent insignificant IC values in both visual and SC coordinates; open circles represent significant IC values in SC coordinates and insignificant IC values in visual coordinates.

5.5 DISCUSSION

Early studies revealed that the SC contains a logarithmically distributed map in visual coordinates, a result which requires its motor commands to be exponentially transformed for saccade vectors to conform to visual space (Sparks 1986). The nature of this conversion causes the output of an averaging scheme to become dependent on whether its computation occurs before or after the exponential transformation. VA and CM mechanisms, therefore, carry different interpretations for decoding eye movements. We stress this difference due to the observation that an averaging computation is often considered an acceptable decoding method, yet statements of this manner are generally qualitative and noncommittal on the implementation strategy (e.g., Sooksawate et al. 2011). And although there is a significantly different result to each sequence, the two schemes are commonly classified under the umbrella of population vector averaging. We simulated both VA and CM models with two simultaneous populations of activities and found that they predict different saccade endpoint distributions. Specifically, differentially weighing the two populations produce endpoint distributions that reside on a straight line in the VA model but conform to a curved geometry in the CM model (Fig. 26C). These predictions were tested by examining the distribution of weighted averaging saccade endpoints through simultaneous stimulation of two sites in the SC. Regression of the data revealed good linear fits in the visual field, as predicted by the VA decoding sequence. Furthermore, when endpoint distributions were log-transformed into SC coordinates, we found that the millimeter coordinates calculated by the CM model did not align well with the coordinates of the transformed data. Therefore, we conclude that our results favor the networked sequence of decoding that is implicit to the VA model.

5.5.1 Neural Implementation of Decoding Mechanisms

Implementation of both VA and CM mechanisms requires two steps: decoding population activity using a normalization (averaging) based algorithm and an exponential transformation to align movements in visual coordinates. While physiological and theoretical evidence for normalization has been provided in various systems such as visual cortex of

primates (Carandini and Heeger 1994) and olfactory processing in the locust (Papadopoulou et al. 2011b), a neural correlate in the saccadic system has been elusive. A vector summation algorithm that does not require normalization has been proposed as an alternate mechanism for decoding SC activity (Goossens and Van Opstal 2006; Van Gisbergen et al. 1987); this mechanism is discussed below.

Projections from the SC to the burst generator are weighted according to the site of origin (Moschovakis et al. 1998). Specifically, the efficacy of the projections increases for neurons originating from regions encoding increasingly larger amplitude vectors. This trend in projection weights conforms to the transformation needed to convert saccade commands into visual coordinates and, at least qualitatively, is consistent with the requirements of the VA mechanism. However, it should be noted that the monotonic increase in weight is not equivalent to the exponential relationship required of the VA algorithm.

Neural implementation of the CM mechanism is potentially more complicated and is not explicitly supported by our data. Nevertheless, we speculate on potential schemes. Let's first consider decoding saccade metrics from a single active region in the SC, such as activation resulting from a single target. The reconstruction of a population response from neural recordings in the SC has demonstrated that activity is well represented by a static Gaussian mound that rises and falls (Anderson et al. 1998). In this manner, the cells at the center of the active population will have the highest firing rate and the longest burst duration. Therefore, one such implementation may be that the center cells are the only significant representation of the intended saccade vector (Van Opstal and Kappen 1993). Another pivotal feature is that because CM decoding occurs before the exponential transformation, another explicit transformation would be needed to properly generate saccades in the visual field. Such an operation could be performed in the cerebellum and/or the nucleus reticularis tegmenti pontis, to which the SC projects heavily (Harting 1977; Huerta and Harting 1984; Scudder et al. 1996) and whose functional role in processing SC activity is still unclear.

The CM mechanism is most prominent not as the primary saccadic decoding mechanism but rather when implemented prior to population decoding in-order to explain a neural correlate for the generation of regular-latency averaging saccades (Arai et al. 1994; Glimcher and Sparks 1993). Presiding through the use of lateral interactions, a CM correlate occurs when a mass distribution of activity, resulting from multiple visual stimuli, can form a single population at an

intermediate location in the SC. The single population can then be deciphered through a different mechanism (e.g., VA and VS). Nevertheless, we demonstrate in this investigation that implementing a process of this nature generates non-intuitive results (see: relation to averaging saccade mechanisms). It seems more reasonable to speculate that lateral interactions in the SC manipulate the spatial and temporal register of activity to form broad population profiles (Edelman and Keller 1998) that allows for the incorporation of information from the visual stimuli. Therefore, one must be cautious when describing and/or using an averaging scheme to explain saccade generation, as the implementation is important for appropriately characterizing decoding properties in the oculomotor system.

A vector summation model could also be a plausible candidate to contrast with the CM model. This computation also assumes a sequence in which the decoding operation occurs after the neural activity has been exponentially transformed, but stipulates that the weighted vector contribution of each neuron in the active population is summed and not normalized (Goossens and Van Opstal 2006; Van Gisbergen et al. 1987). Furthermore, when the computation incorporates spatial interactions in the SC the model can predict stimulation induced activity patterns and produce saccade vector predictions that align with the VA model (Van Opstal and Van Gisbergen 1989). Interestingly, the model's predicted discharge patterns correspond nicely with the neural activity correlated to express latency averaging saccades. Therefore, the neural mechanism described by a VS model could also be a likely candidate to explain decoding SC activity, and does not alter the finding that decoding occurs after exponential transformation. We chose to limit our focus on the VA model due to its loose interpretation with the CM model.

5.5.2 Relation to Averaging Saccade Mechanisms

Edelman and Keller's (1998) examination of averaging saccades of express latencies in a two target task revealed that activity in the deeper layers of the SC best matches the profile of two simultaneous populations corresponding to the two visual targets. Therefore, the discharge of neurons was centered at loci corresponding to the paired target locations and not the site encoding the elicited saccade vector. Their finding exemplifies the reflexive nature of the task which allows visual activity to be immediately pipelined to the motor layers (Dorris et al. 1997).

We simulated these findings (Fig. 31A) to distinguish between the VA and CM mechanisms and found results that conform to the predictions of the VA hypothesis.

Averaging saccades can also be generated at regular (non-express) reaction times. How is activity distributed across SC neurons for this subset of movements? Glimcher and Sparks (1993) suggested that the initial visual activity dependent on target configuration is processed to generate a single population centered at an intermediate location. To simulate this finding a target pair location was chosen and equation (6) was first used to determine an intermediate coordinate location (u_o,v_o) between the two simultaneous populations generated from the input target pair. Next equation (3) was used to generate a single population at the calculated coordinates (u_o,v_o). Finally, the VA computation as stated in the methods was used to decode the single population and output a saccade vector. Interestingly, we found that simulations of our model generated saccade vectors that overshot a vector average in visual coordinates (Fig. 31B). Furthermore, when the strength of each population was varied incrementally we discovered that the model predicted endpoints that lie on the curved geometries that matched those of the CM model (magenta trace). This result is a consequence of the required CM decoding needed to calculate the intermediate location of the single population.

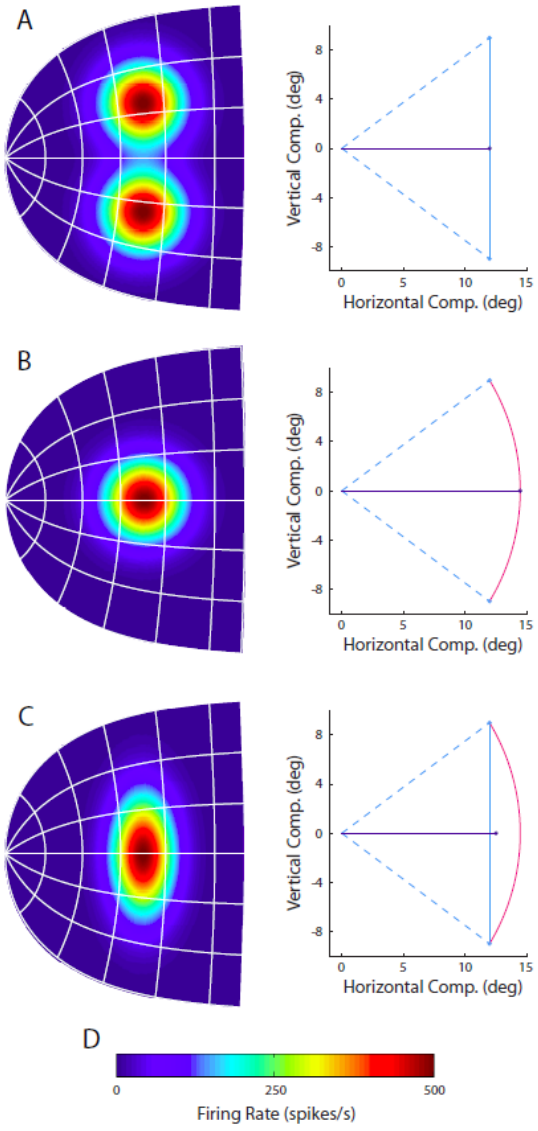

Figure 31. Simulations of the VA model to account for the generation of averaging saccades **(A)** (Left) Two, equal strength populations of active neurons positioned at sites encoded by a chosen target pair location (12o,12 o) and (12 o,-12 o).(Right) Solid blue line represents the saccade vector prediction generated by the VA model when decoding the simultaneous activity distributions. Dashed cyan lines represent single site vector prediction generated when each population is decoded separately. Solid (vertical) cyan line represents the geometry of the VA model predicted by differentially weighing the two populations. **(B)** (Left) Single population of activity formed at an intermediate location between the two populations shown in *A* (see: relation to averaging saccade mechanism). The width of this population is identical to those used for saccades directed to a single target. (Right) Solid blue line represents the VA saccade output when decoding this population activity. Solid magenta line represents the geometry of the endpoints generated by the VA model as the spatial center of the population shifts from one target location to the other. **(C)** (Left) Population activity centered at an intermediate location between the populations shown in *A* but with broad directional spread. The two dimensional variance of this population is conceptual and was manually set to simulation the broad activity profiles reported in Edelman and Keller (1998). (Right) Solid blue line represents saccade output from the VA model when decoding this activity. Note that its endpoint falls much closer to the output predicted by averaging vectors in visual space (cyan trace). **(D)** Color scale represents the firing rate (spikes/s) of population activity shown in the left hand column.

Research and computational models that use the CM mechanism to explain and simulate averaging saccades will generate vectors that overshoot the expected weighted average (Arai et al. 1994). The hypermetric movements simulated by this architecture do not conform to experimental findings. Other studies have reported that SC activity during regular latency averaging saccades exhibits a representation that is intermediate between two target-activated populations and a single saccade-related ensemble (Edelman and Keller 1998; Van Opstal and Van Gisbergen 1990). We simulated the VA model (Fig. 31C) with the incorporation of widespread SC activity (the population profile was manually altered to mimic the findings discussed in Van Opstal and Van Gisbergen 1990; Edelman and Keller 1998) and found that the VA model indeed produces vector predictions closer to observed averaging saccades. This would imply that although averaging saccades of regular reaction times do not exactly match the profile of two simultaneous populations, the activity remains broad enough to incorporate sufficient information from the target configuration, allowing the decoding mechanism to generate saccades that land near or in-between the visual stimuli.

Averaging saccades of express and regular latencies not only differ in their spatial distribution of activity but also have been shown to have different dynamics, where the firing rates at express latencies are much lower (Edelman and Keller 1998). We simulated whether a reduction in SC activity would affect our model predictions. Accordingly, we reduced the output firing rate patterns of each model by 40%. The averaging saccade predictions from the VA and CM models were similar for the attenuated and intact activity profiles (not shown). We anticipated this conclusion as both models derive the metrics of saccades with an averaging formula that relies on the spatial distribution of activity and not the level of activity. We recognize that such a method is probably too simplistic to describe neural mechanisms; however, the crude approximation of an averaging scheme does resemble the data allowing for a sufficient investigation of decoding sequence. Furthermore, we cannot assume that supra-threshold stimulation induces low levels of neural activity such as during averaging saccades at express latencies, yet stimulation still elicits averaging saccade endpoints that qualitatively match naturally evoked averaging saccades. Van Opstal and Van Gisbergen (1989) proposed a potential method for predicting patterns of dual stimulation activity; however, the paper focused only on current-distance activation. Additional research is needed to determine how a large range of both current intensity and frequency stimulation induces neural activity in the SC.

5.5.3 Interpretation of Stimulation Results

The use of supra-threshold stimulation parameters likely drives SC neurons at a high frequency and corrupts the time scale necessary for networked neurons to interact. Therefore, our experimental technique for generating distributions of weighted averaging saccade endpoints may bypass the network necessary to observe the results of a CM mechanism. Nevertheless, under the assumption that stimulation only activates the output of the SC, our data still implies that there is a system that is fully capable of producing weighted averaging movements (i.e., transformation before decoding), regardless of the brute force stimulation technique. The weighted projections from the SC to the burst generator (see discussion above; Moschovakis et al. 1998) suggest that the transformation occurs downstream of the SC. However, it is important to recognize that ascending outputs of the SC could also contribute to the transformation. For example, stimulation of the deep layers could activate neurons in the superficial layers (Isa and Hall 2009; Vokoun et al. 2010), which in turn could recruit the intraparietal cortex via the pulvinar (Clower et al. 2001). Neurons in the deep SC layers could also recruit the frontal eye fields via the mediodorsal thalamus (Sommer and Wurtz 2004). In addition, these and other oculomotor areas with direct projections to the SC could be activated antidromically. We speculate that structures activated through the ascending output are not likely to exert a role in producing SC stimulation-evoked saccades because their inactivation does not produce deficits in mediating motoric control (Sommer and Wurtz 2002; Wilke et al. 2010). Furthermore, the primary FEF output pathway involved in saccade generation is likely relayed through the SC (Hanes and Wurtz 2001), and the same could be true for other cortical regions. These results collectively imply that saccades evoked by SC stimulation are primarily mediated through descending outputs to the brain stem.

We must assume that current intensity primarily influences the spatial extent of activation, and frequency mainly controls the temporal features of activity (McIlwain 1982; Ranck 1975; Tehovnik 1996; Vokoun et al. 2010). From an experimental perspective, our data demonstrate that current intensity versus frequency generates comparable averaging saccade distributions. We speculate that this result could be due to using stimulation parameters in the supra-threshold range, where spatial and temporal integration mechanisms may become functionally equivalent. Another possible explanation could arise from the intrinsic properties of

the SC, which could shape stimulation induced activity to maintain features of naturally generated discharge patterns. Further investigation is needed to elucidate how stimulation evokes activity in the SC (Katnani and Gandhi 2010). From a modeling perspective, our simulations vary population strength by changing the firing rate or level of activity, thus, aligning with the assumptions behind how stimulation frequency induces activity. To observe the effects of current intensity we also simulated each model by varying the width (σ) of the population as opposed to the firing rate. We found that the saccade vector predictions of the CM model only significantly changed with population widths that generated drastic border effects ($\sigma > 1.5$ mm). In contrast, the VA predictions changed well before border effects due to the non-linear nature of the SC saccade vector map. To resolve such an issue the model's scaling constant (see Methods) must change along with the population width. Nevertheless, regardless of any change in the derived saccade vectors, the geometry of the predicted saccade distributions from each model always remained the same. This is an important result as the focus of this study is not to distinguish the properties of decoding mechanisms in the SC, but to probe the order of operations which occur during saccade generation.

Lastly, we cannot assume that dual microstimulation induces patterns of activity in the SC that matches visually-evoked activity; however, since our stimulation induced endpoint distributions qualitatively match visually guided averaging saccade endpoint distributions (Chou et al. 1999; Edelman and Keller 1998; Glimcher and Sparks 1993; Van Opstal and Van Gisbergen 1990), it seems reasonable to assume that the order of operations that occurs (exponential transformation then decoding), whether driven by stimulation or visual targets, is similar.

5.5.4 Previous Studies Using Dual Microstimulation in the Oculomotor System

Assessment of vector averaging in the oculomotor system through dual microstimulation is limited. Dual microstimulation studies in the 1960's and 70's (Robinson 1972; Robinson and Fuchs 1969; Schiller et al. 1979) were typically sub-experiments resulting in a qualitative assessment of the elicited saccades and nothing more than a single illustration. In fact, stimulation-induced vector averaging in the SC has only been briefly reported in one

investigation of the colliculus (see Figure 5 in Robinson 1972), where weighted vector averaging was not quantified and no alternate mechanisms to account for the observed saccade patterns were considered. Recent dual microstimulation experiments in the oculomotor system have employed temporal shifts between the stimulation trains elicited at each electrode. Noto and Gnadt (2009) evaluated the generation of curved saccades, while Brecht et al (2004) attempted to differentiate between VA and VS. Our analysis of endpoint distributions provides a systematic and in-depth analysis of the long standing but poorly tested weighted vector averaging hypothesis, which is necessary to link averaging saccades across literature in the oculomotor field.

6.0 CONCLUSION

6.1.1 Summary

When immersed within a visual environment with many potential stimuli, the oculomotor system must undergo a series of processes to appropriately control eye movement behavior. From the standpoint of the superior colliculus (SC) these processes can be generalized into transforming sensory information into a motor command that provides the proper spatial and temporal patterns of activity to drive an accurate eye movement. The laboratory paradigm used to understand the details of collicular function, usually involves presenting multiple visual stimuli, in which either free behavior or a specific task is instructed (e.g., saccade to a specific stimulus). Typically, single unit neurons in the SC are recorded during the task to determine the patterns of activity associated with the generated behavior. Although such work has been monumental in advancing knowledge on oculomotor control, there is still a great deal of clarity needed in the field. The saccadic system is considered ballistic-like in the sense that relatively invariant motor commands in the SC produce stereotypical saccades. The minimal amount of observed variability makes it difficult to establish a relationship for characterization, thereby making it difficult to understand emerging and significant features in motor decoding. As a result, there is a longstanding controversy on how population activity in the SC is integrated and decoded to produce an eye movement. Previous investigations have employed perturbations during their experimental paradigm (i.e., inactivation, air-puffs; Goossens and Van Opstal 2000b; Lee et al. 1988) in an attempt to generate variability in the saccadic system and test potential neural mechanisms for decoding. Nevertheless, a definitive neural substrate for motoric control in the oculomotor system remains elusive. In a different respect, but along the same lines, the order of operations that occur during the generation of a saccade is also not well-defined. As a result, there exists a disunited understanding of the implementation strategy for saccadic motor

control. We have attempted to contribute to the understanding of these obscure concepts through the use of neural stimulation in the SC. We utilize varying levels of microstimulation to diverging from the natural processes of the saccadic system. By manually inducing activation patterns, we can forcibly evoke variable behavior in order to make inference on the properties of the neural system that generated such behavior. In doing so, we have provided insightful information on the processes of motor control in the saccadic system.

In our first study we present the results of a controlled systematic microstimulation experiment to provide important insights into the mechanisms underlying saccade generation. Our results demonstrate that activity induced for motor control in the saccadic system reflects a greater sensitivity to the temporal, as opposed to the spatial, features of activity. Furthermore, integration of the temporal profile was found to be critical in generating the proper neural command to define the optimal metrics and kinematics of eye movements, while the spatial distribution seemed to impact the strength of the command. The overall result contributed to understanding the significance of distributed activity features in saccade generation. In the second study, we differentiate between two controversial models that have dominated the oculomotor field in hypothesizing the proper mechanism for deciphering SC activity: vector averaging and vector summation. Our results demonstrate that both models are insufficient to account for the observed data, revealing that additional network properties (i.e., dynamic intracollicular interaction, saccadic gating) are needed to properly describing motor decoding. Furthermore, we perform a supplementary experiment that probed the potential contribution of these properties, specifically the gating of the saccadic system, by combining reflexive blinks with microstimulation. The result, although not exclusively, favored a summation mechanism, which collectively, with our work (Katnani et al. 2012) and other evidence (Goossens and Van Opstal 2006; Groh 2001; Groh 2011; Van Opstal and Goossens 2008), strongly supports vector summation and provides a level of clarification to the longstanding controversy. In the final study, we define whether decoding occurs before or after exponential transformation. By simulating the two sequences and then experimentally verifying their predictions, we demonstrate that decoding occurs after transformation. The finding unifies the decoding implementation across the oculomotor field. Moreover, a definitive order of operations elucidated how distributed neural activity, representing multiple visual stimuli, is processed into a single motor command. The contribution is significant for two reasons. The first is that the

proposed process establishes a new line of thought that counters the previously cemented ideals. The second is that the process incorporates dynamic intracollicular interactions, again demonstrating the need for integrating additional network properties in understanding neural mechanisms for motor decoding (also discussed in our second study).

6.1.2 Limitations and Future Direction

Although neural stimulation is a favorable technique used to characterize brain areas with behavior, the methodology is not without its limitations. It is not well-known how electrical stimulus influences the activation and propagation of spatial and temporal features of neural activity. Thus to draw inferences about the function of a neural system based on stimulation-evoked behavior, one must make assumptions and therefore have a marked amount of uncertainty. Cutting edge techniques, such as voltage dye and optogenetics may help to resolve this issue by providing a method in which stimulation-induced activity can be visualized. Indeed, both techniques in cortical and sub-cortical tissue have already generated some interesting results (Diester et al. 2011; Histed et al. 2009; Vokoun et al. 2011). Another potential avenue to remedy the limitations of neural stimulation could be mediated through neural field models. The objective would be to use an experimental database, such as the one generated in our first study, to characterize the intrinsic connectivity of a neural network. Simulations of the model with stimulation-induced activity should then generate behavior that resembles those obtained experimentally. A fully functional model of this nature could be used to predict the spatial and temporal profile of induced activity, to test decoding mechanisms, and to reveal emerging properties in the neural network. Nevertheless, the effects of microstimulation and the properties of a neural network depend on the neutrophil of the brain area being study. A number of models already exist for certain sub-cortical and cortical areas in the brain (Butson et al. 2007; Kawato et al. 1987; Markounikau et al. 2010; McIntyre et al. 2006; Wennekers 2002) and have helped to advance the study of motor control. A well-developed model of the collicular network trained on microstimulation results does not yet exist. The quantified results generated in our first study would provide a suitable database for the development of such a model, which would be an interesting area for future research.

Microstimulation is the not only methodology worth pursuing to understand motor control. Neural recording is a more elegant and faithful technique that is vital to understanding mechanisms for decoding. Future research that can design clever paradigms that naturally generate behavioral variability (i.e., reflexive tasks with multiple targets) will be extremely beneficial; as such experiments avoid the insertion of motor signals that may mask certain functions of neural substrates. However, a limitation to neural recording in the SC exists due to the structures depth in the brain, which prevents multi-unit recording. Single-unit studies do not fully capture network properties and therefore lend themselves vulnerable to assumption, albeit much less than microstimulation. Nevertheless, the ability to record multiple neurons simultaneously in superficial motor areas in cortex (i.e., FEF, M1, PMd) provides a reference for future collicular studies. Integrating concepts from such areas may help to design specific experiments for the saccadic system that can test for common traits and reveal canonical properties.

6.1.3 Final Thoughts

Understanding the neural processes that allow us to appropriately control behavior is an important area for research. With current day advancements in technology, the application of such knowledge will be crucial to improving health care and quality of life. For example, neuroprostheses are assistive devices that compensates for loss of motor function through a brain-machine interface (BMI). Another example stems from deep brain stimulation (DBS), which utilizes electric stimulation in sub-cortical motor areas to restore proper motor function. The viability of these therapeutic treatments relies heavily on the understanding of neural function in motor control. The work in this thesis contributes to that knowledge by assessing the functions of the oculomotor system. The constrained neural network has been thoroughly studied and provides an advantageous testing ground to understand motor function with limited complexity. Accordingly, many concepts have translated from the saccadic system to benefit research in other brain areas such as motor cortex and basal ganglia, which are prime areas of focus for BMI and DBS work. The integration and combination of research and concepts across all motor systems will be crucial in advancing these applications. In the pursuit of that goal,

however, we must realize that the complexity of combining technology with our understanding of the brain will only continue to grow. As a result, collaboration and standardization is needed in order to cause a significant impact that will not only cause short term but also long term benefit for growth.

BIBLIOGRAPHY

Anderson RW, Keller EL, Gandhi NJ, and Das S. Two dimensional saccade-related population activity in superior colliculus in monkey. *J Neurophysiol* 80: 798-817, 1998.

Arai K, Keller EL, and Edelman JA. Two-dimensional neural network model of the primate saccadic system. *Neural Networks* 7: 1115-1135, 1994.

Arai K, McPeek RM, and Keller EL. Properties of saccadic responses in monkey when multiple competing visual stimuli are present. *J Neurophysiol* 91: 890-900, 2004.

Badler JB and Keller EL. Decoding of a motor command vector from distributed activity in superior colliculus. *Biol Cybern* 86: 179-189, 2002.

Basso MA and Wurtz RH. Modulation of neuronal activity by target uncertainty. *Nature* 389: 66-69, 1997.

Behan M and Kime NM. Intrinsic circuitry in the deep layers of the cat superior colliculus. *Vis Neurosci* 13: 1031-1042, 1996.

Berthoz A, A G, and J D. Some collicular efferent neurons code saccadic eye velocity. *Neurosci Lett* 72: 289-294, 1986.

Box G. The exploration and exploitation of response surfaces: some general considerations and examples. *Biometrics* 10: 16-60, 1954.

Box G, Connor L, Cousins W, Davies O, Himsworth F, and Sillitto G. The design and analysis of industrial experiments. *Oliver and Boyd*, 1953.

Brecht M, Singer W, and Engel AK. Amplitude and direction of saccadic eye movements depend on the synchronicity of collicular population activity. *J Neurophysiol* 92: 424-432, 2004.

Bryant CL and Gandhi NJ. Real-time data acquisition and control system for the measurement of motor and neural data. *J Neurosci Methods* 142: 193-200, 2005.

Butovas S and Schwarz C. Spatiotemporal effects of microstimulation in rat neocortex: a parametric study using multielectrode recordings. *J Neurophysiol* 90: 3024-3039, 2003.

Butson CR, Cooper SE, Henderson JM, and McIntyre CC. Patient-specific analysis of the volume of tissue activated during deep brain stimulation. *Neuroimage* 34: 661-670, 2007.

Büttner U and Büttner-Ennever JA. Present concepts of oculomotor organization. In: *Neuroanatomy of the Oculomotor System*, edited by Büttner-Ennever JA. Amsterdam: Elsevier, 1988, p. 3-32.

Carandini M and Heeger DJ. Summation and division by neurons in primate visual cortex. *Science* 264: 1333-1336, 1994.

Carpenter RH, Reddi BA, and Anderson AJ. A simple two-stage model predicts response time distributions. *J Physiol* 587: 4051-4062, 2009.

Chou IH, Sommer MA, and Schiller PH. Express averaging saccades in monkeys. *Vision Res* 39: 4200-4216., 1999.

Clower DM, West RA, Lynch JC, and Strick PL. The inferior parietal lobule is the target of output from the superior colliculus, hippocampus, and cerebellum. *J Neurosci* 21: 6283-6291, 2001.

Cohen B and Komatsuzaki A. Eye movements induced by stimulation of the pontine reticular formation: evidence for integration in oculomotor pathways. *Exp Neurol* 36: 101-117, 1972.

Cohen M and Newsome W. What electrical microstimulation has revealed about the neural basis of cognition. *Curr Opin Neurobiol* 14: 169-177, 2004.

Coren S and Hoenig P. Effect of non-target stimuli upon length of voluntary saccades. *Percept Mot Skills* 34: 499-508, 1972.

Cynader M and Berman N. Receptive-field organization of monkey superior colliculus. *J Neurophysiol* 35: 187-201, 1972.

Diester I, Kaufman MT, Mogri M, Pashaie R, Goo W, Yizhar O, Ramakrishnan C, Deisseroth K, and Shenoy KV. An optogenetic toolbox designed for primates. *Nat Neurosci* 14: 387-397, 2011.

Dorris MC, Paré M, and Munoz DP. Neuronal activity in monkey superior colliculus related to the initiation of saccadic eye movements. *J Neurosci* 17: 8566-8579, 1997.

Edelman JA and Keller EL. Dependence on target configuration of express saccade-related activity in the primate superior colliculus. *J Neurophysiol* 80: 1407-1426, 1998.

Furuya N and Markham CH. Direct inhibitory synaptic linkage of pause neurons with burst inhibitory neurons. *Brain Res* 245: 139-143, 1982.

Gandhi NJ. Interactions between gaze-evoked blinks and gaze shifts in monkeys. *Exp Brain Res* 216: 321-339, 2012.

Gandhi NJ, Barton EJ, and Sparks DL. Coordination of eye and head components of movements evoked by stimulation of the paramedian pontine reticular formation. *Exp Brain Res* 189: 35-47, 2008.

Gandhi NJ and Bonadonna DK. Temporal interactions of air-puff evoked blinks and saccadic eye movements: Insights into motor preparation. *J Neurophysiol* 93: 1718-1729, 2005.

Gandhi NJ and Katnani HA. Motor Functions of the Superior Colliculus. *Annu Rev Neurosci* 34: 203-229, 2011.

Georgopoulos A, Schwartz A, and Kettner R. Neuronal population coding of movement direction. *Science* 233: 1416-1419, 1986.

Glimcher PW and Sparks DL. Representation of averaging saccades in the superior colliculus of the monkey. *Exp Brain Res* 95: 429-435, 1993.

Gnadt JW, Lu SM, Breznen B, Basso MA, Henriquez VM, and Evinger C. Influence of the superior colliculus on the primate blink reflex. *Exp Brain Res* 116: 389-398., 1997.

Godijn R and Theeuwes J. Programming of endogenous and exogenous saccades: evidence for a competitive integration model. *J Exp Psychol Hum Percept Perform* 28: 1039-1054, 2002.

Goossens H and Van Opstal A. Optimal control of saccades by spatial-temporal activity patterns in monkey superior colliculus. *PLoS Computational Biology*, in press, 2012.

Goossens HH and Van Opstal AJ. Blink-perturbed saccades in monkey. I. Behavioral analysis. *J Neurophysiol* 83: 3411-3429, 2000a.

Goossens HH and Van Opstal AJ. Blink-perturbed saccades in monkey. II. Superior colliculus activity. *J Neurophysiol* 83: 3430-3452, 2000b.

Goossens HH and Van Opstal AJ. Dynamic ensemble coding of saccades in the monkey superior colliculus. *J Neurophysiol* 95: 2326-2341, 2006.

Graziano MS, Taylor CS, and Moore T. Complex movements evoked by microstimulation of precentral cortex. *Neuron* 34: 841-851, 2002.

Grill W and Mortimer J. Stimulus Waveforms for Selective Neural Stimulation. *IEEE Eng Med Biol* 14: 375-385, 1995.

Groh JM. Converting neural signals from place codes to rate codes. *Biol Cybern* 85: 159-165., 2001.

Groh JM. Effects of initial eye position on saccades evoked by microstimulation in the primate superior colliculus: implications for models of the SC read-out process. *Frontiers in Integrative Neuroscience* 4, 2011.

Guillaume A and Pélisson D. Gaze shifts evoked by electrical stimulation of the superior colliculus in the head-unrestrained cat. I. Effect of the locus and of the parameters of stimulation. *Eur J Neurosci* 14: 1331-1344, 2001.

Guo Y, Rubin JE, McIntyre CC, Vitek JL, and Terman D. Thalamocortical relay fidelity varies across subthalamic nucleus deep brain stimulation protocols in a data-driven computational model. *Journal of neurophysiology* 99: 1477-1492, 2008.

Hall WC and Moschovakis A. *The Superior Colliculus: New Approaches for Studying Sensorimotor Integration*. Boca Raton: CRC Press, 2004.

Hanes DP and Schall JD. Neural control of voluntary movement initiation. *Science* 274: 427-430, 1996.

Hanes DP and Wurtz RH. Interaction of the frontal eye field and superior colliculus for saccade generation. *J Neurophysiol* 85: 804-815, 2001.

Harting JK. Descending pathways from the superior collicullus: an autoradiographic analysis in the rhesus monkey (Macaca mulatta). *J Comp Neurol* 173: 583-612, 1977.

Hashimoto T, Elder CM, Okun MS, Patrick SK, and Vitek JL. Stimulation of the subthalamic nucleus changes the firing pattern of pallidal neurons. *The Journal of neuroscience : the official journal of the Society for Neuroscience* 23: 1916-1923, 2003.

Hepp K and Henn V. Spatio-temporal recoding of rapid eye movement signals in the monkey paramedian pontine reticular formation (PPRF). *Exp Brain Res* 52: 105-120, 1983.

Hikosaka O and Wurtz RH. Modification of saccadic eye movements by GABA-related substances. I. Effect of muscimol and bicuculline in monkey superior colliculus. *J Neurophysiol* 53: 266-291, 1985a.

Hikosaka O and Wurtz RH. Modification of saccadic eye movements by GABA-related substances. II. Effects of muscimol in monkey substantia nigra pars reticulata. *J Neurophysiol* 53: 292-308, 1985b.

Histed M, Bonin V, and Reid R. Direct activation of sparse, distributed populations of cortical neurons by electrical microstimulation. *Neuron* 63: 508-522, 2009.

Histed MH, Ni AM, and Maunsell JH. Insights into cortical mechanisms of behavior from microstimulation experiments. *Prog Neurobiol*, 2012.

Holtzheimer PE and Mayberg HS. Deep brain stimulation for psychiatric disorders. *Annu Rev Neurosci* 34: 289-307, 2011.

Huerta MF and Harting JK. The mammalian superior colliculus: Studies of its morphology and connections. In: *Comparative Neurology of the Optic Tectum*, edited by Vanegas H. New York: Plenum Publishing, 1984, p. 687-773.

Isa T and Hall WC. Exploring the superior colliculus in vitro. *J Neurophysiol* 102: 2581-2593, 2009.

Jürgens R, Becker W, and Kornhuber HH. Natural and drug-induced variations of velocity and duration of human saccadic eye movements: evidence for a control of the neural pulse generator by local feedback. *Biol Cybern* 39: 87-96, 1981.

Katnani HA and Gandhi NJ. Analysis of current and frequency stimulation permutations in the superior colliculus. *Society for Neurosciences Abstract* Program No. 77.9, 2010.

Katnani HA and Gandhi NJ. Order of operations for decoding superior colliculus activity for saccade generation. *J Neurophysiol* 106: 1250-1259, 2011.

Katnani HA, van Opstal AJ, and Gandhi NJ. A test of spatial temporal decoding mechanisms in the superior colliculus. *Journal of neurophysiology*, 2012.

Kawato M, Furukawa K, and Suzuki R. A hierarchical neural-network model for control and learning of voluntary movement. *Biological cybernetics* 57: 169-185, 1987.

Keller A. Intrinsic synaptic organization of the motor cortex. *Cereb Cortex* 3: 430-441, 1993.

Keller EL. Participation of medial pontine reticular formation in eye movement generation in monkey. *J Neurophysiol* 37: 316-332, 1974.

Kim B and Basso MA. A probabilistic strategy for understanding action selection. *J Neurosci* 30: 2340-2355, 2010.

Kimmel D and Moore T. Temporal patterning of saccadic eye movement signals. *J Neurosci* 27: 7619-7630, 2007.

Langer TP and Kaneko CR. Brainstem afferents to the oculomotor omnipause neurons in monkey. *J Comp Neurol* 295: 413-427, 1990.

Lee C, Rohrer WH, and Sparks DL. Population coding of saccadic eye movements by neurons in the superior colliculus. *Nature* 332: 357-360, 1988.

Lee P and Hall WC. An in vitro study of horizontal connections in the intermediate layer of the superior colliculus. *J Neurosci* 26: 4763-4768, 2006.

Lee PH, Helms MC, Augustine GJ, and Hall WC. Role of intrinsic synaptic circuitry in collicular sensorimotor integration. *Proceedings of the National Academy of Sciences USA* 94: 13299-13304, 1997.

Lefèvre P, Quaia C, and Optican LM. Distributed model of control of saccades by superior colliculus and cerebellum. *Neural Networks* 11: 1175-1190, 1998.

Li X and Basso MA. Competitive Stimulus Interactions within Single Response Fields of Superior Colliculus Neurons. *J Neurosci* 25: 11357-11373, 2005.

Logothetis NK, Augath M, Murayama Y, Rauch A, Sultan F, Goense J, Oeltermann A, and Merkle H. The effects of electrical microstimulation on cortical signal propagation. *Nat Neurosci* 13: 1283-1291, 2010.

Luschei ES and Fuchs AF. Activity of brain stem neurons during eye movements of alert monkeys. *J Neurophysiol* 35: 445-461, 1972.

Markounikau V, Igel C, Grinvald A, and Jancke D. A dynamic neural field model of mesoscopic cortical activity captured with voltage-sensitive dye imaging. *PLoS Computational Biology* 6, 2010.

McHaffie JG and Stein BE. Eye movements evoked by electrical stimulation in the superior colliculus of rats and hamsters. *Brain Res* 247: 243-253, 1982.

McIlwain JT. Lateral spread of neural excitation during microstimulation in intermediate gray layer of cat's superior colliculus. *J Neurophysiol* 47: 167-178, 1982.

McIntyre C, Savasta M, Goff L, and Vitek J. Uncovering the mechanim(s) of action of deep brain stimulation: activation, inhibition, or both. *Clinical Neurophysiology* 115: 1239-1248, 2004.

McIntyre CC, Butson CR, Maks CB, and Noecker AM. Optimizing deep brain stimulation parameter selection with detailed models of the electrode-tissue interface. *Conf Proc IEEE Eng Med Biol Soc* 1: 893-895, 2006.

McIntyre CC and Grill WM. Selective microstimulation of central nervous system neurons. *Ann Biomed Eng* 28: 219-233, 2000.

McPeek RM, Han JH, and Keller EL. Competition between saccade goals in the superior colliculus produces saccade curvature. *J Neurophysiol* 89: 2577-2590, 2003.

McPeek RM and Keller EL. Saccade target selection in the superior colliculus during a visual search task. *J Neurophysiol* 88: 2019-2034, 2002.

Meredith MA and Ramoa AS. Intrinsic circuitry of the superior colliculus: pharmacophysiological identification of horizontally oriented inhibitory interneurons. *J Neurophysiol* 79: 1597-1602, 1998.

Merrill DR, Bikson M, and Jefferys JG. Electrical stimulation of excitable tissue: design of efficacious and safe protocols. *J Neurosci Methods* 141: 171-198, 2005.

Moro E, Esselink R, Xie J, Hommel M, Benabid A, and Pollak P. The impact on parkinson's disease of electrical parameter settings in STN stimulation. *Neurology* 59: 706-713, 2002.

Moschovakis AK, Kitama T, Dalezios Y, Petit J, Brandi AM, and Grantyn AA. An anatomical substrate for the spatiotemporal transformation. *J Neurosci* 18: 10219-10229, 1998.

Moschovakis AK, Scudder CA, and Highstein SM. Structure of the primate oculomotor burst generator. I. Medium-lead burst neurons with upward on-directions. *Journal of neurophysiology* 65: 203-217, 1991a.

Moschovakis AK, Scudder CA, Highstein SM, and Warren JD. Structure of the primate oculomotor burst generator. II. Medium-lead burst neurons with downward on-directions. *Journal of neurophysiology* 65: 218-229, 1991b.

Munoz DP and Istvan PJ. Lateral inhibitory interactions in the intermediate layers of the monkey superior colliculus. *J Neurophysiol* 79: 1193-1209, 1998.

Munoz DP and Wurtz RH. Saccade-related activity in monkey superior colliculus. I. Characteristics of burst and buildup cells. *J Neurophysiol* 73: 2313-2333, 1995.

Mysore S and Knudsen E. The role of a midbrain network in competitive stimulus selection. *Curr Opin Neurobiol* 21: 653-660, 2011.

Nakao S, Curthoys IS, and Markham CH. Direct inhibitory projection of pause neurons to nystagmus-related pontomedullary reticular burst neurons in the cat. *Exp Brain Res* 40: 283-293, 1980.

Nichols MJ and Sparks DL. Component stretching during oblique stimulation-evoked saccades: the role of the superior colliculus. *J Neurophysiol* 76: 582-600, 1996.

Noto CT and Gnadt JW. Saccade trajectories evoked by sequential and colliding stimulation of the monkey superior colliculus. *Brain Research* 1295: 99-118, 2009.

Optican LM. A field theory of saccade generation: temporal-to-spatial transform in the superior colliculus. *Vision Research* 35: 3313-3320, 1995.

Ottes FP, Van Gisbergen JA, and Eggermont JJ. Visuomotor fields of the superior colliculus: a quantitative model. *Vision Research* 26: 857-873, 1986.

Papadopoulou M, Cassenaer S, Nowotny T, and Laurent G. Normalization for sparse encoding of odors by a wide-field interneuron. *Science* 332: 721-725, 2011a.

Papadopoulou M, Cassenaer S, Nowotny T, and Laurent G. Normalization for sparse encoding of odors by a wide-field interneuron. *Science* 332: 721-725, 2011b.

Perlmutter J and Mink J. Deep Brain Stimulation. *Annu Rev Neurosci* 29: 229-257, 2006.

Pettit DL, Helms MC, Lee P, Augustine GJ, and Hall WC. Local excitatory circuits in the intermediate gray layer of the superior colliculus. *J Neurophysiol* 81: 1424-1427, 1999.

Port NL and Wurtz RH. Sequential activity of simultaneously recorded neurons in the superior colliculus during curved saccades. *J Neurophysiol* 90: 1887-1903, 2003.

Quaia C, Lefèvre P, and Optican LM. Model of the control of saccades by superior colliculus and cerebellum. *J Neurophysiol* 82: 999-1018, 1999.

Quessy S and Freedman EG. Electrical stimulation of rhesus monkey nucleus reticularis gigantocellularis. I. Characteristics of evoked head movements. *Exp Brain Res* 156: 342-356, 2004.

Ranck JB, Jr. Which elements are excited in electrical stimulation of mammalian central nervous system: a review. *Brain Res* 98: 417-440, 1975.

Rebesco JM and Miller LE. Stimulus-driven changes in sensorimotor behavior and neuronal functional connectivity application to brain-machine interfaces and neurorehabilitation. *Prog Brain Res* 192: 83-102, 2011.

Robinson DA. Eye movements evoked by collicular stimulation in the alert monkey. *Vision Research* 12: 1795-1808, 1972.

Robinson DA. A method for measuring eye movement using a scleral search coil in a magnetic field. *IEEE Trans Bio-Med Eng* BME-10: 137-145, 1963.

Robinson DA. Oculomotor control signals. In: *Basic Mechanisms of Ocular Motility and Their Clinical Implications*, edited by Bach-y-Rita P and Lennerstrand G. Oxford: Pergamon, 1975, p. 337-374.

Robinson DA and Fuchs AF. Eye movements evoked by stimulation of frontal eye fields. *J Neurophysiol* 32: 637-648, 1969.

Sasaki S and Shimazu H. Reticulovestibular organization participating in generation of horizontal fast eye movement. *Ann N Y Acad Sci* 374: 130-143, 1981.

Schiller PH, True SD, and Conway JL. Paired stimulation of the frontal eye fields and the superior colliculus of the rhesus monkey. *Brain Res* 179: 162-164, 1979.

Schultz KP, Williams CR, and Busettini C. Macaque pontine omnipause neurons play no direct role in the generation of eye blinks. *J Neurophysiol* 103: 2255-2274, 2010.

Scudder CA, Kaneko CS, and Fuchs AF. The brainstem burst generator for saccadic eye movements: A modern synthesis. *Exp Brain Res* 142: 439-462, 2002.

Scudder CA, Moschovakis AK, Karabelas AB, and Highstein SM. Anatomy and physiology of saccadic long-lead burst neurons recorded in the alert squirrel monkey. I. Descending projections from the mesencephalon. *J Neurophysiol* 76: 332-352, 1996.

Sommer MA and Wurtz RH. A pathway in primate brain for internal monitoring of movements. *Science* 296: 1480-1482, 2002.

Sommer MA and Wurtz RH. What the brain stem tells the frontal cortex. I. Oculomotor signals sent from superior colliculus to frontal eye field via mediodorsal thalamus. *J Neurophysiol* 91: 1381-1402, 2004.

Sooksawate T, Isa K, Behan M, Yanagawa Y, and Isa T. Organization of GABAergic inhibition in the motor output layer of the superior colliculus. *Eur J Neurosci* 33: 421-432, 2011.

Sparks DL. Translation of sensory signals into commands for control of saccadic eye movements: role of primate superior colliculus. *Physiol Rev* 66: 118-171, 1986.

Sparks DL and Gandhi NJ. Single cell signals: an oculomotor perspective. *Prog Brain Res* 142: 35-53, 2003.

Sparks DL and Hartwich-Young R. The deep layers of the superior colliculus. *Rev Oculomot Res* 3: 213-255, 1989.

Sparks DL, Holland R, and Guthrie BL. Size and distribution of movement fields in the monkey superior colliculus. *Brain Res* 113: 21-34, 1976.

Sparks DL and Mays LE. Signal transformations required for the generation of saccadic eye movements. *Annu Rev Neurosci* 13: 309-336, 1990.

Sparks DL and Mays LE. Spatial localization of saccade targets. I. Compensation for stimulation-induced perturbations in eye position. *J Neurophysiol* 49: 45-63, 1983.

Stanford TR, Freedman EG, and Sparks DL. Site and parameters of microstimulation: evidence for independent effects on the properties of saccades evoked from the primate superior colliculus. *J Neurophysiol* 76: 3360-3381, 1996.

Stein BE and Meredith MA. *The Merging of the Senses*. Cambridge, MA: MIT Press, 1993.

Stoney SD, Jr., Thompson WD, and Asanuma H. Excitation of pyramidal tract cells by intracortical microstimulation: effective extent of stimulating current. *J Neurophysiol* 31: 659-669, 1968.

Straschill M and Hoffmann KP. Activity of movement sensitive neurons of the cat's tectum opticum during spontaneous eye movements. *Exp Brain Res* 11: 318-326, 1970.

Straschill M and Rieger P. Eye movements evoked by focal stimulation of the cat's superior colliculus. *Brain Res* 59: 211-227, 1973.

Strassman A, Evinger C, McCrea RA, Baker RG, and Highstein SM. Anatomy and physiology of intracellularly labelled omnipause neurons in the cat and squirrel monkey. *Exp Brain Res* 67: 436-440, 1987.

Strassman A, Highstein SM, and McCrea RA. Anatomy and physiology of saccadic burst neurons in the alert squirrel monkey. I. Excitatory burst neurons. *J Comp Neurol* 249: 337-357, 1986.

Takahashi M, Sugiuchi Y, and Shinoda Y. Topographic organization of excitatory and inhibitory commissural connections in the superior colliculi and their functional roles in saccade generation. *J Neurophysiol* 104: 3146-3167, 2010.

Tehovnik EJ. Electrical stimulation of neural tissue to evoke behavioral responses. *J Neurosci Methods* 65: 1-17, 1996.

Van Gisbergen JA, Robinson DA, and Gielen S. A quantitative analysis of generation of saccadic eye movements by burst neurons. *J Neurophysiol* 45: 417-442, 1981.

Van Gisbergen JA, Van Opstal AJ, and Tax AA. Collicular ensemble coding of saccades based on vector summation. *Neuroscience* 21: 541-555, 1987.

Van Horn MR, Mitchell DE, Massot C, and Cullen KE. Local Neural Processing and the Generation of Dynamic Motor Commands within the Saccadic Premotor Network. *J Neurosci* 30: 10905-10917, 2010.

Van Opstal A and Goossens H. Linear ensemble-coding in midbrain superior colliculus specifies the saccade kinematics. *Biol Cybern* 98: 561-577, 2008.

Van Opstal AJ and Kappen H. A two-dimensional ensemble coding model for spatial-temporal transformation of saccades in monkey superior colliculus. *Network* 4: 19-38, 1993.

Van Opstal AJ and Van Gisbergen JA. A nonlinear model for collicular spatial interactions underlying the metrical properties of electrically elicited saccades. *Biol Cybern* 60: 171-183, 1989.

Van Opstal AJ and Van Gisbergen JA. Role of monkey superior colliculus in saccade averaging. *Exp Brain Res* 79: 143-149, 1990.

Van Opstal AJ and Van Gisbergen JA. Skewness of saccadic velocity profiles: a unifying parameter for normal and slow saccades. *Vision Research* 27: 731-745, 1987.

Van Opstal AJ, Van Gisbergen JA, and Smit AC. Comparison of saccades evoked by visual stimulation and collicular electrical stimulation in the alert monkey. *Exp Brain Res* 79: 299-312., 1990.

Vokoun CR, Jackson MB, and Basso MA. Circuit dynamics of the superior colliculus revealed by in vitro voltage imaging. *Ann N Y Acad Sci* 1233: 41-47, 2011.

Vokoun CR, Jackson MB, and Basso MA. Intralaminar and Interlaminar Activity within the Rodent Superior Colliculus Visualized with Voltage Imaging. *J Neurosci* 30: 10667-10682, 2010.

Walton MMG, Sparks DL, and Gandhi NJ. Simulations of saccade curvature by models that place superior colliculus upstream from the local feedback loop. *J Neurophysiol* 93: 2354-2358, 2005.

Wennekers T. Dynamic approximation of spatiotemporal receptive fields in nonlinear neural field models. *Neural Comput* 14: 1801-1825, 2002.

Wilke M, Turchi J, Smith K, Mishkin M, and Leopold DA. Pulvinar inactivation disrupts selection of movement plans. *J Neurosci* 30: 8650-8659, 2010.

Williamson SS, Zivotofsky AZ, and Basso MA. Modulation of gaze-evoked blinks depends primarily on extraretinal factors. *J Neurophysiol* 93: 627-632, 2005.

Wurtz RH and Goldberg ME. Activity of superior colliculus in behaving monkey. III. Cells discharging before eye movements. *J Neurophysiol* 35: 575-586, 1972.

Yoshida K, Iwamoto Y, Chimoto S, and Shimazu H. Saccade-related inhibitory input to pontine omnipause neurons: an intracellular study in alert cats. *J Neurophysiol* 82: 1198-1208, 1999.